School of Surveying and Land Information

Determination of Water Column Characteristics in Coastal Environments using Remote Sensing

Peter HICK

"This thesis is presented as part of the requirements for the award of the Degree

of

Doctor of Philosophy

of the

Curtin University of Technology"

February 1997

PREFACE

"My life-long fascination with the aquatic environment began from my childhood homes, one high on a sand dune above Scarborough Beach, the other on the Serpentine River. The inevitable consequence of this is a passion for surfing, fishing, diving and sailing, all of which require an understanding of the ever-changing look of these waters. My other fascination, and my career choice, was to translate environmental information into the spatial domain, or maps, and remote sensing research has given me the opportunity to blend my hobbies and scientific curiosity with my work".

ABSTRACT

This thesis illustrates the specific aspects that influence or limit the application of remotely-sensed data for information retrieval from coastal marine, estuarine and riverine environments. The thesis is drawn principally from ten separate studies and is divided into discrete sections, or experiments, that provide an understanding of the fundamental aspects of the effects of the atmosphere, water surface, water column and bottom on sensor-received reflected signal.

The results show the importance of precise calculation of acquisition parameters and the absolute importance of relevant reference data. Most instrumentation for remote sensing at visible wavelengths has been developed for terrestrial applications where signal is rarely limiting and target features are relatively static. For in-water applications, where signal is small and noise can be large, the features to be sensed may be temporally dynamic and obscured.

However, the work presented also shows the great benefit and spatial cost-effectiveness that can be obtained if the spectral and temporal specification is adequately considered. The prime motivation for such applications usually comes from the requirement to detect and quantify water column characteristics, such as phytoplankton forming as algal blooms, and bottom stratigraphic condition, such as benthic habitat mapping for fishery or conservation purposes.

ACKNOWLEDGMENTS

I wish to recognise the contributions of the following people and their organisations. The Commonwealth Scientific Industrial Research Organisation (CSIRO) has been the principal financial supporter of most of this work and without that support I could not have completed this thesis. I wish to particularly acknowledge the significance of the contribution and friendship of my colleagues and collaborators Miss Cindy Ong for image processing advice and support and Dr Peter Jernakoff for marine biological contributions.

Much of the work reported in the thesis is drawn from collaborative research and experience gained within CSIRO, especially the Algal Bloom Research Program and the Perth Coastal Waters Study, and is directly supported with biological and physical inputs from collaborators such as Dr Jernakoff, Miss Ong, as well as Dr Chari Pattiaratchi, Richard Scoones, Vas Hosja and Jim Burt. Valuable advice in the design of the studies, analyses, processing of data and preparation of the manuscript was provided by Jill Ashton, Jeremy Wallace, Suzanne Furby and Dr Peter Thompson. Dr Frank Honey of SpecTerra Systems supplied the DMSV.

I would also like to acknowledge Dr John Parslow, Dr Hugh Kirkman, Dr Trevor Ward and Peter Jolly of the workshop staff at CSIRO Division of Fisheries; Alex Wyllie and Robert "Red" Shaw of the Remote Sensing Applications Centre (DOLA); officers of the Waterways Commission and Swan River Trust, including Wasele Hosja, Sarah Grigo, Dr Bruce Hamilton, Robert Atkins, Malcolm Robb and the

inspectors who operated the "Jack Mattison"; Roger Schultz, Dean Cunningham and Ron Dercoles of the WA Chemistry Centre; Donald DeVries and Dr David Jupp of COSSA (the CSIRO Office of Space Science and Applications).

This work received funds and/or research-in-kind from the CSIRO Division of Fisheries, the CSIRO Blue-Green Algal Program, COSSA, the Waterways Commission of Western Australia, M.G. Kailis and Broome Pearls Pty Ltd. In the early phases of the work Dr Pattiaratchi (CWR), Dr Richard Smith (CSIRO), Wally Russell (CSIRO), Bob Gozzard, Capt. Mitch Blakers (Geoscan), Cec Maher (COSSA), Claire Anthony (All Saints College), Capt Rodney MacLachlan (R V Tartan II), Howard Fairbanks (R V Tartan II), Graeme Behn (CALM) all made valued contributions to these outcomes.

Special thanks are directed to Curtin University where I have had the pleasure of being a part-time student since the late seventies having completed three major endeavours culminating in this thesis. I wish to express my gratitude to Mrs Kylie Bessant, and Dr Will Featherstone and Graeme Wright for their encouragement help and advice. Professor Graham Lodwick, who reviewed the manuscript, and guided the successful examination outcome deserves my highest praise and regard. Finally, I would like to thank my wife and family for support and for putting up with my nocturnal study habits.

thankyou

TABLE OF CONTENTS

Page

PREFACE ii

ABSTRACT iii

ACKNOWLEDGMENTS iv

TABLE OF CONTENTS vi

LIST OF FIGURES xiii

LIST OF TABLES xv

LIST OF ACRONYMS xvi

Chapter

1 INTRODUCTION 1

1.1 Background 1

1.2 Why do this Work? 1

1.3 Review of Relevant Studies 5

1.4 Research Program 12

1.5 Chapter Arrangement 16

2 REMOTE SENSING OF WATER BODIES 18

2.1 Electromagnetic Spectrum 18

2.1.1 Ultraviolet 19

2.1.2 Visible Wavelengths 20

2.1.3 Near Infrared 21

2.1.4 Mid-Infrared 22

2.1.5 Thermal Infrared 22

2.1.6 Microwave 23

2.2 Reflectance from a Waterbody 23

2.2.1 Water-leaving or Upwelling Radiance 24

2.2.2 Penetration of Light into Water or Attenuation Coefficients 25

2.2.3 Bottom Contribution 27

2.2.4 Separation of Components 28

Table of Contents (continued)

Chapter **Page**

2.2.5 Signal-to-Noise Ratios 29
2.3 Data Sources 30
2.3.1 Compact Airborne Spectrographic Imager (CASI) 30
2.3.2 Digital Multi Spectral Video (DMSV) 31
2.3.3 Geoscan Airborne Multi-Spectral Scanner 31
2.3.4 Ocean Colour Scanner 32
2.3.5 Landsat Thematic Mapper 32
2.3.6 SPOT 33
2.4 Field Spectral Measurements 33
2.4.1 DSIR Radiometer 34
2.4.2 Irricrop Multi-Spectral Radiometer 34
2.4.3 Ocean Optics Spectrometer 35
2.5 Summary 36

3 DETERMINATION OF SURFACE SCATTERING EFFECTS 38
3.1 Introduction 38
3.1.1 Atmospheric Correction 39
3.1.2 Image Brightness Variation Caused by Wind-fields 40
3.1.3 Bi-directional Reflectance from Wide Field-of-View Sensors 41
3.1.4 Hot-spots 42
3.1.5 Correction Procedures 42
3.2 Coastal Waters Experiment 45
3.2.1 Background and Aims 45
3.2.2 Methodology 46
3.2.3 Results 48
3.2.3.1 Brightness correction using band ratios 48
3.2.3.2 Brightness correction using across-track modelling 49
3.2.4 Conclusions 50
3.3 Peel Inlet Experiment 52
3.3.1 Background and Aims 52
3.3.2 Methodology 53

Table of Contents (continued)

Chapter **Page**

3.3.3 Results....54
3.3.4 Conclusions....54
3.4 Swan Estuary Experiment....56
3.4.1 Background and Aims....56
3.4.2 Methodology....57
3.4.3 Results....58
3.4.3.1 Effect of look-angle and solar angle....58
3.4.3.2 Effect of windspeed....60
3.4.4 Conclusions....61
3.5 Summary....61

4 DETERMINATION OF WATER COLUMN CHARACTERISTICS....65
4.1 Introduction....65
4.1.1 Phytoplankton (plants in the water column)....66
4.1.1.1 Euglenophyta....66
4.1.1.2 Chlorophyta....66
4.1.1.3 Chrysophyta....67
4.1.1.4 Pyrrophyta....67
4.1.1.5 Phaeophyta....68
4.1.2 Remote Sensing of Algal Pigments....68
4.2 Swan-Coastal OCS-Geoscan Comparison....69
4.2.1 Background and Aims....70
4.2.1.1 Background studies....70
4.2.1.2 Study location....72
4.2.2 Methodology....74
4.2.2.1 Ocean Colour Scanner....74
4.2.2.2 Geoscan Scanner....75
4.2.2.3 Signal to noise calculations....75
4.2.2.4 Data acquisition....76
4.2.3 Results....77
4.2.3.1 Spectral band comparison....77

Table of Contents (continued)

Chapter **Page**

4.2.3.2 Signal to Noise comparison....81
4.2.4 Conclusions....81
4.3 Swan River Study: CASI Experiment....83
4.3.1 Background and Aims....83
4.3.1.1 Study area....85
4.3.1.2 In-water spectral data....85
4.3.2 Methodology....89
4.3.2.1 CASI instrument....90
4.3.2.2 Site sampling methods....92
4.3.2.3 Analysis methods for CASI data....93
4.3.3 Results....94
4.3.3.1 DSIR radiometer....94
4.3.3.2 Comparison of biological and spectral-mode CASI data....97
4.3.3.3 Comparison of biological data with spatial-mode CASI data....99
4.3.3.4 Variable band selection results....102
4.3.3.5 Image classification....103
4.3.3.6 Simulation of simple multi-band video system....103
4.3.4 Conclusions....108
4.4 Swan River Study: DMSV Experiment....110
4.4.1 Aims....110
4.4.1.1 Background....110
4.4.1.2 Study area....111
4.4.2 Methodology....111
4.4.2.1 Field reference data collection....111
4.4.2.2 Airborne data collection....114
4.4.2.3 Calibration of DMSV data to reflectance....115
4.4.2.4 Image rectification....116
4.4.2.5 Image analysis....116
4.4.3 Results....117
4.4.3.1 Composition of algal bloom types....117

Table of Contents (continued)

Chapter **Page**

4.4.3.2 Composition of bloom pigments 117
4.4.3.3 Spatial, temporal and depth variability in algal bloom chlorophyll 118
4.4.3.4 Secchi disk index of light penetration 120
4.4.3.5 Total suspended solids 121
4.4.3.6 Relationship between chlorophyll, Secchi depth and total suspended solids 121
4.4.3.7 Spectral characteristics of Gymnodinium 123
4.4.3.8 DMSV data compared with algal bloom concentration 124
4.4.4 Conclusions 124
4.5 Summary 127

5 DETERMINATION OF BOTTOM CHARACTERISTICS 129
5.1 Introduction 129
5.1.1 Upwelling radiance from a waterbody 130
5.1.1.1 Substrate radiance 131
5.1.1.2 Bathymetric determination 133
5.1.1.3 Signal to noise considerations 134
5.2 Broome Project 135
5.2.1 Background 135
5.2.2 Aims 137
5.2.3 Methodology 138
5.2.4 Results 139
5.2.4.1 Ocean reflectance 139
5.2.4.2 Data filtering 142
5.2.4.3 Atmospheric effects 145
5.2.4.4 Ocean floor features 147
5.2.4.5 Pearl-catch relationship results 148
5.2.5 Conclusions 152
5.3 Geographe Bay Project 155
5.3.1 Aims 155

Table of Contents (continued)

Chapter **Page**

5.3.2 Methodology 158
5.3.3 Results 158
5.3.4 Conclusions 160
5.4 Coastal Waters Project 161
5.4.1 Aims 161
5.4.1.1 Study area 161
5.4.1.2 Benthic habitats 163
5.4.2 Methodology 167
5.4.2.1 Data acquisition 167
5.4.2.2 Data processing 168
5.4.3 Results 169
5.4.3.1 Validation program 169
5.4.3.2 Habitat distribution 172
5.4.4 Conclusions 174
5.5 Marmion Lagoon Project 175
5.5.1 Aims 175
5.5.1.1 Background 176
5.5.1.2 Study site 176
5.5.2 Methodology 178
5.5.2.1 Preliminary habitat study 178
5.5.2.2 CASI habitat study 180
5.5.3 Results 181
5.5.3.1 Preliminary habitat study 181
5.5.3.2 CASI habitat study 182
5.5.4 Conclusions 187
5.6 Summary 188

6 CONCLUSIONS AND RECOMMENDATIONS 189
6.1 Conclusions 189
6.1.1 Image Reflectance Characteristics 189
6.1.1.1 Atmospheric and radiometric correction 190

Table of Contents (continued)

Chapter **Page**

6.1.1.2 Image brightness variation 192
6.1.1.3 Hot-spots 193
6.1.2 Water Column Characteristics 194
6.1.2.1 Swan-Coastal OCS-Geoscan Comparison 195
6.1.2.2 Swan River Study: CASI experiment 197
6.1.2.3 Swan River Study: DMSV experiment 199
6.1.3 Bottom Characteristics 202
6.1.3.1 Broome Project 203
6.1.3.2 Geographe Bay Project 205
6.1.3.3 Perth Coastal Waters Project 206
6.1.3.4 Marmion Lagoon Project 207
6.2 Recommendations 208
6.2.1 Surface Reflectance Effects 208
6.2.2 Water Column Characteristics 212
6.2.3 Bottom Characteristics 216

REFERENCES 220

LIST OF FIGURES

Figure		Page
1.1	North-western corner of Peel Inlet, near Mandurah, WA	4
1.2	Location map of all study sites	14
2.1	Solar energy paths for remote sensing over water	24
3.1	Across-track brightness from calibrated airborne imaging spectrometer	44
3.2	Study location for Geoscan and DMSV data acquisition	47
3.3	Curve of column means for band 1 of Geoscan data	50
3.4	Curve of column means after first stage correction	50
3.5	Part of Geoscan data for Coastal Waters study	51
3.6	Raw DMSV data acquired over part of Peel Inlet	55
3.7	DMSV scene processed using 3 x 3 kernel	55
3.8	DMSV scene processed with three digital count differential	55
3.9	Spectra from Swan River at varying sun angles	59
3.10	Vertical spectra of Swan River water at a range of wind-speeds	59
3.11	Relative upwelling radiance as a function of wind-speed	62
4.1	Location of flightlines and study sites near Perth, WA	73
4.2	Filter functions for both scanners	76
4.3	Plot of Geoscan band 1/5 ratio and Log C	80
4.4	Plot of OCS bands 2/7 against Log C for all sites	80
4.5	Location map of Swan River showing wetlands and six monitoring sites	84
4.6	In-water spectral measurements from Irricrop radiometer	87
4.7	In-water spectral measurements from Swan/Canning River system	88
4.8	DSIR meter spectra for site 1	96
4.9	DSIR meter spectra for site 2	96
4.10	CASI spectral curves extracted from spectral-mode data	97
4.11	CASI spectra for site 2 and an adjacent wetlands site	99
4.12	Canonical variate analysis for river sites using bands 3-14	100
4.13	Canonical variate analysis for river and wetlands using bands 3-14	101
4.14	CASI classification of Swan River using best-possible-subset bands	104
4.15	CASI classification using only three simulated DMSV spectral bands	105
4.16	Relationship between total chlorophyll and *in vivo* fluorescence	112

List of Figures (continued)

Figure		Page
4.17	Composition (± SE) of algal groups within the bloom	117
4.18	Proportion (±) SE of total bloom concentrations	118
4.19	Six calibrated DMSV frames, 19, 20 January near Ron Courtney Is	119
4.20	Secchi depth penetration	121
4.21	Reflectance spectra of *Gymnodinium* at three concentrations	123
5.1	Location diagram of Broome study area	136
5.2	Satellite-measured radiance and its relationship to depth	139
5.3	Transect line seven from Pacific Lady cruise	140
5.4	Graphs of solar elevation from winter to summer solstice at 20°S	141
5.5	Effect of varying weightings of an "east" directional filter	142
5.6	Kernels designed to provide directional filtering	142
5.7	Band 1 enhancement (a), weighted edge filters in (b), (c) (d)	143
5.8	Direction filters to highlight discontinuities and heterogeneity	144
5.9	Landsat TM band displays for part of Broome Study Area	146
5.10	Holocene global marine transgression based on Fairbridge (1961)	148
5.11	Geographe Bay study area	156
5.12	TM image and Admiralty Chart AUS 334 (depth in fathoms)	159
5.13	Location map for the Coastal Waters Project	162
5.14	Part of Geoscan data for Coastal Waters Project	170
5.15	Part of classified image of Coastal Waters Project	171
5.16	Air photo of Little Island with examples of transects	177
5.17	Spectrum of bare sand (transect 1) at depth of 8.0 m	184
5.18	Spectra of bare sand at 8.0 m and Ecklonia at 1.0 m	184
5.19	Spectra of Ecklonia at 1 m (trans 8) and at 3.0-4.0 m (trans 10)	185
5.20	Spectra of Ecklonia-dominated reef at depths ranging from 3-9 m	185
5.21	Spectra of Posidonia and Amphibolis seagrasses	186
5.22	Spectra for sand, shallow reef, deeper reef and seagrass	186

LIST OF TABLES

Table		Page
4.1	Correlation matrix for all scanner bands against chlorophyll	78
4.2	Sites and total chlorophyll used in analysis	78
4.3	Calculation of signal to noise ratios	82
4.4	Wavebands of CASI, DMSV and DSIR spectrometer	91
4.5	Chemical and biological measurements, 18/2/1993	96
4.6	CVA of CASI spatial-mode data using bands 3-14 for river sites	100
4.7	CVA of CASI spatial-mode data, bands 3-14 for river and wetland sites	101
4.8	Optimum separation using a variable selection procedure and cumulative percentage for 12 bands for river sites only	102
4.9	Optimum separation using variable selection procedure and cumulative percentage for 12 bands for river sites and wetland sites	102
4.10	Concurrence of classes between best seven CASI bands and three CASI bands corresponding to DMSV	107
4.11	Field reference data collected during the study	112
5.1	Diver versus image assessment of bottom type	149
5.2	Trawl data versus image assessment	151
5.3	Tests of significance (χ^2) between pearl-bottom, prawn catch and image	152
5.4	Transects used in spectral analysis for habitat mapping	183

LIST OF ACRONYMS

AMG	Australian Map Grid
AMSS	Airborne Multi Spectral Scanner
ATSR	Along Track Scanning Radiometer
AVHRR	Advanced Very High Resolution Radiometer
BRDF	Bi-directional Reflectance Distribution Function
CALM	Conservation and Land Management (Department of)
CASI	Compact Airborne Spectrographic Imager
CCD	Charged-Couple Device
COSSA	CSIRO Office for Space Science and Applications
CPUE	Catch Per Unit Effort
CSIRO	Commonwealth Scientific Industrial Research Organisation
CVA	Canonical Variate Analysis
CWR	Centre for Water Research (University of WA)
CZCS	Coastal Zone Colour Scanner
DEP	Department of Environmental Protection
DMSV	Digital Multi-Spectral Video
DOLA	Department of Land Administration
DSIR	Department of Scientific Industrial Research (NZ)
ERS	European Resources Satellite
FOV	Field Of View
GPS	Global Positioning System
INS	Inertial Navigation System
IFOV	Instantaneous Field Of View
MSR	Multi-Spectral Radiometer
MSS	Multi-Spectral Scanner
NOAA	National Oceanographic and Atmospheric Administration
OCS	Ocean Colour Scanner
PAR	Photosynthetically Available Radiation
SNR	Signal to Noise Ratio
SPOT	Satellite Pour l'Observation de la Terre
STS	SpecTerra Systems
TM	Thematic Mapper
WAWA	Water Authority of Western Australia

Chapter 1

INTRODUCTION

1.1 Background

Remote sensing of aquatic environments presents a discrete range of problems that can, if ignored, render the exercise a waste of time. This thesis sets out to illustrate, through a series of studies, the advantages and pitfalls of using spatial data gathered from a remote sensor to simply measure the characteristics of the surface, the column and the features at the bottom of a water body.

The main emphasis within this thesis is to illustrate the specific aspects that influence or limit the use of remotely sensed data. This thesis is drawn principally from ten separate studies of both the author's own research projects and collaborative projects, in which the author has been the major contributor of the remote sensing component.

This thesis is divided into discrete sections, or study topics, that will provide an understanding of those fundamental aspects and, hopefully, will help the marine and aquatic remote sensing user community, by example from these case studies, to obtain the best information possible from remotely sensed data.

1.2 Why do this Work?

Particular emphasis is placed on optimum operational outcomes from the acquisition of remotely-sensed data. These demands may be from the fishing, maritime,

exploration, extraction industries or environmental authorities. Information is needed for these users at specific or generic times and must conform with planimetric requirements. The impetus for this work has grown in part from the included projects that rely on meeting critical specification for remotely-sensed data acquisition that is not satisfactorily achieved because of constraints that should be possible to predict.

Key studies such as Van Stokkom *et al.* (1993), who reviewed the quantitative use of passive optical remote sensing over coastal and inland water bodies assert that insufficient understanding of the physical mechanisms involved with water bodies, and technical limitations of instruments are limiting the usefulness of remotely sensed data. That review paper crystallised many of my views and highlighted many of the case studies to which my research has been related. In their conclusions they comment that "one could easily get the impression that remote sensing over water is like dealing with Murphy's Law and therefore decide to abandon the attempt". They also say "taking into account the great importance of water management throughout the world, and the potential of remote sensing, one should use it to its full quantitative potential"

This thesis combines a series of studies in coastal marine, estuarine and riverine settings that address remote sensing of the water column as a whole but is divided into the aspects of surface, column and bottom.

The first work in the Peel-Harvey estuary was published in Hick (1979). This was a study undertaken in the early seventies using Landsat MSS 80 m data from 1972, and

is interesting as the problems encountered with that work were symptomatic of almost all of the subsequent studies. This demonstrated that it was possible to map, and therefore monitor, the distribution of the troublesome Cladophora algal bloom using satellite data. The reason for the failure to adopt this breakthrough in monitoring is evident in Figure 1.1 which is the line-printer output displaying the image products created from this "highly-suspicious" new high-flying spy technology.

It was not until the next year, when simultaneous colour and false colour infrared photography was acquired with the satellite data, that the concept received "grudging" potential acknowledgment by the inlet management authority. However, it must be recognised that the enormous relative cost of computers, capable of processing the vast amounts of data generated by satellites, was a great disincentive to the wider adoption of this technology.

Many years later a much more extensive and quantitative collaborative study using multi-date Landsat TM data was reported in Lavery *et al.* (1993). This study in the Peel-Harvey estuarine system supported the satellite data with extensive field and collateral data and it was still not possible to convince managers to incorporate remotely sensed data into their routine "boat and bucket" monitoring strategy.

Intervening studies by Honey and Hick (1976a) and Honey *et al.* (1980) on wetland classification using Landsat Multi-Spectral Scanner data were among the first more widely accepted applications of the objectivity possible with multi-temporal and multi-spectral spatial descriptions of water body components.

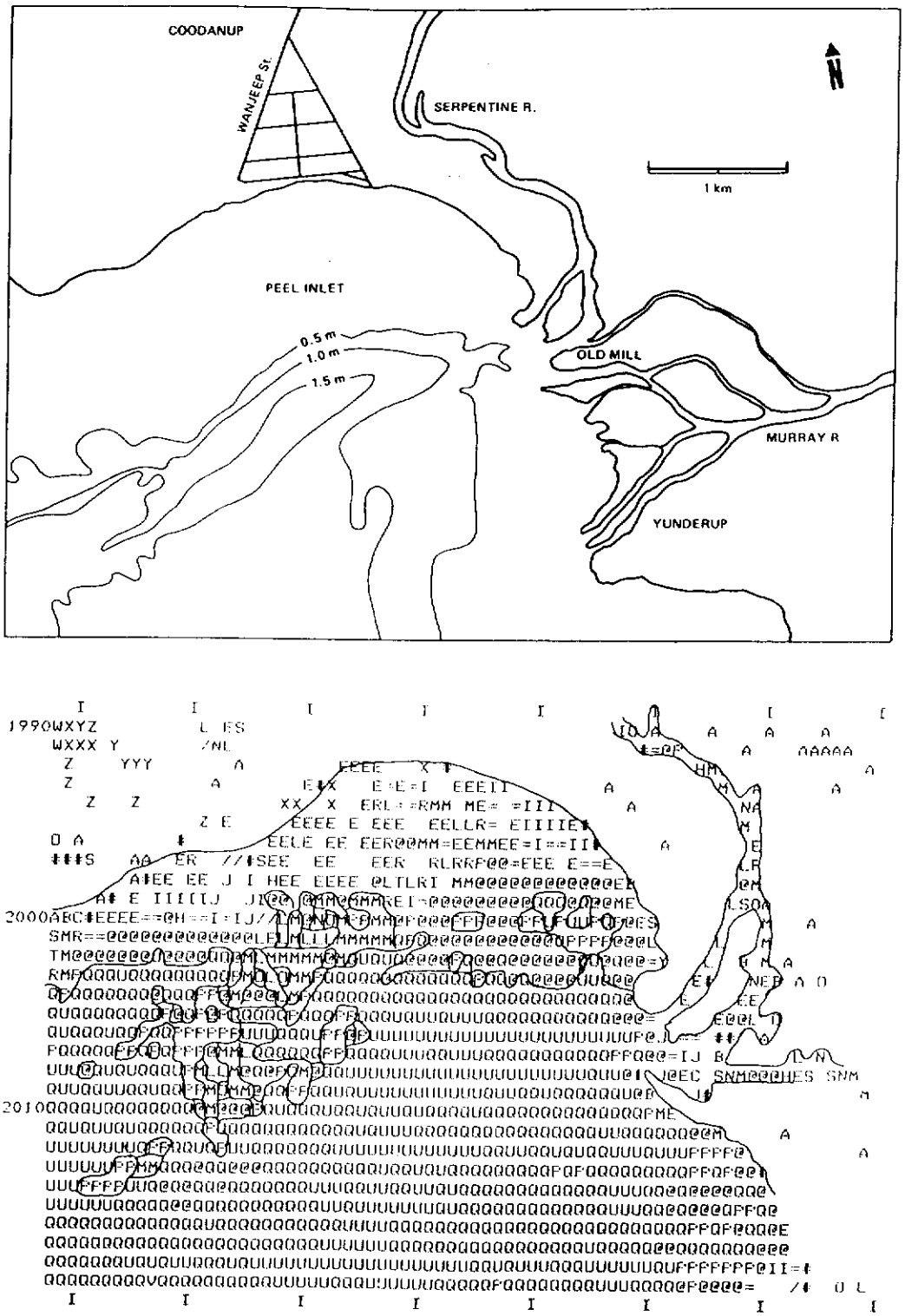

Figure 1.1: North-western corner of Peel Inlet, near Mandurah, WA

Therefore this work was undertaken, in part, to address the realisation that the technology has not been adopted into coastal management strategies, and in part to explore some of the complexities and disappointing results that may have influenced coastal managers to avoid the use of remotely-acquired spatial data.

1.3 Review of Relevant Studies

A review of the literature that is relevant to these studies, principally from within the Australian environment, is summarised here. Every endeavour has been made to accurately cite the work of others, and where interpretations and evaluations have been made, it has been done with the utmost respect for those authors.

Qualitative interpretations of water bodies, produced from remotely sensed data, have suffered from noise within the data that make definitive measurement unreliable. Many examples of descriptions of suspended sediments, presence of algae and pigments, and other physical and biological parameters have been correlated with in-situ measurements, with the aim of predictive capability only to be less than acceptable when other conditions change. An extensive review of the practicality of remote measurement of inland waters was undertaken by CSIRO prior to the commencement of the National Algal Bloom Research Program, Jupp *et al.* (1992a). The following is partly condensed from that review and partly from my own observations.

The role and diversity of the interactions of light with water is found in the work of Jerlov (1976) and Kirk (1983) which shows that biological competition for light and

nutrients in water is complex. The use of airborne and satellite-borne sensors to measure and map the spatial extent, colour and temperature of water masses has become widespread and fundamental to research into the spatial environmental processes which they support.

Remote sensing for determining water column properties in the ocean has mostly used satellite data, principally the Coastal Zone Colour Scanner (CZCS) and to a lesser extent Landsat satellite data (Smith and Wilson, 1981; Sturm, 1981; Gordon *et al.*, 1983). CZCS data provide the most advanced broad scale examples of remote sensing of water parameters and chlorophyll, and Pattiaratchi *et al.* (1990) show the relationship to ocean productivity and thermal structures associated with the Leeuwin Current.

This study took advantage of the specific situation where ocean chlorophyll concentrations are caused essentially by phytoplankton abundance, where there is little inanimate suspended sediment in the water column and where remotely-sensed images normally contain areas of clear ocean water as a reference. Algorithms for CZCS data, based on the blue/green region of the light spectrum, were developed by Dr John Parslow, of the CSIRO Division of Fisheries, for mapping the surface pigments associated with the phytoplankton and for estimating ocean productivity at a global level.

Coastal waters and estuaries provide a situation that is more complex and there is considerable on-going research into developing algorithms and scanner design which

will allow these dynamic and important areas of the sea to be effectively monitored using remote sensing.

Poor correlation between estimates of chlorophyll, based on ocean algorithms, and the actual distribution were reported in Port Phillip Bay, near Melbourne, Victoria. Some observers felt that this may have been caused by a number of problems, such as the difficulty of relating field data and satellite data precisely in space and time. The relevance of these observations was considered throughout the studies reported in this thesis as will become apparent in the chapter and sections relating to water column characteristics. A fair conclusion, at the time of these anecdotal reports, was drawn by both Jupp *et al.* (1992a) and, on the west coast, by Lavery *et al.* (1993), that changes in methodology were needed in more turbid waters. Nevertheless, the spatial patterns of water mass dynamics, derivable from these data and from Landsat data, were worth capturing.

CZCS was successfully used to monitor blooms in a turbid estuary by Stumpf and Tyler (1988). Their methods used data taken at the time of overpass and were based on correlating the satellite data with in-water measurements. As with other studies, they achieved very good statistical correlations between water constituent concentrations and the remotely sensed measurements in these more complex waters. Since the algorithms based on the blue/green region of the spectrum and successfully applied in the ocean are only recently being extended to estuaries, it seemed unlikely that they were appropriate in turbid, gelvin (yellow/green) rich inland waters without modification. Subsequent work by myself and my collaborator Dr Peter Jernakoff, in

the humic-rich Swan River and reported later in this thesis, add substance to this observation.

Tassan (1987) shows how the methodology developed to analyse the CZCS data may be successfully modified for the finer resolution and different spectral bands of the Landsat Thematic Mapper (TM). The methods he described are based on an extension of CZCS atmospheric corrections and a variety of ratio-based algorithms for concentrations of chlorophyll and suspended sediments using the blue/green bands. The consistency of the algorithms between different scenes depends on consistent correlations existing between suspended solids and concentration of chlorophyll.

In Tassan and Sturm (1986), methods similar to those of Tassan (1987) were established for turbid coastal waters as a result of careful attention to atmospheric correction. It is significant, supporting the claim that the spectral focus must shift in turbid waters, that the algorithms providing best results in their work used wavebands in the 500 to 700 nm (green/red) region.

Work undertaken in the late eighties (Lavery *et al.*, 1993) show how Tassan's methods for atmospherically correcting Landsat TM data may be profitably applied in an estuarine system. By using field data taken at different times, that study showed that it is possible to construct regressions between atmospherically corrected TM data and (assumed dependent) variables, such as salinity, total pigments and Secchi disk depth (as a measure of particulate concentration causing light attenuation), that are

time-consistent. The work shows that TM data should not be ignored in those inland water situations where the water bodies have sufficient extent. However, it is likely that for inland waters, atmospheric correction methods need more collateral data since Tassan's method, like the deep ocean algorithms, relies on having reference water with either known properties or zero water radiance effects.

Like the majority of contemporary studies into water property/remote sensing applications, the conclusions in Lavery *et al.* (1993) are based on correlations between field data and remotely sensed data. Correlations do not generally transfer well from one location to another as they depend on consistent underlying associations between the constituents. In Chesapeake Bay, Harding *et al.* (1992) applied chlorophyll algorithms to data acquired by airborne remote sensing. The spectral bands used were centred on the blue/green region at 460, 490 and 520 nm. The results were mixed and demonstrated the extent to which different algorithms are needed in turbid waters.

Dekker *et al.* (1991) showed the value of modelling the underwater light field and photosynthetically available radiation (PAR) using high resolution in-water and airborne spectral data of turbid lakes in the Netherlands. Using the methods described by Kirk (1981a, 1981b), they found that the water masses they were studying were clearly separated by their PAR absorption and scattering coefficients. The components of a complete atmospheric, water surface and subsurface measurement model for aircraft remote sensing of water masses have been established and tested by Guzzi *et al.* (1987) and Zibordi *et al.* (1990).

The need for cost-effective techniques to detect algal blooms and to monitor the widely-distributed waterbodies throughout Western Australia has become an urgent priority. Pattiaratchi *et al.* (1992) and Lavery *et al.* (1993) have shown the potential for the routine use of satellite-derived remotely sensed data for quantitatively measuring chlorophyll concentrations in Peel Inlet and Cockburn Sound. However, these studies were unable to show that speciation in chlorophyll pigments could be determined at the broad-band resolutions of the current satellite systems. Also, problems with cloud cover at satellite overpass times in the Perth area means there is only about a 40 percent probability of clear acquisitions.

It is widely accepted that the spatial extent of visible effects of phytoplankton and chlorophyllous materials can only be measured practically using an appropriate form of narrow-band remotely sensed data. Jupp *et al.* (1992b) in their extensive studies of blue-green algal blooms in Lake Mokoan concluded that the main limitation to using remotely sensed data was a lack of simultaneous in-water and atmospheric measurements. This thesis relies heavily on field spectral measurements, and in-water spectral techniques were developed for this work. The principles and the logistical aspects of field spectral measurement are covered in Milton (1987) and Yamaguchi and Lyon (1985). Jupp *et al.* (1992b) also stress the importance of using a calibrated data set.

Hick *et al.* (1992) compared two airborne multispectral scanners flown a short distance apart over a range of riverine, estuarine, lacustrine and oceanic sites. These sites near Perth and Rottnest Island had total chlorophyll pigment concentrations

ranging from 2μg/l to 800μg/l and showed that strong correlations for total log chlorophyll to optimum scanner band combinations could be achieved in predicting pigment concentrations.

Landsat TM data have been used, at scales compatible with the 30 m resolution, for the delineation of mapping substrate features in shallow coastal waters. A research project in the La Grange area (Hick and Scoones, 1988; Scoones and Hick, 1990) surveyed the distribution of habitat for pearl oysters and prawns in the Broome area. Local studies performed in, or associated with, the CSIRO WA Remote Sensing Group (Lyons, 1976; Hick, 1979; Honey and Byrne, 1978; Young, 1984; Hick *et al.*, 1994) have indicated that the full potential of remotely sensed data for water penetration had not been achieved.

The benefits of satellite data over aerial photographs are that a narrower field-of-view (FOV) reduces the solar-flaring effects, and multiband digital data can mathematically remove the effects of pathlength and surface scatter (Lyzenga, 1978). Satellite data may also have less geometric rectification problems and the archive of TM data, now collected since 1986, has a 16 day repeat cycle.

Surface roughness or wave slope distributions as measured by Cox and Munk (1954; 1956) account for scattering as a function of both wind direction and velocity. This is further complicated if surface foam is present. Koepke (1985) contradicts the assumptions in this area by Wald and Monget (1983). Methods of measuring surface

roughness, and hence facet scattering, have been developed and correlated with measurable parameters such as windspeed, fetch and deep ocean swell records.

Cox and Monk (1954; 1956), Jerlov (1976), Gordon and Jacobs (1977) and many others produced qualitative and quantitative data and models for the effects of surface roughness on bi-directional reflectance. Serious conjecture then appeared in the literature with Koepke (1985) disputing the results of Wald and Monget (1983). Both groups of researchers hinted at angular effects but, as they were principally addressing satellite applications and surface angular effects of wave facets, they did not seriously address the upwelling angular brightness effects that appear in wide-angle airborne imagery invariably captured on "calm" days. Monahan and O'Muircheartaigh (1986) reviewed whitecaps and the passive remote sensing of the ocean surface, especially in the microwave region, and showed the effect of surface temperature on whitecap formation. Since that time little further work has been published in the traditional remote sensing literature and correction of brightness variations, whilst consuming significant research effort for terrestrial imagery, has only a few researchers looking at water problems.

1.4 Research Program

Spaceborne and airborne data were used for a range of projects in the Perth region and the problems encountered in meeting the specifications for these projects provide research examples for the purpose of this thesis. Figure 1.2 shows the locations of all of the study sites from which the examples of research outcomes have been drawn.

Examples from ten separate experiments, including collaborative studies, are used to address those parameters over which some control or modification of practice can have an effect on the successful use for a given purpose of remotely sensed data. Field spectral measurements coupled with simultaneous physical, chemical and biological characteristics, and their relationship with the remotely sensed data, are used to provide a range of examples to support the subsequent recommendations.

To determine the extent of problems associated with surface scattering and procedures for removal or correction, three separate studies are included. These are: the Coastal Waters Experiment, that used airborne scanner data in 1991 for the purpose of habitat mapping; the Peel Inlet experiment that used airborne video data, on a windy day in 1993, as part of a monitoring program to assess the effects of channel construction; and the Swan Estuary Experiment in 1996, that used a spectrometer to determine the surface scattering effects with changing solar angles and variable windspeed.

The determination of water column characteristics has also been included with three sequential experiments that demonstrate the development and application of the technology. These are: firstly in 1990, the initial comparison of the two airborne scanners, flown simultaneously over a range of targets to determine the suitability of multispectral data for quantifying high and low levels of phytoplankton pigments; this was followed by the Swan River Study using an airborne imaging spectrometer in 1992/3 for the detection and quantification of algal blooms; and then in 1994/5, also in the Swan River, by the study using multispectral airborne video which was

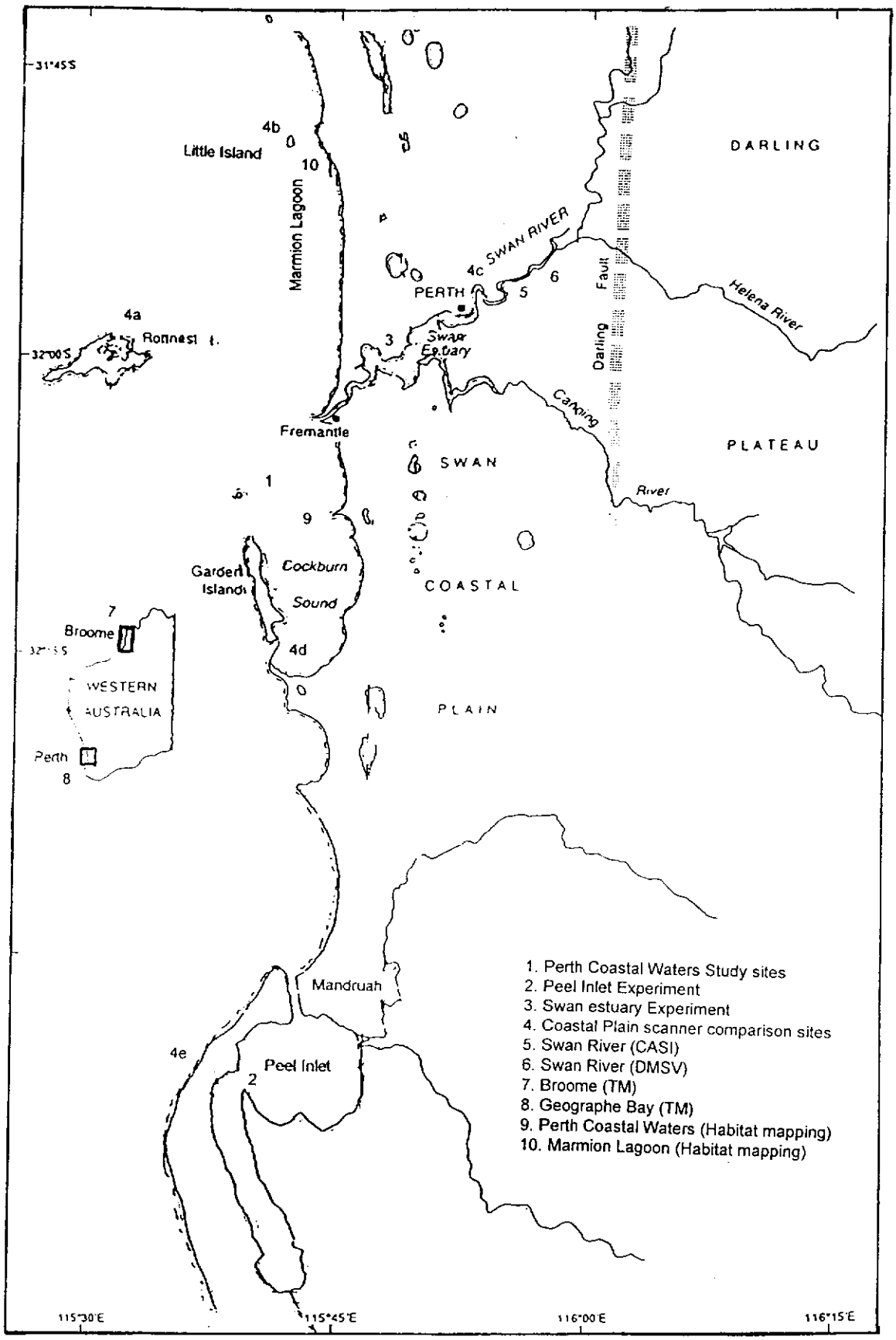

Figure 1.2: Location map of all study sites

designed to determine the operational logistical problems of routine quantitative algal bloom assessment.

The third series of four experiments is included to show and evaluate the use of remotely sensed data to describe the characteristics of the bottom of the water column. These are: the Broome Study which, in 1987/8, used satellite data for evaluation of pearling and prawning grounds; followed by the Geographe Bay study in 1991/2 that also used satellite data to define the acquisition specifications for habitat mapping at depths approaching 50 m; then the Perth Coastal Waters Study in 1990, that used Geoscan data; and finally, the Marmion Lagoon experiment in 1993, that used an airborne spectrometer to separate the spectral signatures of different benthic materials at different depths, also for the purpose of quantitative habitat mapping.

Data acquisition planning for terrestrial targets, such as urban studies, agriculture or forestry, using diagnostic vegetation-related wavebands are usually only constrained by cloud or other static or easily predictable limits. The critical nature of measuring information from the relatively low levels of reflected energy from highly-dynamic surfaces such as oceans, lakes or rivers presents the planner with a different set of problems.

These results are structured to provide a predictive planning capability for the probability of determining:

(i) Atmospheric and solar illumination constraints,

(ii) Surface scattering from prevailing wind and current turbidity conditions,

(iii) Pigment speciation, phenology and concentrations,

(iv) Determination of substrate components and benthic speciation, and

(v) Validity of bathymetric algorithms where multiple scattering affects reflected energy.

Experimental use and application of remotely sensed satellite data from the Kimberley and south-west coastline during the period of 1987-91 and field and airborne measurements made in the Swan River and in the ocean near Perth over the summers of 1992/3, 1993/4 and 1994/5 are included. The raw data and processed imagery provide quantitative correlations of field-measured and remotely-measured cases.

These examples are restricted principally to the visible and the complementary near-reflected infrared regions of the electromagnetic spectrum because this region has historically held, and potentially holds, the greatest chance of providing useable and repeatable information. The potential for "active" instruments such as radar and fluorescence scanners is still in the laboratory stage, and thermal data presents a different range of problems.

1.5 Chapter Arrangement

The first chapter comprises the introduction and an initial literature review.

The second chapter covers some remote sensing principles and the specific details of the remote sensing platforms and spectral instruments that were used for data collection for the experiments and examples given in the thesis.

The third chapter covers the effects on the signal received by a sensor of atmosphere and solar irradiance at water-penetrating wavelengths, surface scattering from, and through, the water skin as a function of bi-directional reflectance and surface roughness. The chapter includes three studies that were undertaken to minimise or correct these effects.

The fourth chapter covers three studies as chronological phases of methodology development for application of remotely sensed data for determining the organic and inorganic water column characteristics, with particular emphasis on phytoplankton and algal blooms.

The fifth chapter concentrates on four studies that demonstrate the capabilities of both satellite and airborne remotely sensed data to provide maximum water penetration for delineation of substrate stratigraphy, and shows the relevance of these findings to fishing, mining and conservation.

The sixth and final chapter summarises the specific outcomes of all the studies and focuses on the practical applicability of the results to setting specifications, acquisition planning, pre- and post-processing and information extraction and delivery.

Chapter 2

REMOTE SENSING OF WATER BODIES

2.1 Electromagnetic Spectrum

Electromagnetic radiation includes a very wide range of energy, from X-rays through visible light to radio waves. One thing that all types have in common is that they can be transmitted through a vacuum, and do not require movement of the molecules of the material through which they travel in the way that sound waves do. Only a portion of the huge electromagnetic spectrum is actually used for remote sensing and even less is of value for describing the characteristics of a water body. The radiation is classified according to its wavelength, from 300 nm in the ultraviolet region up to about 1 m, the longest wavelength used for microwave remote sensing.

The upper and lower limits of the spectrum used for remote sensing are constrained by the physical interactions between the radiation and the materials which make up the Earth's surface. Since remote sensing is concerned with studies of the surface, and immediate sub-surface in a few cases such as water, it is essential that radiation, either from natural sources such as the sun, or from an artificial source, such as an active radar system, be reflected, emitted or scattered back to the sensor in order to make an observation.

When the wavelength of the radiation diminishes to the same order of magnitude as the spacings between the molecules in surface materials, the radiation is not reflected

from the surface but penetrates the material. It may then be diffracted or scattered, but only a small proportion of the incident radiation will ever find its way back to the sensor. This sets the lower limit of radiation useable for remote sensing to the ultraviolet region, although practical considerations actually set the practical limit for most applications at the lower end of the visible light region. The upper limit of the useful portion of the spectrum is set by the necessity to have reasonably detailed imagery of the surface of the Earth. The spectrum is divided into six main sections on practical grounds, influenced strongly by the absorption of large sections of the spectrum by water vapour in the Earth's atmosphere. The useable portions cover so-called "atmospheric windows", wavelengths at which the atmosphere is essentially transparent.

2.1.1 Ultraviolet

The ultraviolet region of the spectrum could be of great interest, but the problem is that atmospheric absorption is very strong at this wavelength, and little ultraviolet radiation from the sun actually reaches the Earth's surface. This is a problem for remote sensing, but an advantage for most living things, which find excessive ultraviolet radiation toxic. Active ultraviolet remote sensing, using ultraviolet lasers on aircraft or helicopter platforms, has been tested for monitoring oil slicks. The fluorescence of oil films on the surface of the sea can assist in the identification of the type and source of the oil. The fluorescence induced by ultraviolet radiation is mainly in the visible portion of the spectrum, less subject to atmospheric absorption.

2.1.2 Visible Wavelengths

These are the wavelengths which are the main focus of this thesis and at which most conventional camera systems operate. The comparative ease with which radiation at these wavelengths can be focussed and detected meant that most of the early spaceborne scanners operated in this region. It is one of the largest atmospheric windows covering the region that is perceived by our unaided eyes, and is the part of the electromagnetic spectrum that is of most importance to water quality studies. This appears a very fortunate coincidence until one realises that the existence of this window is precisely why animal eyes have evolved special sensitivity at these wavelengths. If there were strong atmospheric absorption of the region that we now term the "visible" portion of the spectrum, we might instead "see" in the mid-infrared or even in the thermal portion of the spectrum, and call these the "visible wavelengths".

Visible light is more strongly dispersed by atmospheric haze, dust and pollutants than radiation at infrared wavelengths. This results in a loss of contrast in visible wavelength imagery, low digital values being increased and high values decreased by atmospheric scattering. Despite these limitations, visible wavelength remote sensing is important in many fields.

The fact that visible light penetrates water to an extent dependent on the water purity, and is scattered back by suspended material, whereas radiation at infrared wavelengths is almost totally absorbed by water, makes visible wavelength remote sensing essential for studies of water quality, pollution and coastal bathymetry.

2.1.3 Near Infrared

This region of the spectrum is essentially a continuation of the main visible wavelength atmospheric window, and radiation at these wavelengths behaves in a very similar way to visible light. Hence, it is sometimes referred to as the reflected infrared, and can be focussed by fairly standard optical systems, and recorded by photographic emulsions, unlike the longer wavelengths in the mid-infrared and thermal infrared.

The total amount of electromagnetic energy available at a sensor is greater in this region than in the visible portion, and absorption and scattering by atmospheric pollutants is less. This results in a higher dynamic range for most sensors in the near infrared, and thus a higher signal to noise ratio. Imagery is usually sharp with good contrast especially in land-sea interfaces.

Ratios of radiances in the near infrared to radiances at visible wavelengths are very important in vegetation studies and use has been made of this to detect actively photosynthesising plant material at the water's surface. The almost total absorption of near infrared radiation by water, compared with the scattering of visible light, allows the use of the reflected infrared for accurate discrimination of aquatic vegetation. Coherence of scattering from sunglint and surface foam also make this region important in deterministic algorithms and surface scatter corrections.

2.1.4 Mid-Infrared

The Mid-Infrared, or short-wave infrared, actually includes two "atmospheric windows", one centred at about 1500 nm and the other at 2200 nm, each with its own particular characteristics. The relatively low levels of radiation available at these wavelengths, the fact that this radiation is absorbed by all but the most exotic glasses used in optical systems, the requirement for cooling of detectors operating at these wavelengths in order to maintain acceptable signal to noise ratios, and the almost total absorption by water surfaces have restricted the use of this region to mainly soil and geological applications.

2.1.5 Thermal Infrared

Remote sensing in this region is constrained by similar problems as in the mid-infrared. Conventional optics cannot be used and detectors must be cooled to ensure acceptable noise levels. Development of spaceborne thermal infrared sensors has been driven by the meteorological community, who require accurate measurements of sea surface and cloud top temperatures, and the only operational spaceborne multispectral thermal scanners are the Advanced Very High Resolution Radiometer (AVHRR) on the National Oceanographic and Atmosphere Administration (NOAA) satellites and the Along-Track Scanning Radiometer (ATSR) on the Earth Resources Satellite (ERS)-1, each with one channel in the 3,500 nm window and two in the 10,000 nm region. These sensors are all carefully calibrated and can provide very accurate temperature measurements of homogeneous surfaces. The single thermal band on Landsat Thematic Mapper (TM) is not so well calibrated, and generally gives only qualitative indications of temperature. Some useful applications of airborne

thermal imaging have been used to describe marine and lacustrine processes and detect inputs from thermally different sources.

2.1.6 Microwave

The microwave portion of the spectrum can be rather arbitrarily divided into a series of bands. These subdivisions are historical and derive from aviation, military and civilian radar systems, rather than from remote sensing of the type that is considered here. In general, the short wavelengths are most strongly absorbed by natural materials, especially water, while the longer wavelengths penetrate further into soils and overburden, especially if they are dry. Microwave emissions, or brightness temperatures, have been studied extensively to determine sea-state, as sea foam emissions (white-caps) have been able to predict ocean surface wind fields.

2.2 Reflectance from a Waterbody

The total reflected energy received at the sensor is shown in Figure 2.1. The sum of energy upwelling from the water surface, scattered back from the surface and back from the atmosphere is the recorded signal. Atmospheric back-scatter varies as a function of wavelength. In-water spectral measurements are designed to provide, as a function of wavelength, four factors.

(i) Total water-leaving radiance,

(ii) Radiance from the surface,

(iii) Radiance from the column, and

(iv) Radiance from the bottom.

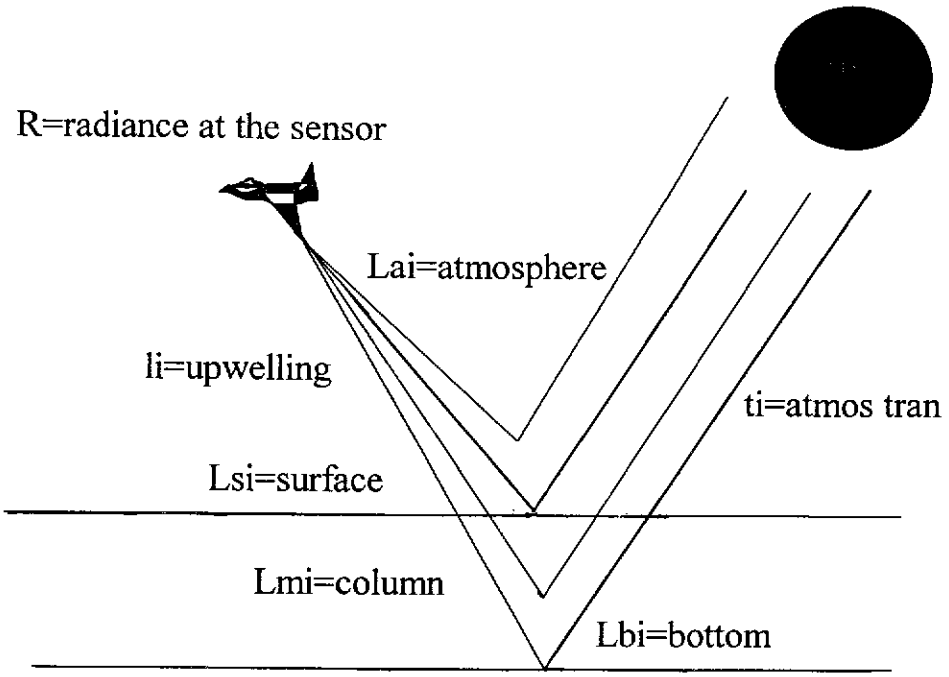

Figure 2.1: Solar energy paths for remote sensing over water.

2.2.1 Water-leaving or Upwelling Radiance

The basic models for radiance R, the measured energy recorded at the sensor, for waveband i, may be resolved into components involving the atmosphere and radiation leaving the water surface such that:

$$R = ti\,(Li + Lsi) + Lai \qquad (2.1)$$

where:

R is radiance recorded at the sensor,

ti is total atmospheric transmittance,

Li is radiance from the water column,

Lsi is radiance returning from the water surface, and

Lai is radiance scattered into the sensor field of view by the atmosphere.

Radiation emerging from the water column Li includes effects of depth, sea floor type and particulates in the water column. In cloud-free imagery, of the type usually selected for this work, assumptions may have to be made that ti, Lai and the reflected component of Lsi are uniform across the image. If this is not the case, where sun angles produce "sun glint", and solar azimuth and elevation give across-track illumination variation, correction may need to be applied to Li and Lsi for some scenes. Corrections to Lai, the atmospheric component, may be possible by using other wavebands.

Li has constituent components which need further consideration. These may be suspended sediments, dissolved substances or chlorophyll-based material in the water column, or the textural components of the sea floor. Li can be measured with a radiometer at the sea-surface and calibrated against a Lambertian standard. Lsi can then be crudely derived by radiometric samples above and below the ocean surface skin.

2.2.2 Penetration of Light into Water or Attenuation Coefficients

The penetration of light into water is defined for remote sensing purposes as the depth above which 90 percent of the diffusely reflected irradiance (excluding specular reflectance) originates. Gordon and McCluney (1975) showed that for a homogeneous ocean this is the depth at which the downwelling in-water irradiance falls to 1/e of its value at the surface. Following is a simple water reflectance model which accounts for most of the signal received for a given band over clear shallow water but neglects the effects of scattering in the column and at the water surface.

$$Li = Lsi + ki\ Lbi \exp(-Ki\ f\ D) \qquad (2.2)$$

where for band i,

Lsi is the radiance of deep water,

ki is a constant for solar irradiance, atmospheric transmittance and surface refraction,

Lbi is bottom radiance,

Ki is the attenuation coefficient of the water for band (i),

f is the geometric factor for pathlength, and

D is depth.

Lyzenga (1981) offered a single index for substrate radiance based on a log ratio of two bands xi/xj plotted on an axis, with variability of substrate being a function of distance from the axis. Beirwirth *et al.* (1993) used another approach to derive substrate reflectance and depth in the same algorithm. They used the multispectral data and water attenuation coefficients to produce images of bottom reflectance and depth.

It is important to understand the limitations of remote sensing of the ocean floor. This thesis examines these limitations and discusses the methods which need to be considered in the context of spectral band selection, atmospheric scattering, water column transmission, the nature of bottom materials and data processing techniques.

2.2.3 Bottom Contribution

The next consideration, which is vitally important for studies that focus on substrate stratigraphy and habitat mapping, is to separate from the water-leaving radiance Li, the bottom component Lbi, from the scattering and absorption by materials in the water column. This can be done with the use of in-water spectral measurements as reported by Jernakoff and Hick (1994).

A very good general approximation suggested by Jupp (1988) is based on Equations 2.1 and 2.2. Using the same symbolic terms describes the way water properties, substrate reflectance and water depth affect resultant signal. Here

$$Li = \exp(-2\, ki\, D) \qquad (2.3)$$

where:

ki is the effective attenuation coefficient of the water mass, and

D is depth below the water surface.

Li and Lsi are affected by solar elevation. Illumination increases with solar altitude but so does the surface backscatter and sunglint component Lsi. Surface roughness or spatial reflecting facets can significantly reduce the usefulness of image data.

The bathymetric determinations based on some linear relationship of shallow ocean depth and reflected solar energy from the ocean bottom were defined by Doak *et al.* (1980) and the model is given here:

$$D = -1 / 2 (ki - kj) \ln (band\ j - Vsj)\ Voi / (band\ i - Vsi)\ Voj \qquad (2.4)$$

where:

D is known depth

ki is water attenuation for band i

kj is water attenuation for band j

Vsi is deep water signal for band i

Voi is limiting signal as depth nears zero

2.2.4 Separation of Components

The approach to be taken for the measurement of above- and in-water spectra is determined on the basis of the following basic models for radiance R, the measured energy recorded at the sensor at waveband i, that may again be resolved into components involving the atmosphere and radiation leaving the water surface such that:

$$Ri = ti\ (Li + Lsi) + Lai \qquad (2.5)$$

The above-water measurement of radiation emerging from the water column Li includes effects of depth, bottom type and particulates in the water column, as well as the reflected component Lsi. In the case where sun angles produce "sun glint" or "ripple-flaring", correction may need to be applied to Li and Lsi.

Li has constituent components which need further consideration. These may be suspended solids, such as sediments, dissolved substances or chlorophyll-based material in the water column, or the textural components of the bottom. Li is

measured either against a Lambertian standard or, as is the case with the Irricrop multispectral radiometer (MSR), against a measure of irradiance ti + Lai = tmi from the upward-pointing diffuser. Lsi is then derived, in a crude form, by spectral sampling above and below the water's surface skin. This may be modelled as follows:

$$Li = tmi\ (Lbi + (1\text{-}tmi))\ Lmi \qquad (2.6)$$

where:

Li is the measurable radiance from the water column,

tmi is the effective transmittance,

Lbi is the radiance from the substrate material, and

Lmi is the radiance of deep water.

As may occur when tmi varies between 0 and 1, Li varies between Lmi and Lbi, i.e. deep water to no water cover at all, or in the case in the Swan River to date, where Lbi and Lmi are low or zero.

2.2.5 Signal-to-Noise Ratios

Signal-to-noise ratios are not generally a problem with conventional applications of satellite data. However, for in-water related image processing, where instrument quantisation values for target materials are often of the order of ±5 or less, processing is aimed at the maximum information retrieval. The enhancement is limited by the radiometric resolution of the sensors, and the signal to noise ratio SNR can introduce image degradation that would be unacceptable for most terrestrial applications.

However, for qualitative interpretation of linear or reasonably homogeneous patterns a lower than normal SNR is often acceptable.

2.3 Data Sources

Airborne data used in the study have been acquired from the Compact Airborne Spectrographic Imager (CASI), SpecTerra Digital Multi-Spectral Video (DMSV), Geoscan Mk2 Airborne Multi-Spectral Scanner (AMSS) and the Ocean Colour Scanner (OCS). Satellite data from Landsat TM and Satellite Pour l'Observation de la Terre (SPOT) have also been used. Field spectral measurements are from modified Exotech 4-band Radiometers, Irricrop Cropscan MSR and the recently developed Ocean Optics miniature spectrometer (Jernakoff and Hick, 1994).

2.3.1 Compact Airborne Spectrographic Imager (CASI)

The CASI was brought to Australia from Canada by COSSA, and was flown over a range of sites in February 1993. Some of the sites had simultaneous spectral, physical and chemical ground-truthing of the surface, water column and substrate for both marine and estuarine targets.

The CASI can be flown in one of two modes (Babey and Anger, 1989). In spatial mode up to 15 full image bands between approximately 400-900 nm can be acquired across a field of view of 35 degrees. In spectral mode, 288 contiguous bands covering the same wavelength range, are recorded for 39 evenly-spaced picture elements for the same field of view. It was flown in a Britten-Norman Islander aircraft in which was installed a gyroscope, to record aircraft roll, a Global Positioning System (GPS) and an optical drift-site for site location.

The flight lines were flown in both spectral and spatial modes, over four days (15 to 18 February 1993) with simultaneous spectral measurements of the water column and Lambertian targets with an underwater spectral radiometer. Several of the lines were repeated with different solar geometry and wind conditions for the purpose of complementary research for this study.

2.3.2 Digital Multi Spectral Video (DMSV)

The DMSV is built by SpecTerra Systems (STS) in Perth. It is four bore-sighted Charge-Couple Device (CCD) array cameras with selectable narrow (25 nm) band-pass filters centred at 450 nm (blue), 550 nm (green), 650 nm (red) and 770 nm (infrared) usually fitted. The image is "frame-grabbed" in 8-bit quantisation and has a similar geometric specification to aerial photography. A four band image comprises 740 x 578 picture elements each representing about 2 m when flown at 3,000 m above the target. Data from this instrument are used in this study to demonstrate many aspects of the research and application to "operational" routine management practices.

2.3.3 Geoscan Airborne Multi-Spectral Scanner

The Geoscan Airborne Multi-Spectral Scanner (Mk2) is a 46 channel instrument which can simultaneously record up to 24 bands of information in the visible, reflected, and thermal infrared regions. Of use for water studies are band 1 (482-514 nm), band 2 (534-585 nm), band 3 (588-653 nm), band 4 (680-703 nm) and band 5 (703-726 nm) (Hick *et. al.*, 1992). Much early work with this instrument provided examples of the limitations of using airborne systems for aquatic studies.

The Geoscan scanner has an instantaneous field of view (IFOV) of 3.0 mrad and a field of view (FOV) of 90 degrees. Data collected for the Perth Coastal Waters Study, parts of which are included in this thesis, were flown at 3,000 m, giving a pixel resolution of 10 m, and a swath width of 6 km. Each raw scan-line data record comprises 768 pixels. The data are digitised into 8 bits, with gain and offset automatically adjusted and recorded prior to data acquisition. Variations in aircraft roll, pitch and yaw are corrected by "sample-timing" for roll, and by an inertially-stabilised integral mount for pitch and yaw.

2.3.4 Ocean Colour Scanner

The CSIRO OCS is a nine channel, rotating mirror instrument with bands in the visible and near-infrared regions (380-980 nm). The OCS was designed to be flown in the CSIRO research aircraft, a Fokker F27 (VH-CAT), at an altitude of 3,000 m giving an approximate scan width of 6 km. An IFOV of 4 mrad gives a nominal 10 m spatial resolution on a 600 pixel-wide, roll-corrected path. Inertial navigation system (INS) data are fed into the 12 bit data stream, which in turn is stored on Exabyte tapes.

2.3.5 Landsat Thematic Mapper

The Landsat TM instrument has six wavebands with a ground resolution of 30 m in the reflected channels and a thermal band. With a 9.30 AM local acquisition time and a repeat cycle of sixteen days, TM gives scene areas in excess of 30,000 sq. km. The position of TM band 1 (450-520 nm) is ideally situated to avoid atmospheric absorption and permit maximum measurement of water-leaving upwelling radiance. The other water-penetrating band of some use in the TM instrument, band 2 (520-600

nm), can provide information on water column characteristics, and any of the infrared bands can help to delineate the dry land/water interface.

The Thematic Mapper detector arrays have across-track, multi-line mirror systems which may not be identically calibrated. These can produce horizontal striping in the data. Algorithms which sample entire rows or columns and then apply a mean-average correction can remove much of the striping caused by detector arrays without significant data degradation.

2.3.6 SPOT

Data from the French SPOT satellite offer some significant opportunities for use in water studies. SPOT data are available in multispectral mode with three bands (500-600 nm), (600-700 nm) and (700-800 nm) at 20 m nominal ground resolution, and in panchromatic mode with a single band (500-800 nm) with a 10 m nominal ground resolution. SPOT's local time acquisition is an hour later than TM and this can sometimes compensate for the reduced water-penetrating capabilities of the SPOT band choice (500-600 nm for SPOT versus 450-520 nm for TM).

2.4 Field Spectral Measurements

Spectral measurements, taken from boats and jetties, are of the total upwelling radiance, surface scattering, particulate scattering and transmission through the waterbody. As mentioned earlier, these may be from suspended solids, such as sediments, dissolved substances or chlorophyll-based material in the water column, or the textural components of the bottom. Li is measured either against a Lambertian standard or as is the case with the Irricrop against a simultaneous measure of

irradiance ti + Lai = tmi from the upward-pointing diffuser. Lsi is then derived, in a crude form, by spectral sampling above and below the water's surface.

The instruments used to measure these components have been the New Zealand-manufactured Department of Scientific and Industrial Research (DSIR) 8-band radiometer, the Irricrop Cropscan MSR and a triple configuration of 1024-element spectrometers based on the Ocean Optics ST1000 spectrometer.

2.4.1 DSIR Radiometer

The DSIR Mk2, Eight Channel Radiometer has narrow bands centred at 440 nm (band width 12.5 nm), 480 nm (9.5), 520 nm (10.5), 560 nm (9.5), 620 nm (10.8), 670 nm (11.5), 780 nm (11.7) and 860 nm (10.7) and a field of view of 20 degrees. From these eight channels, an interpolation of a reflectance curve is possible. For the in-water spectral measurements, a water-tight radiometer housing with a clear perspex viewing window is mounted astern of the boat in a suspension frame. This enables the radiometer within the housing to be pointed upward, with a diffuse filter, or downward for calculation of radiance or irradiance. The radiometer is suspended from a boom, clear of the boat, to reduce the effect of shadowing or reflectance from the boat hull, and spectral measurements are made just above the surface, and with the radiometer housing centred at 1 and 2 m below the surface.

2.4.2 Irricrop Multi-Spectral Radiometer

The Irricrop Technologies "Cropscan" radiometer uses simultaneously a combination of eight upward (diffuse) and eight downward (15 deg FOV) detectors with nominal band-centres at 450, 500, 550, 600, 650, 700, 750 and 800 nm. The specially-adapted

underwater housing is suspended from the boom, ensuring that during measurements the instruments remain stable in the water column pointing directly upward/ downward. The radiometers are connected via a waterproof cable to a laptop computer on a boat. Readings are made under full sun with a sun angle generally less than 45 degrees with cloudless skies and away from any shade generated by the boat. Spectral measurements are made just above the surface, at the surface, and with the radiometer housing centred at 1 and 2 m below the surface.

2.4.3 Ocean Optics Spectrometer

This miniature fibre-optic solid-state instrument measures high resolution spectra (1024 wavelengths) using holographic diffraction gratings in the reflected ultraviolet, visible and near-infrared. It can be coupled directly to a portable computer to display and record both target and reference spectra. A choice of optical fibre diameters and collecting optics can provide the opportunity to resolve either absorption or reflectance spectra to 2 nm from a narrow or diffuse field-of-view. The silicon detector can measure between 350-1000 nm and, with the quartz detector, fluorescence can be measured in the range 220-440 nm.

This instrument was initially developed for laboratory or workbench applications but adaptations to the basic instrument for specific applications in this thesis made this a versatile and flexible option. To take advantage of this capability required the development of underwater sensor heads, spectrally compatible plumbing and optical fibre configurations. The use of this integrated system, coupled to GPS in a moving boat or moored in fixed sampling point was developed. The simplicity of connecting

the optical fibre to any optical device and simultaneously measure incoming or sourced energy and target radiance made this instrument useful for real-time optical water-quality research applications, bloom type detection and concentration, and monitoring and management strategies.

2.5 Summary

The physical constraints to extraction of useable information from a remote platform can be addressed if the issues of illumination, scattering and signal processing are well understood. It can be assumed that these aspects have been considered by sensor and instrument designers because the evolution of routinely available systems, such as the Landsat TM sensor, and specific task systems, such as airborne scanners, are being matched by the development of highly sensitive field validation instruments, such as the Ocean Optics spectrometer.

It is indeed fortunate that this range of instruments was available for trial application and evaluation at a time when the requirement and demand for knowledge of the coastal and marine environment is high. However, there is no doubt that the next generation of sensors will have greater spectral, spatial and temporal capabilities. Despite this, the range of instruments from satellites, aircraft and for field measurement was entirely adequate to satisfy the objectives of this research.

The following three chapters are intended to show that very useful information can be gained from remotely sensed data about the constituents of the water column, if appropriate consideration is made for atmospheric and surface scattering, and field

validation. It will also be shown that corrections can be applied to data that will significantly improve the value of the information, if the basic guidelines to acquisition are followed. These relate to an understanding of the question, or questions, that are being asked of the data. These questions must take account of the physical and biological conditions of the surrogate signal recorded at the sensor that is being interpreted as quantitative information.

Consideration of appropriate spatial, i.e. minimum scale resolvable features, as well as spectral, i.e. the detectable diagnostic "colour" of those features, and temporal, i.e. the time that those features are of maximum contrast to background materials, is essential. The following ten experiments are designed to demonstrate the importance of these considerations.

Chapter 3

DETERMINATION OF SURFACE SCATTERING EFFECTS

3.1 Introduction

Images of the same area, acquired on different dates, may have very different radiance values received by the sensor. This can be caused by differences in solar illumination, depending on the time of day or year, differences in atmospheric scattering and absorption, or by changes in up-welling radiance at the surface of the area to be studied. The latter is almost always the one for which remote sensing seeks to retrieve information in studies of multi-date imagery. However, in some circumstances investigators might wish to use remote sensing to monitor atmospheric pollution, and might correct for solar elevation and surface-state to arrive at a measure of atmospheric scattering and absorption.

Radiometric correction to compensate for sun elevation differences between image dates and for differences in sensor calibration is an essential precursor to the detection of change. By a comparison of reflectance values this is a relatively easy process. Since most earth-observation satellites pass over each point on the earth at roughly the same local sun time, solar illumination variations are mainly a function of the season. The solar elevation and azimuth at the time of image acquisition are normally recorded in the header of the digital image, and it is a relatively simple matter to adjust the digital values of a series of images to a constant solar elevation, so that all images appear to have been acquired at the same time of year. If the

scanner has a relatively narrow angle of view, then solar illumination can be assumed to be constant across the whole of the image. A simple correction for solar illumination is based on the fact that illumination varies with the cosine of the solar elevation angle, and imagery can thus be corrected for an arbitrarily fixed elevation.

Often band ratios can eliminate much of the effect of solar elevation. With some airborne scanners, e.g. the Geoscan and CASI, and for imagery from meteorological satellites, radiometric correction is more complicated. The wide scan angle of these systems leads to significant solar elevation differences, or differences in the angles between the sun and sensor across the width of the image, and these may require compensation prior to any quantitative analysis. In its simplest form, the correction is an arithmetic one, based on a simple model of the scanner geometry, although more precise correction may require incorporation of bi-directional reflectance. These radiometric corrections can remove differences caused by solar elevation and because of the relative positions of pixels within broad scan swaths.

3.1.1 Atmospheric Correction

Atmospheric correction is a greater problem, and there are a range of techniques of varying complexity to achieve this. Kneizys *et al.* (1983), and subsequent upgrades of their Lowtran and Modtran software codes, offer interactive capability to correct for the effects of variable atmosphere. It is fortunate that atmospheric effects in terrestrial applications are usually relatively minor in comparison with solar elevation effects, and some remote sensing can be carried out without the need for atmospheric

correction. However, the removal of atmospheric effects from visible wavelength data over water is very important.

Atmospheric effects can contribute most of the signal reaching a sensor over water, especially at wavelengths that penetrate water, and this is caused by a complex mixture of scattering and absorption by gases, aerosols and solids. A common approach is the "darkest pixel" method, where the water-leaving radiance in the near infrared is assumed to be zero, and the signal received at the satellite is entirely from atmospheric effects. The effects of air molecule scattering can be calculated and removed, leaving the radiance produced from aerosol scattering. It is then possible to produce ratios relating the effects of aerosol scattering in the near infrared to the aerosol scattering at other wavelengths, and thus to remove atmospheric effects from visible wavelength data. The corrected radiance values can then be related to physical properties, such as concentrations of chlorophyll and sediments in the water.

3.1.2 Image Brightness Variation Caused by Wind-fields

The action of wind creates wave facets that increase the reflective region as a function of wave face angle to the sun and the sensor. Obvious brightness variation is apparent when the still water surface is acting as a reflector and returning an image of the sun to the sensor. This should rarely happen in well planned acquisitions. Increasing wind speed increases the facet angles and as a consequence the proportion of an imaged area affected by "sunglint" also increases. At wind velocities above about 25 km/hr surface waves begin to break causing two major effects. The first is the increased albedo of the breaking wave and the subsequent foam and bubble-

stream and, secondly, in shallow nearshore situations, sediments and biological material may be resuspended and/or mixed throughout the water column also increasing albedo and shifting spectral maxima.

3.1.3 Bi-directional Reflectance from Wide Field-of-View Sensors

Imagery obtained over land from aircraft, both with aerial photography and "frame-grabbed" video images, has brightness variations that must be considered. The same effects are theoretically affecting imagery over water. Steps can be taken to minimise these effects at the mission planning stage and by post-processing of the data. On terrestrial imagery they are caused mainly by three things. These are scattering by particles and aerosols in the atmosphere, bi-directional reflectance and sensor optical geometry.

Added to these, when imaging water, is the effect of sunglint, or solar flaring, which is the reflection of the sun into the field of view of the sensor. In the case of a "flat" water body, ie. without any surface waves or ripples, the effect on the image is theoretically confined to a single spot, which can be avoided by selective acquisition at times when solar elevations are less than the field of view of the sensor. Because the sun is the source of energy for illumination of the target it stands to reason that the best signal to noise ratio obtained by the sensor will be at the highest possible solar elevations. The effects of surface roughness or wave facets increase the region around the solar reflection spot and the extent of intrusion into the field of view is, as mentioned earlier, a function of windspeed.

3.1.4 Hot-spots

The brightness variation, called the "hot-spot", presents problems which must be addressed on imagery that includes land and water targets. In cases such as river monitoring, where runs of calibrated images are to be joined in a mosaic on a regular time frame for temporal comparisons, this effect must be removed. It is caused on the image at the point on the ground in line with the aircraft and the sun, and at its centre the shadow of the aircraft can sometimes be seen. This point of the image has the potential to provide maximum information from the water column but causes processing problems for terrestrial targets. This is because the maximum image brightness appears concentrically around that point, as there is no visible shadow from vegetation or particulate structure (backscatter only). As the distance away from the point increases, so does the amount of visible shadow in the image (forward and multiple scattering) causing reduced total reflectance.

3.1.5 Correction Procedures

The most common method of removing the effect of image brightness variation relies on calculating an average brightness surface from a sequence of frames in the flight line (the more the better, preferably over deep water and on a constant or reciprocal bearing and attitude), and subtracting that mean (usually smoothed) surface from the image. Other methods need to be used if multiple uniform frames are not available. These may be based on band-ratios (Hick *et al.*, 1994), or on empirical corrections that account for solar elevation and azimuth and for flight direction (Pickup *et al.*, 1993).

Rayleigh scattering causes brightness variation in images and varies with particles in the atmosphere and as a function of pathlength and wavelength. This is clearly shown in the example in Figure 3.1, which graphs the across-track brightness from calibrated airborne imaging spectrometer data with a scan angle of 35 degrees (Hick *et al.*, 1994), over a smooth water target, above the inversion layer, on a day that had considerable visible haze. The six wavelengths chosen for the figure are representative of the bands that were being considered for use in an airborne multi-spectral video system.

Pickup *et al.* (1993) indicate that a single equation, based on view angle, can be used for brightness normalisation as a function of wavelength for each image. Their findings show that this produces better results than the commonly-used band ratio techniques. Figure 3.1 is a good example of wavelength-dependant scattering brightness effects across a scanned image of deep ocean. These data have been extracted from the video-based Compact Airborne Spectrographic Imager, and show the effect of Rayleigh scattering at the shorter (blue) wavelengths as compared with the significantly reduced effect at the longer wavelengths.

However, Pickup *et al.* (1993) seem to be at variance with King (1991) who, in his analysis of video data, showed that where the linear trends were consistent in all bands, simple band ratios were an effective means of reducing brightness variations caused by view angle. Pickup *et al.* (1993) produced contingency coefficients for an overlap area on two adjacent images which had different brightness values caused by view angle.

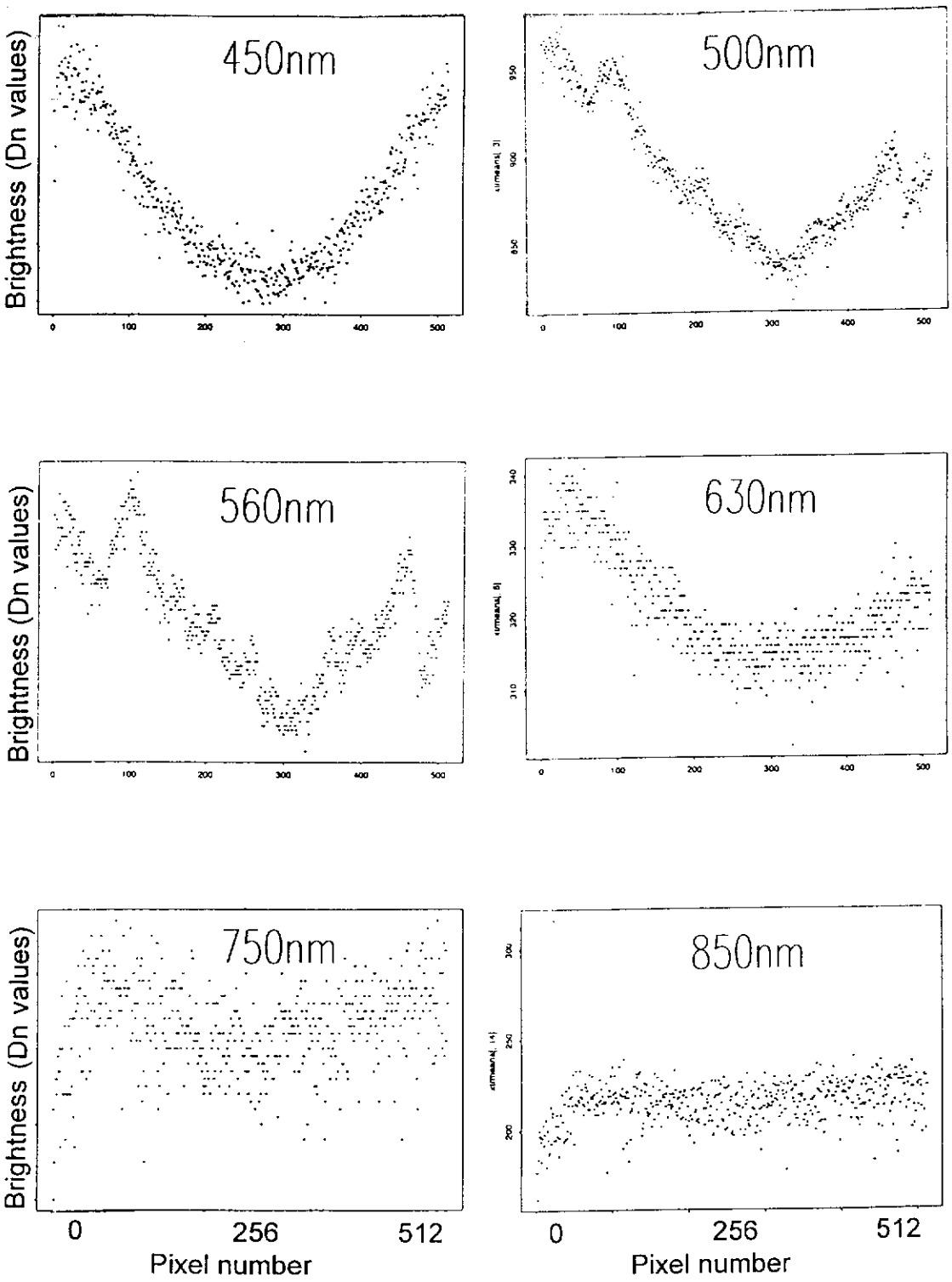

Figure 3.1: Across-track brightness from calibrated airborne imaging spectrometer

The following three examples show the extent of the problems of scene brightness variation and the approaches that were adopted to quantify and solve these effects. The first project was planned to provide information on the coastal waters near Perth, but only the aspects that relate to the correction of scene brightness are discussed here, with the results of the habitat mapping being reported in Chapter 5. Because of the size of the area to be acquired, it was realised that the acquisition time-span would present a significant scene brightness correction problem despite the best possible control of flight planning. The second experiment demonstrated the removal of facet and wave effects from video frames, and the third experiment in this chapter characterised the spectral effects of surface scattering.

3.2 Coastal Waters Experiment

3.2.1 Background and Aims

The metropolitan coastline of Perth, Western Australia, is used extensively for industrial, commercial and recreational purposes. With approximately 70 percent of the State's population (1.7 million) living within 20 km of the metropolitan coastline, these waters are arguably the most valuable part of Western Australia's 10,000 km of coast. In 1991, the State Government initiated complementary studies by the Department of Environmental Protection (DEP) and the Water Authority of Western Australia (WAWA) into the cumulative impacts of waste inputs, particularly nutrients, to Perth's coastal waters (Simpson *et al.*, 1993).

Protection of the coastal waters off Perth requires information on key habitats. Inventory and baseline surveys of some of these areas were required, which included

a need to accurately map the main benthic habitats as a reference for quantifying future habitat changes.

3.2.2 Methodology

On 12 February 1993, between 0900 and 1000 hrs the Geoscan Airborne Multi-Spectral Scanner was flown over the entire study area, well north of Little Island, south to Mandurah, and offshore to the 30 m bathymetric contour, including Rottnest Island, part of which is included in the experimental scene brightness correction for this thesis (Figure 3.2). The instrument, installed in a Cessna 404, was flown at 16,000 ft (4,800 m) giving a nominal pixel resolution of 10 m and a swath width of 10 km. Sixteen spectral bands in the visible, near infra-red and thermal infra-red were recorded with the gains and offsets being adjusted for water penetration and a tan θ (angular sampling function) correction for panoramic distortions. In ideal conditions in Perth's coastal waters, the Geoscan bands 1 (482-514 nm), 2 (534-585 nm) and 3 (588-653 nm) are capable of penetrating water to depths of 25, 18 and 6 m respectively (Jupp, 1988).

Optimal conditions for acquiring maximum information from Geoscan data generally occur in these waters during the quiescent period around the summer equinox (February to April). In the present study the following criteria were defined as acceptable conditions to acquire data: solar elevation between 35 and 50 degrees (maximum illumination with minimum solar flaring); sea swell less than 1m; windspeed less than 10 knots; low haze; cloud cover less than five percent.

However, despite the flexibility for timing of the flight, an un-forecast wind-shift during the flight produced surface scattering effects in some parts of the raw image.

Four control targets were deployed from vessels during the flight period in areas that were considered to have insufficient features for spatial rectification purposes. These

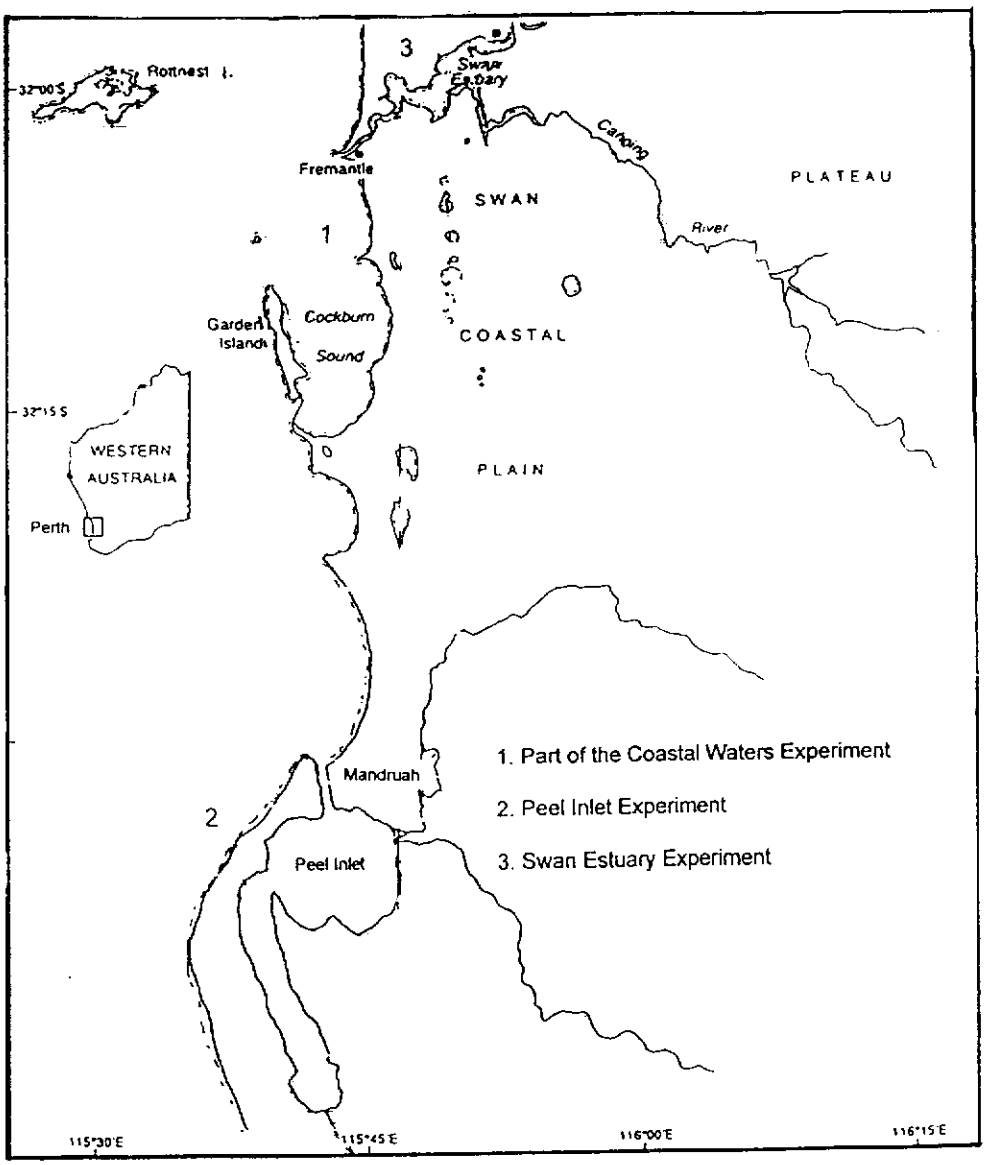

Figure 3.2: Study location for Geoscan and DMSV data acquisition

targets were fixed using both differential GPS and traditional survey triangulation from shore-based theodolites.

The scanner image was registered to a SPOT panchromatic (10 m) satellite image that was acquired on 22 January 1993, and had been registered to the Australian Map Grid (AMG). The tessellation technique of Craig and Green (1987) was used to rectify the Geoscan images to an accuracy of ± 20 m using a SPOT panchromatic image as a map base. Digital bathymetric data were also incorporated into the image to assist the separation of habitat types. The areas were mapped as silt, sand with sparse seagrass, seagrass meadows, coarse sand and subtidal reef.

The flightlines, which followed the general north-south direction of the coast, contained a proportion of sun-glint caused by specular reflection from the sea surface. This was the dominant influence affecting the eastern end of each scan line. Specular reflections from long-period swell waves also caused interference on some parts of the image.

3.2.3 Results

3.2.3.1 Brightness correction using band ratios

Rayleigh scattering resulted in systematic across track effects in the shorter wavelength Geoscan bands, especially bands 1 and 2, where higher digital counts were recorded as the scan angle increased, giving longer atmospheric pathlengths. Hick *et al.* (1992) showed that correction of illumination effects is possible by using ratios between visible and near-infrared bands. This technique was tried but it was

not possible to remove the across track illumination effects on this dataset. The result of this technique was suitable to identify offshore control points for spatial rectification of the image but the image was not suitable for the purpose of habitat classification.

3.2.3.2 Brightness correction using across-track modelling

A two-stage correction procedure was developed to remove across-track illumination and wave facet effects. The first stage involved calculating the combined effect of Rayleigh scattering and specular reflection effects. This was done by extracting data for 50 rows by 1024 columns of deep (over 30 m) ocean which contained no detectable bottom features. Figure 3.3 shows the curve of column means of this sample for band 1and includes the solar flaring, the steep rise on the right hand side of the graph, and the wave facet effects, being the perturbations on the line. The product of the subtraction of this model from the image data is an image free of across-track illumination effects but containing wave facet effects. This was smoothed by fitting a moving average filter (using a window of 60 pixels) combined with a cubic polynomial over the area of greatest curvature. The resulting smoothed curve was then subtracted from band 1 of the raw image. Figure 3.4 is the curve of column means after the first stage correction.

In the second stage correction, it was assumed that the infrared bands have no water penetration capabilities but have similar wave facet contributions. The removal of wave facet effects was performed by regressing the visible bands 1 (460-525 nm) and 2 (525-580 nm) against the infrared band 7 (750-800 nm) over an area of deep ocean.

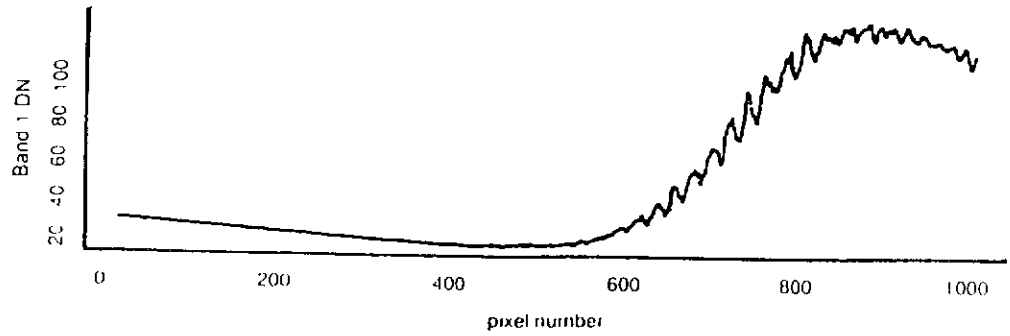

Figure 3.3: Curve of column means for band 1 of Geoscan data

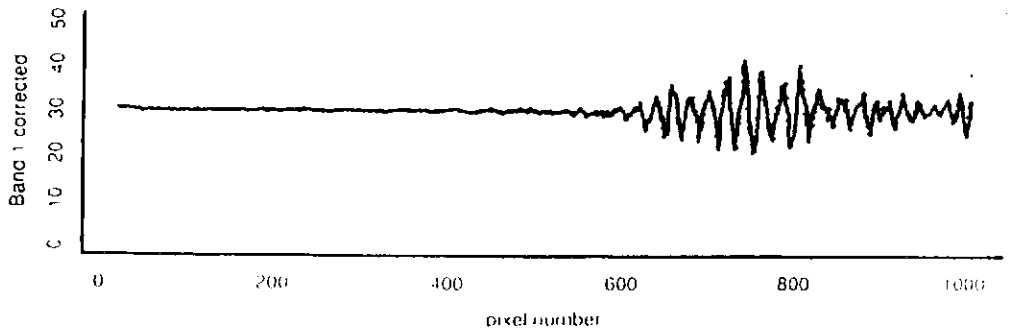

Figure 3.4: Curve of column means after first stage correction

The resulting image was subtracted from the across-track free image. The residual is an image with all visibly detectable across-track and wave facet effects removed to within the level of instrument noise and rendering the data acceptable for use in training for classifications.

3.2.4 Conclusions

As mentioned earlier, the specific outcomes of the habitat mapping are more relevant to Chapter 5 where they are covered in detail. However, the imagery that resulted from these correction procedures, of which Figure 3.5 is an example, had the multiple effects of scene brightness variation caused by atmosphere, solar geometry

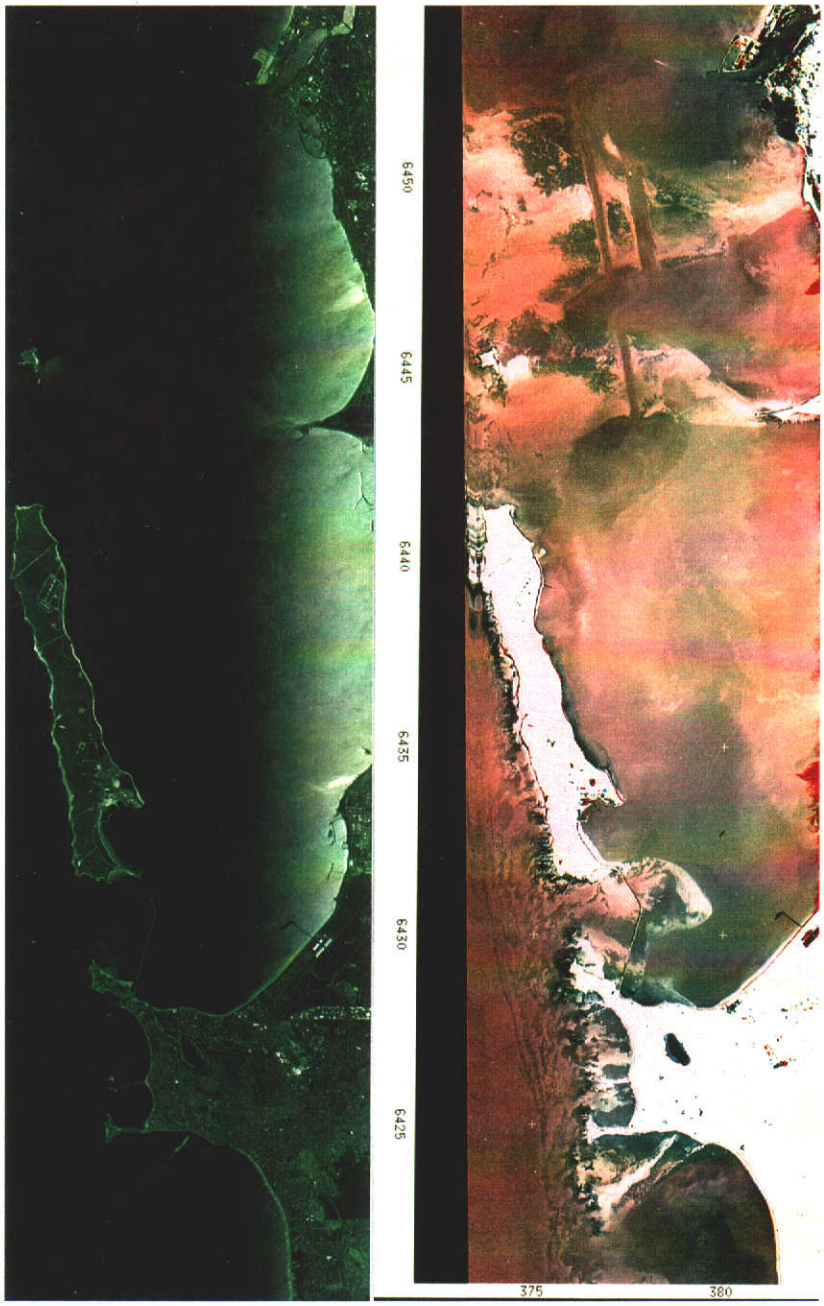

(a) Raw colour composite (b) Processed data

Figure 3.5: Part of Geoscan data for Coastal Waters study

and surface scattering removed to an extent that permitted a supervised classification to be applied. This indicated that traditional multi-band techniques for removing the effects of depth from the image were inappropriate, in contrast with the findings of Bierwirth *et al.* (1993). Consequently, the approach adopted in this study to classify benthic habitats used a combination of spectral information and water depth, after the combined effects of surface scattering had been removed from the raw data.

This example also shows the dilemma that faces this sort of high-resolution habitat mapping requirement. The wide scan angle of systems, such as Geoscan, have limitations of flying altitude and speed for economical area coverage. This is further compounded with the large data sets and changing solar and meteorological conditions between the commencement and completion of data acquisition.

3.3 Peel Inlet Experiment

3.3.1 Background and Aims

Despite the best possible attempts at selecting acquisition parameters to minimise surface effects and maximise signal from either the bottom or the water column, some imagery requires processing before the maximum information content is revealed. DMSV data, acquired for benthic habitat mapping in the Peel Inlet, near Mandurah (see Figure 3.2), had wave facet scattering that obscured useful information It was argued that the benthic flora in the vicinity of a new access channel could change from estuarine to more marine macro-phytic assemblages. Remotely sensed data were proposed as a spatially quantitative strategy for monitoring the effects of a 3 km channel that was cut between the Inlet and the

ocean to improve flushing of the eutrophic system. The issues of the competing influences on the Peel System are well covered in Hodgkin and Birch (1984).

This experiment developed and tested a novel approach to remove complicating effects of the surface-scattered component of total upwelling radiance caused by wave facet effects that were similar to the spatial resolution of the sensor. Monahan and O'Muircheartaigh (1986) showed that the albedo of a "white-cap" is about ten times brighter than the adjacent sea surface. This differential was the basis of the theoretical correction to be developed.

3.3.2 Methodology

The data were acquired at a nominal 2 m resolution, and close inspection of the wave effects show that most of the bright, or saturated pixels, are single wave faces usually only seriously affecting individual pixels. This would obviously change where the waves were larger (leaving larger bubble-streams) or the spatial resolution of the sensor was smaller, requiring a different composition of the kernel.

The method used to remove this effect is a modified scene-dependent smoothing algorithm based on a kernel of 3 x 3 pixels. Signal to noise calculations were made for a part of the scene in deep water that was not affected by significant facet brightness in the opposite corner of the image and in the overlap areas of adjoining scenes. The SNR ratio will change between different datasets and is dependent to a large extent on the conditions of the day and the configuration of the instrument to optimise signal. With knowledge of the expected variability within the 3 x 3, 5 x 5

or other kernel sizes chosen, it is then possible to choose a brightness differential to select and remove the bright pixels caused by the wave facets.

3.3.3 Results

Figure 3.6 shows raw DMSV data that were acquired over part of the Peel Inlet, near Mandurah. Figure 3.7 is the same DMSV scene that has been processed with a 3 x 3 kernel using a brightness differential of two digital counts. This means that when the central pixel of the kernel is greater than two digital counts from the average of the surrounding eight pixels it is reset to the average. This value may be altered for individual bands, or have a maximum cut-off also included. This is important if control, such as geolocation marker buoys or small boats gathering reference data, are not to be lost from the data.

Figure 3.8 is the same scene with a three digital count differential and yet still shows the sampling boat in the lower left hand side of the image. The selection of the value of the centre pixel differential is an iterative process. Considering that the albedo of a "white-cap" is about ten times brighter than the adjacent sea surface, these values seem conservative. The best solution will be related to the spatial resolution of the instrument, and the area of the surface that is affected by the white-cap.

3.3.4 Conclusions

The use of specifically-weighted kernels is not new for cleaning noisy data for terrestrial purposes and the technique is shown to work in some instances in Chapter 5 for exaggerating linear features of marine substrate stratigraphy. However, here,

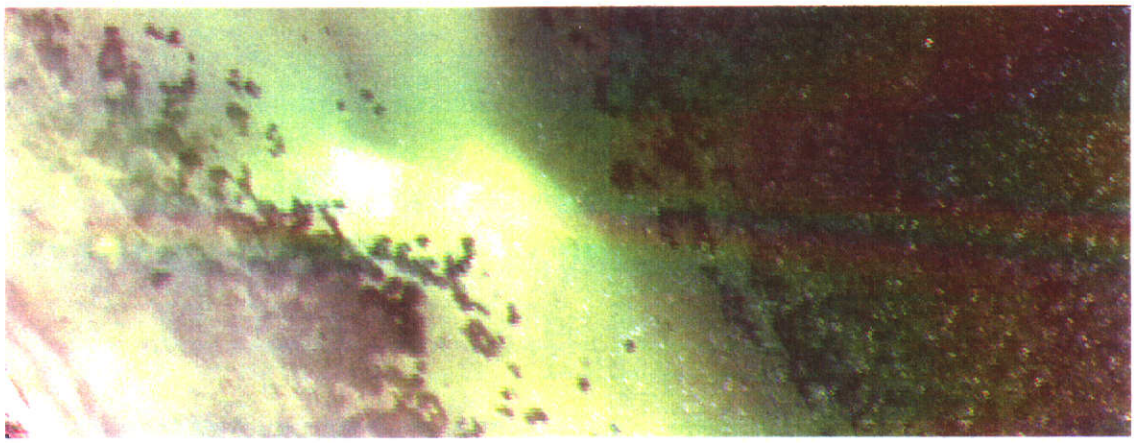

Figure 3.6: Raw DMSV data acquired over part of Peel Inlet

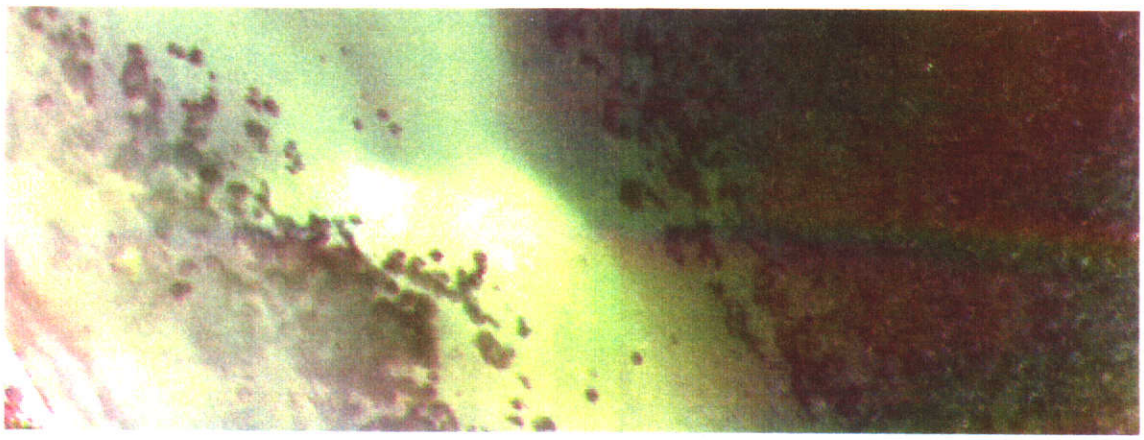

Figure 3.7: DMSV scene processed using 3 x 3 kernel

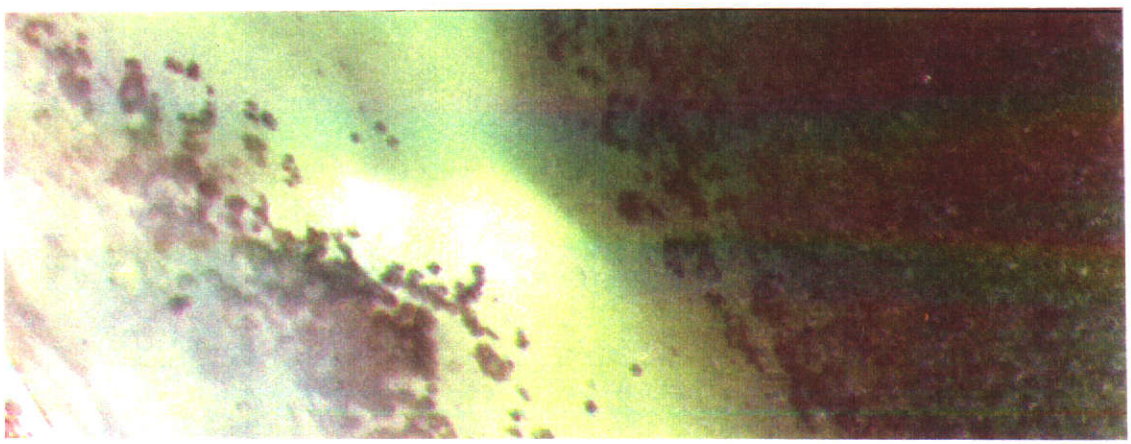

Figure 3.8: DMSV scene processed with three digital count differential

the visual appearance, and hence the ability to interpret visually or with some form of supervised automatic classifier, is substantially improved using this technique.

Normally, in shallow water situations, the presence of whitecaps is also an indication that there is a high probability that particulates from the bottom may be re-suspended causing increased turbidity. Usually data acquisition would be curtailed in such conditions. However, the use of this technique as a surface scattering correction procedure appears to be novel and very effective. The technique adds no new data, but improves the visual and automated interpretability of the imagery to a point that, when used with other scene brightness corrections, makes creating a seamless mosaic of DMSV images possible.

3.4 Swan Estuary Experiment

3.4.1 Background and Aims

An experiment was designed to measure the effect of view angle, solar angle and windspeed on total upwelling radiance. The time chosen to conduct the experiment was to be close to the autumnal equinox because the probability of the range of solar angles, occurring at times of the day when the windspeed range would be likely, was thought to be high. The windspeed range had to reach velocities that would cause the appearance of whitecaps, or wave-induced reflective foam. This occurs at wind-speeds greater than 7 m/sec (25 km/hr). (See Gordon and Jacobs (1977) and later work on the remote sensing signatures of whitecaps by Koepke (1985)).

The experiment was designed to measure spectral characteristics under three conditions:

(i) The effect of look-angle (between ± 30 degrees),

(ii) The effect of solar-angle (between 20-45 degrees), and

(iii) The effect of wind-speed (between 0-30 km/hr, 0-8 m/sec).

3.4.2 Methodology

The Ocean Optics Spectrometer was attached to a boom that was then secured to a specially designed tripod head that could swivel to pre-determined angles. This spectrometer uses an optical fibre to deliver light energy to the holographic diffraction grating and a spectrum is produced instantly and recorded in digital millivolts. This configuration permits a certain amount of data selectivity as the individual spectra are displayed and accepted or rejected. This is done to remove the occasional spectrum that is contaminated by a direct "sun-flash" that may saturate the detector at the chosen integration time. With careful selective operation one standard deviation of the replicated spectra was controlled to be less than 50 millivolts or about five percent of range.

The system was deployed for a day at the starting-box at Perth Flying Squadron Yacht Club on the area known as Melville Water in the Swan River estuary, see Figure 3.2. The location was ideal, as the site was on the north-eastern end of a jetty 7 m above the water. Fetch was in excess of 4 km to the east and 3 km to the south and south-west. The water depth is in excess of 6 m and the organic bottom means that probably little or none of the upwelling radiance was derived from the bottom.

3.4.3 Results

Eventually, such a cloud-free day, with the expected wind conditions, was forecast on the 29 March 1996 and measurements commenced at 0900 hrs through to 1500 hrs. Temperature ranged from 18.2 to 22 degrees Celcius and relative humidity from 62 to 52 percent throughout the day. Calm wind conditions (0-5 km/hr from the east) prevailed until the arrival of the south-westerly sea-breeze around midday (peaking at 30 km/hr mid-afternoon).

The river was not subject to a high background level of phytoplankton, although algal blooms do occur in this section of the estuary, and on this day the integrated cell count was less than 500 cells/ ml and dissolved oxygen 91 to 95 percent. Secchi extinction ranged from 1.8 to 2.2 m during the day. The salinity was in the range 3.78 to 3.80 percent.

3.4.3.1 Effect of look-angle and solar angle

The effect of look-angle produced a predictable result, although there was some evidence that an effect similar to the hot-spot effect on terrestrial imagery was evident on a small, and not readily-repeatable number of replicates, despite the changing solar elevation changes. If backscatter from suspended particulates contributes to the upwelling signal it should be maximum at the solar hot-spot position.

Figure 3.9 shows the mean spectra between 360-850 nm for 10 replicates for the angle range 30 and 15 degrees toward the sun, vertical, and 15 and 30 degrees away

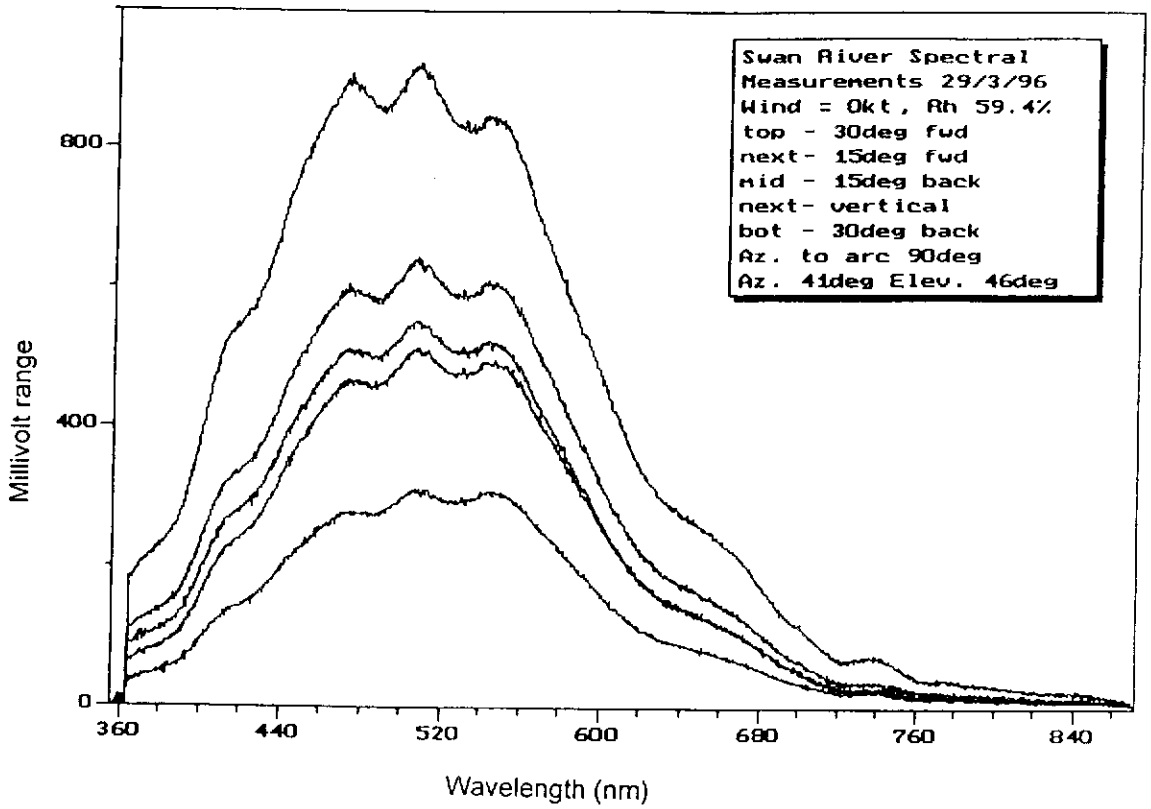

Figure 3.9: Spectra from Swan River at varying sun angles

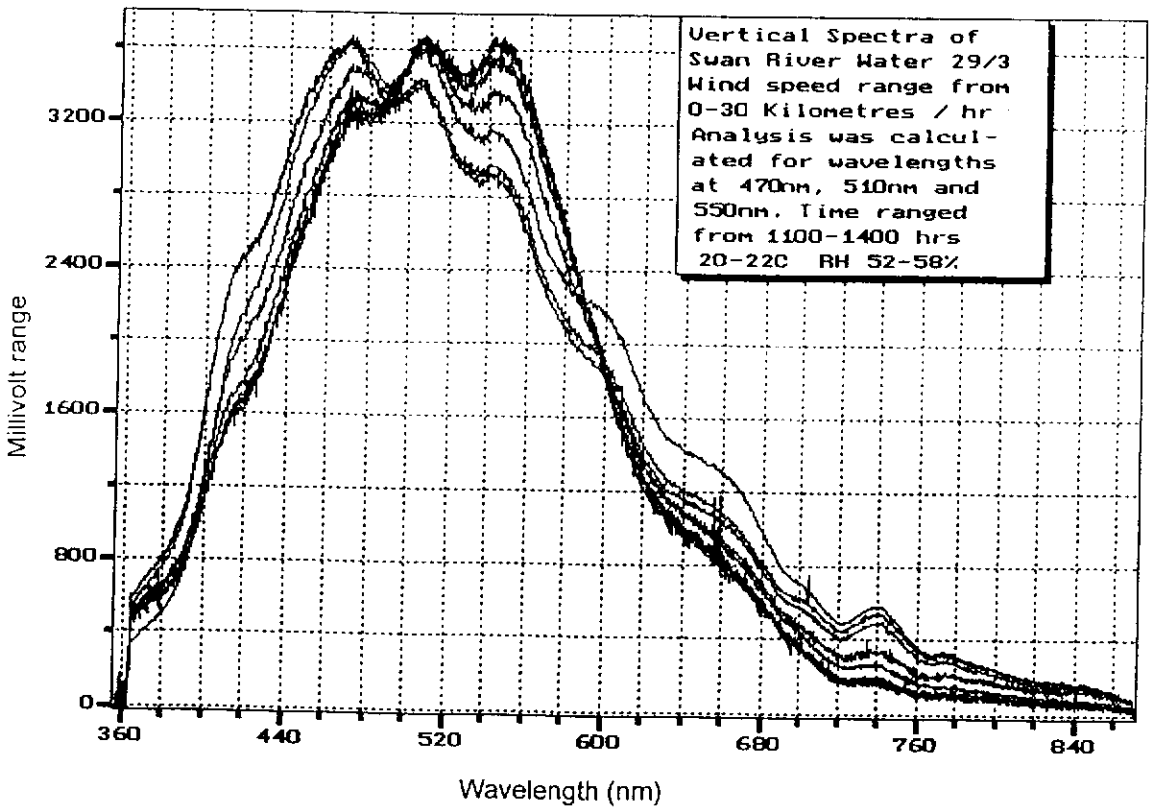

Figure 3.10: Vertical spectra of Swan River water at a range of wind-speeds

from the sun's azimuth. Although variability was high because of the effects of facet reflectance, the results remained consistent throughout the range of solar elevations (20 to 46 degrees). Of particular interest is the higher than expected average spectrum for the 15 degrees away from the sun. This spectrum in some measurements during the morning was equal to, or greater than, the vertical measurement but was subject to the greatest variability. Standard deviation at the maximum peak of the 10 replicates of each spectrum was calculated and some spectra that were obviously affected by random flaring, or sun flashes, were omitted.

If backscatter from suspended particulates contributes to the upwelling signal, it should be maximum at the solar hot-spot position. This interesting, but inconclusive, result should be further investigated in a structured experiment, with more precise control over the particulate and phytoplankton levels and covering a range of view and illumination angles. The implications for brightness correction procedures is significant as most procedures currently used ignore this aspect.

3.4.3.2 Effect of windspeed

The windspeed aspect is demonstrated in Figure 3.10 and shows a series of characteristic water spectra with peaks between 450 and 550 nm. These raw spectra were measured over the day for a wind speed range of 0-30 km/hr (0-8 m/sec). They were normalised to a common base to account for different solar illumination.

Then, for ease of analysis, data were extracted for the visible part of the spectrum approximately at the blue to green/yellow region where, in the first three

wavelengths, maximum variation occurred, and at a point of minimum separation . The wavelengths were at 470 nm (blue/green), 510 nm (dark green) 550 nm (green) and 600 nm (yellow). Figure 3.11 shows three graphs giving the average spectral response of the vertical measurement at a range of wind-speeds at the first three wavelengths. Interpretation of the graphs shows an increase in total upwelling radiance at the mid-wind strengths at 470 nm. Conversely at 510 nm a decrease is shown at the same wind strengths. This maybe supported at 550 nm but by 600 nm no difference is detectable.

3.4.4 Conclusions

This experiment confirms most of the common assumptions relating to the importance of considering environmental conditions at the time of acquisition of remotely sensed data over water. Reflectance from the surface varies as a function of surface scatter and solar angle to the point where the surface acts as a reflector, returning most of the solar irradiance back to the sensor. Maximum upwelling signal from the column is controlled by the same general geometry as terrestrial targets, especially when the column contains particulates contributing to backscattering of light. Maximum useable signal is controlled by these two factors and hence dictates the optimum window for acquisition.

3.5 Summary

This chapter covered the effects on the signal received by a sensor of the atmosphere and solar irradiance at water-penetrating wavelengths, and surface scattering from, and through, the water skin as a function of bi-directional reflectance and surface roughness. It includes three studies undertaken to minimise or correct these effects.

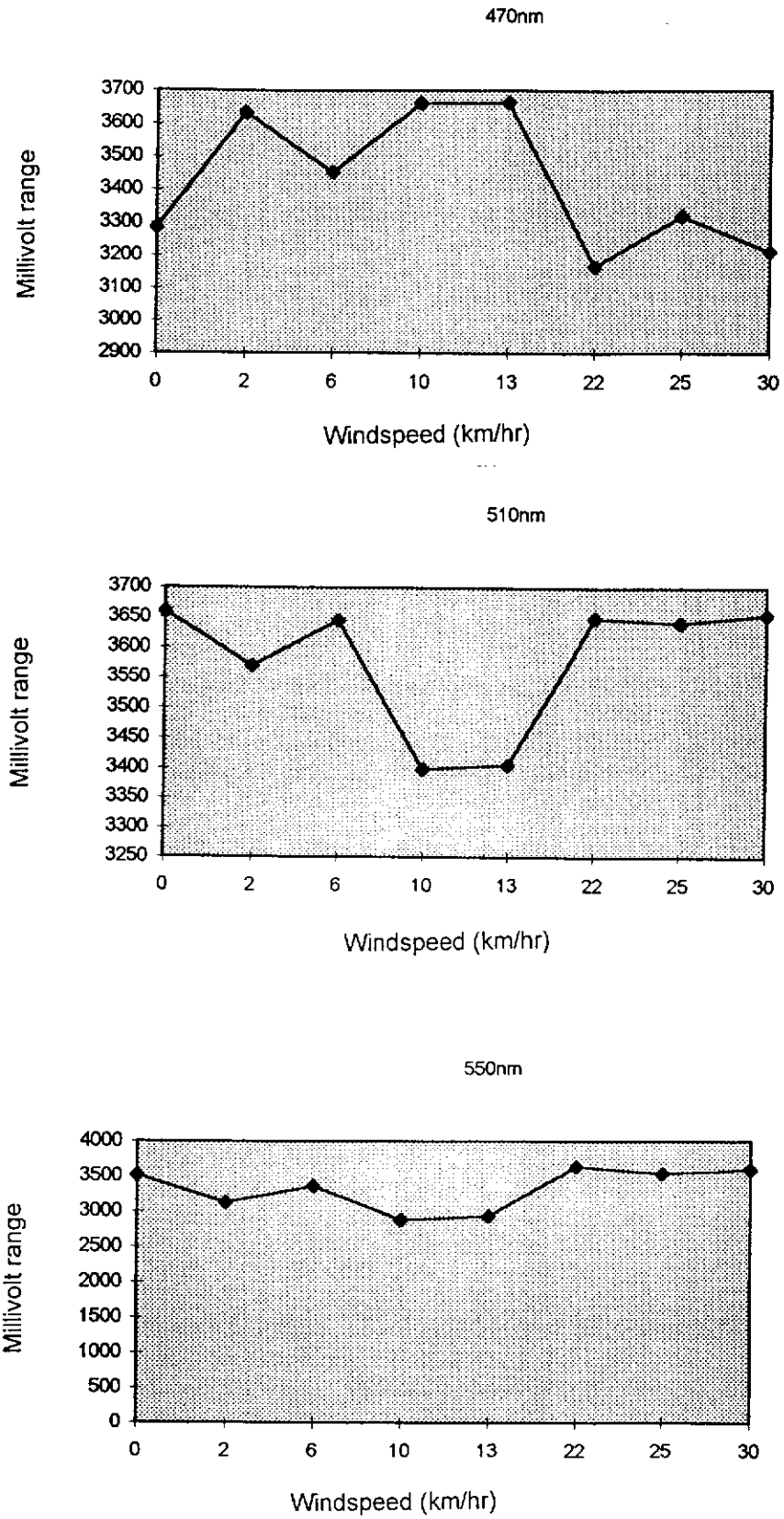

Figure 3.11: Relative upwelling radiance as a function of wind-speed

The effect of look-angle, or FOV, of an instrument is a trade-off between acquisition economics and data quality. As shown earlier in the chapter, instruments, such as the Geoscan with a 90 degree FOV, create major correction problems. However, it was demonstrated that it is possible to use wide FOV instruments and still obtain reasonably good results.

The results of the Swan River experiment indicate that data begin to vary significantly at ± 15 degrees, so instruments such as the DMSV with a 37 degree FOV (accounting for frame overlap) are a sound compromise between efficient acquisition and data quality. Obviously satellite systems, such as TM and SPOT, have a good specification for FOV-related problems.

Similar consideration must be given to solar elevation, as this is also a trade-off between the benefits of better illumination of what is a very low reflectance target, against surface scatter back into the FOV of the instrument. This is further complicated by increases in facet scattering caused by increasing windspeed. The Peel Inlet experiment offered a partial solution for data with a contribution of scattering from white-caps. However, the most significant losses of data are usually from saturation of the instrument detectors, which in most modern airborne instruments have good low-energy sensitivity characteristics.

Therefore the calculation of flight directions and acquisition windows for marine targets should be conservative. Data collection should err toward windless

conditions with lower solar elevations, or increase the overlap (hence the acquisition overheads) in frame-grabbing instruments, or sidelap in scanning systems.

Chapter 4

DETERMINATION OF WATER COLUMN CHARACTERISTICS

4.1 Introduction

It is widely accepted that the spatial extent of visible effects of phytoplankton and chlorophyllous materials can only be measured practically using an appropriate form of remotely sensed data. The need for cost-effective techniques to detect algal blooms and to monitor the widely-distributed waterbodies throughout Western Australia has become an urgent priority. Carpenter and Carpenter (1983), Lillesand *et al.* (1983), Verdin (1985), Dwivedi and Narain (1987) all demonstrated the use of remotely sensed data for measuring water quality. Pattiaratchi *et al.* (1990) and Lavery *et al.* (1993) have shown the potential for the routine use of satellite-derived data for quantitatively measuring chlorophyll concentrations in Western Australian coastal waters.

However, those studies also showed that speciation in chlorophyll pigments could not be determined at the broad-band resolutions of the current satellite systems, and that problems with cloud cover at satellite overpass times in the Perth area means there is only about a 40 percent probability of clear acquisitions. However, Hick *et al.* (1992) when comparing two airborne multispectral-scanners showed that if using optimum scanner band combinations pigment concentrations could be predicted. Jupp *et al.* (1992a) in their extensive studies of blue-green algae blooms in Lake Mokoan concluded that the main limitation to using remotely sensed data was a lack

of simultaneous in-water and atmospheric measurements. They also stressed the importance of using a calibrated data set.

4.1.1 Phytoplankton (plants in the water column)

The organic components of the water column that are of specific interest to this study fall in the division of the plant kingdom group *Thallophyta* which may be unicellular or multicellular. Further subdivision of thallophytes on the basis of presence or absence of chlorophyll and the photosynthetic thallophytes are called *algae*. Fortunately for remote sensing studies of algae, the earliest classifications of algal types were based on colour, which in turn depends on the sort of pigments the cells contain. Other important biological characters, particularly the details of the flagella and cell structure, show that algae of like-structure usually share like-pigmentation and the classification on the basis of colour is still usually acceptable and very relevant to study by remote sensing.

4.1.1.1 Euglenophyta

These algae mostly live in fresh water and are unicellular organisms that show a combination of plant and animal-like characteristics. They have about 25 genera containing about 450 species.

4.1.1.2 Chlorophyta

The Chlorophytes, or green algae, are generally regarded as the group from which higher plants arose. The majority of green algae live in fresh water but there are many marine species. They have many divergent evolutionary tendencies, all beginning with walled and flagellated unicellular organisms. Chlorophyta may range

from motile colonies, to non-motile unicells, to extensive tubelike bodies with numerous nuclei, to multicellular filaments and even three-dimension leaf-like thalluses. A common representative occurring in the Swan river system is the green algae *Chlamydomonas,* which is a unicellular species common in fresh and brackish water and has a single large chloroplast that fills up to two-thirds of the basal area of the cell. Inside the chloroplast are numerous chlorophyll-bearing lamella which are the same as those found in terrestrial plants and include chlorophyll *a* and *b*. They also include the carotenoid pigment.

4.1.1.3 Chrysophyta

Most species in the three groups of algae placed in the chrysophytes (yellow-green and golden-brown algae and diatoms) are various shades of yellow or brown caused by a dominance of carotenoids. However, the diatoms have significant structural differences to the yellow-green and the golden brown algae. Most of the yellow-green and golden brown algae live in fresh or brackish water with only a few marine species, but diatoms are abundant in both fresh and marine habitats where with their silica-rich walls play an important role in the food-web.

4.1.1.4 Pyrrophyta

The Pyrrophytes, or dinoflagellates, are small, usually unicellular, organisms composed largely of cellulose. Photosynthetic species usually have a yellowish-green to brown pigmentation from the abundance of carotenoids, some of which are unique to these organisms. Dinoflagellates are second only to the diatoms as primary producers of organic matter in the marine environment and they bloom in the Swan River system annually. Some species can produce light and are responsible for much

of the luminescence seen in water at night. Some species produce toxins which are poisonous and some species contain a red pigment which when blooming produce the "so-called" red tides that can result in major fish-kills.

4.1.1.5 Phaeophyta

The brown algae, Phaeophyta, are almost exclusively marine and include the brown seaweeds and are always multi-cellular. Like all photosynthetic plants Phaeophyta possess chlorophyll *a*. However, they have chlorophyll *c* instead of chlorophyll *b* found in the euglenoids and the green algae. Large amounts of xanthophyll carotenoid, called fucoxanthin, gives this algae its brownish colour.

4.1.2 Remote Sensing of Algal Pigments

The relationship of remotely sensed data, in the visible-wavelength regions, to chlorophyll-related pigments in water, is well-established. The work reported in this thesis occurred in three distinct sequential phases between 1990 and 1995, and represents the evolving availability of airborne instruments to enable the transfer of the technology from the research arena to the practical application of routine monitoring strategies.

Airborne systems have several advantages over satellites. These include the ability to schedule flights to coincide with optimal weather or bloom conditions, to focus on particular dynamic regions and to choose spatial and spectral parameters. However, there are also disadvantages, such as geometrical scene-brightness variation and platform instability. Navigation errors can also cause problems for mosaicking images between flight lines. Normally the area covered during a flight is smaller

than that from satellites and, therefore, is generally more expensive per unit area. Airborne systems are usually much less expensive than traditional boat-based sampling to cover similar sized areas.

The first experiment reported here compared two airborne multispectral-scanners flown a short distance apart over a range of riverine, estuarine, lacustrine and oceanic sites, which had total chlorophyll pigment concentrations ranging from 2µg/l to 800µg/l. The scanners compared were the CSIRO Ocean Colour Scanner and the Geoscan Mk2 Airborne Multispectral Scanner.

The second experiment was planned to coincide with an algal bloom using data from the Canadian-built Compact Airborne Spectrographic Imager. It was flown in both spectral (288 bands x 39 lines) and spatial (14 bands x 512 lines) modes over the Swan River.

The third experiment describes the potential of airborne digital videography for routine algal bloom monitoring and was flown intensively over three days during a bloom event. The instrument used for this study is the four-channel Digital Multi-Spectral Video, constructed in Western Australia by SpecTerra Systems Pty Ltd.

4.2 Swan-Coastal OCS-Geoscan Comparison

Both instruments are capable of determining the distribution of chlorophyll-related pigments, and the most useful spectral bands are in overlapping wavebands of the two instruments. The use of ratios to eliminate cross-track factors enables between-

band comparisons that relate to reflectance maxima and absorptions of total chlorophyll concentrations. In the analysis, the sites were grouped into high- and low-chlorophyll "case" waters indicating that band selection is dependant on the expected concentrations. The signal-to-noise determinations were based on variance over a range of uniform targets and in each case fell below the test-bench figures, although both instruments gave acceptable imagery.

4.2.1 Background and Aims

The opportunity to compare two airborne multispectral-scanners was taken in October 1990 because at this time of the year the rainfall-induced nutrient inputs into the river, lakes, estuaries and ocean are greatest near Perth. The two scanners were the CSIRO Ocean Colour Scanner (OCS) and the Geoscan Mk2 Airborne Multispectral Scanner. The aims of the study were to compare the relative merits of the systems in near-simultaneous airborne missions coinciding with reference data sampling at 48 sites, 35 of which included water sampling sites, within the scanned paths.

4.2.1.1 Background studies

Previous collaborative studies, Pattiaratchi *et al.* (1990) and Lavery *et al.* (1993), showed the potential for the routine use of satellite-derived remotely sensed data for quantitatively measuring chlorophyll concentrations in aquatic systems in W.A. However, these studies also showed that speciation in chlorophyll pigments could not be determined at the broad-band resolutions of the current satellite systems. This project was therefore designed to evaluate the relative merits of airborne multispectral scanning systems.

Chlorophyll-related pigments, in deep or dark-bottomed water bodies, provide reliable indicators of nutrient enrichment or eutrophication from various physical and chemical inputs. These pigments, present in aquatic plants, are responsible for photosynthesis and have very specific spectral absorption features. However, an important aspect of shallow-water remote sensing is the extraction and characterisation of the reflectance contributions relating to the water medium itself. For low concentrations of chlorophyll (less than $10\mu g/m^3$), Smith and Baker (1981) showed an impressive universal model that accounts for a wide variety of aquatic conditions. In shallow waters the applicability of this model is limited, or unknown, in cases where:

(i) The chlorophyll concentration is high,

(ii) Phytoplankton speciation is critical,

(iii) Suspended or organic materials are in high concentrations, or

(iv) The reflectance from the bottom materials contribute significantly to the remotely-measured signal (O'Neill *et al.*, 1987).

Harding *et al.* (1992) reported the increased use of airborne scanners to remotely sense chlorophyll pigments in clear "case one" oceanic waters, although less attention had been paid to the higher concentration estuarine "case two" waters (Clark, 1981). The broad wavebands of satellite systems, such as the Coastal Zone Color Scanner and Landsat TM, have proven their usefulness for determining oceanic chlorophyll-related pigments (Smith and Baker, 1981; Gordon and Morel, 1983). However, temporal, spatial and perceived spectral limitations of satellite data indicated that airborne systems may provide useful detection and monitoring

capabilities for a wide range of concentrations (Lavery *et al.*, 1993; Anthony *et al.*, 1991).

Recent developments in image rectification techniques now indicate that reliable geolocation of scanner images, using Dirichlet tessellation, can be performed (Wallace *et al.*, 1991). This problem has long been recognised as a limitation to the use of airborne scanner data for routine monitoring (Craig and Green, 1987).

The wide-angle geometry of airborne scanners, especially for data gathering over water bodies, invariably becomes a trade-off between maximising incident radiation and problems of surface backscatter, or sunglint, on the imagery. Calculation of "at scanner" reflectance from radiance counts using standardised targets and correlation with chlorophyll levels can enable direct comparisons of the instruments.

4.2.1.2 Study location

Perth, the capital city of Western Australia (Figure 4.1), is situated on the Swan Coastal Plain which comprises a complex stratification of fluvial, from the weathering of the crystalline Archaean rocks of the Darling Ranges, and eolian sedimentary and marine deposits, derived from Recent epochs of progradation and transgression (MacArthur and Bettenay, 1960). The Plain is crossed by the Swan River which forms the Swan Estuary before joining the Indian Ocean at the port town of Fremantle. The river drains a large part of the Western Australian agricultural region and hence carries a high nutrient loading which encourages the formation of toxic algal blooms. The many lakes and wetlands, which have formed on the coastal

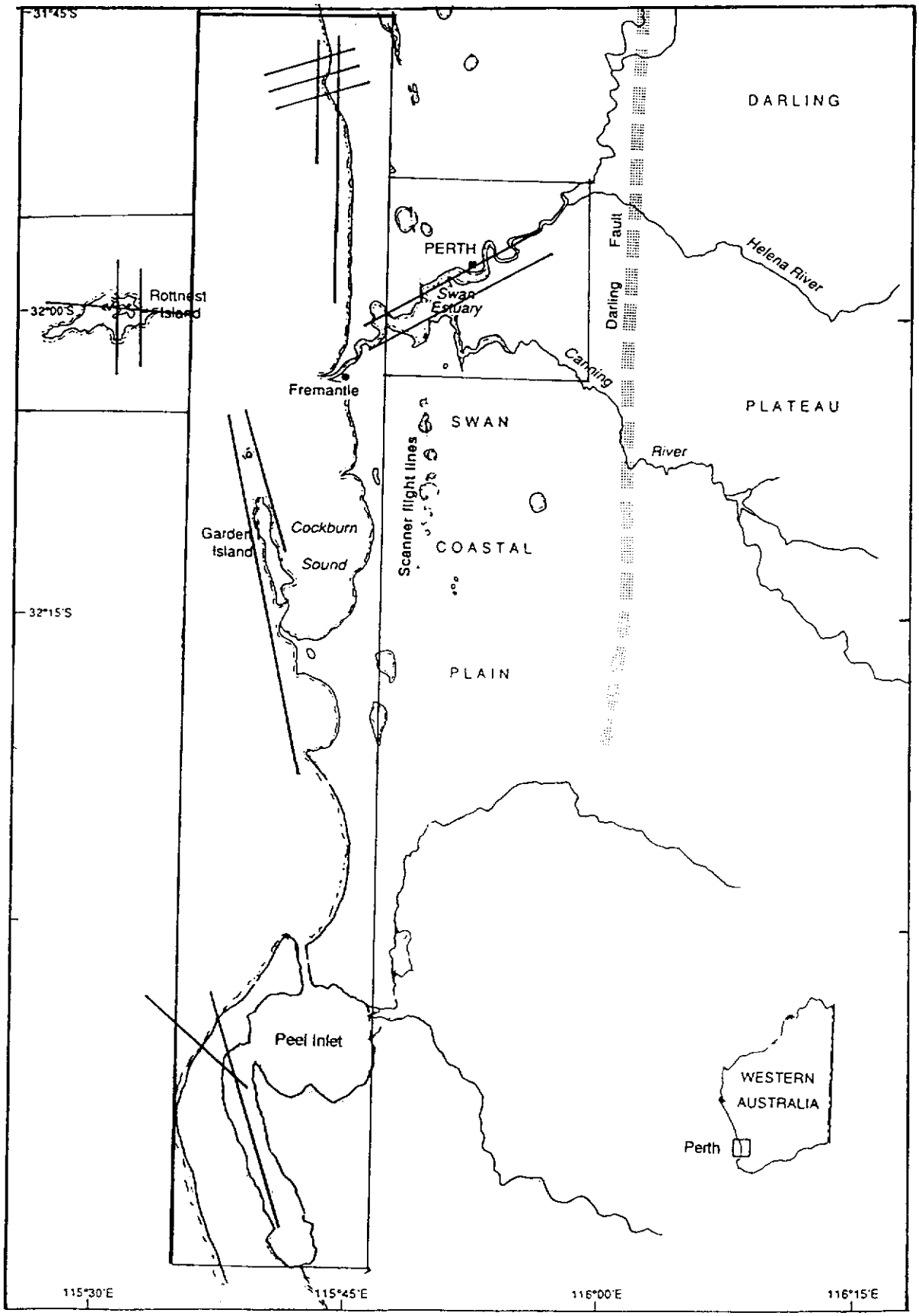

Figure 4.1: Location of flightlines and study sites near Perth, WA.

plain, are usually expressions of the shallow groundwater table and therefore also act as nutrient sinks. Offshore, two inhabited islands contain significant examples of ephemeral brackish to saline wetlands, the most important being Rottnest Island (Hodgkin, 1959).

Total chlorophyll levels range from about 800 µg/l in the highly eutrophic suburban lakes, 200 µg/l in the river to lower than 10 µg/l in the open ocean north of Rottnest Island. The constituent species of pigments also vary widely as a function of salinity and physical characteristics of the waterbody. Two procedures are used to determine chlorophyll concentrations: firstly, spectrophotometric monochromatic determination of chlorophyll *a* in the presence of phaeophytin *a* and thus phaeophytin *a*; and, secondly, spectrophotometric trichromatic determination of chlorophyll *a*, *b*, *c* in waters. Total chlorophyll is the sum of both the components.

4.2.2 Methodology

4.2.2.1 Ocean Colour Scanner

The CSIRO Ocean Colour Scanner is a nine channel, rotating mirror, instrument with bands in the visible and near-infrared regions (380-980 nm). The OCS was designed to be flown in the CSIRO research aircraft, a Fokker F27 (VH-CAT), and at an altitude of 3,000 m gave an approximate scan width of 6 km. An instantaneous FOV of 4.0 mrad gives a nominal 10 m spatial resolution on a 600 pixel-wide, roll-corrected, path. Inertial navigation system data are fed into the 12 bit data stream, which in turn is stored on Exabyte tapes.

4.2.2.2 Geoscan Scanner

The Geoscan Mk 2 Airborne Multispectral Scanner is a 46 channel instrument which can simultaneously record up to 24 bands of information in the visible, reflected, and thermal infrared regions. For this analysis, bands 1-5 were selected (Figure 4.2). These are band 1 (482-514 nm), band 2 (534-585 nm), band 3 (588-653 nm), band 4 (680-703 nm) and band 5 (703-726 nm).

The scanner has an IFOV of 3.0 mrad and a wide FOV $\pm$ 45 degrees from nadir. For this study the instrument was flown in a Cessna 404 (VH-CBM) at 3,000 m, giving a pixel resolution of 10 m, and a swath width of 6 km. Each raw scan-line data record comprises 768 pixels. The data are digitised into 8 bits, with gain and offset automatically adjusted prior to data acquisition. Variations in aircraft roll, pitch and yaw attitude are corrected by sample timing for roll, and by an inertially stabilised integral mount for pitch and yaw. Data are recorded onto 5.25 in optical disks.

Figure 4.2 plots the relative filter functions of the spectral wavebands of the Ocean Colour Scanner and the Geoscan Mk2 Airborne Multispectral Scanner.

4.2.2.3 Signal to noise calculations

Image scanners record a signal that is proportional, or almost proportional, to the energy, or number of photons, per unit of time reaching the detectors. In the absence of signal (S) the system only records noise (N). The ratio of these two readings is (S+N)/N which is equal to the signal to noise ratio only if S/N is significantly greater

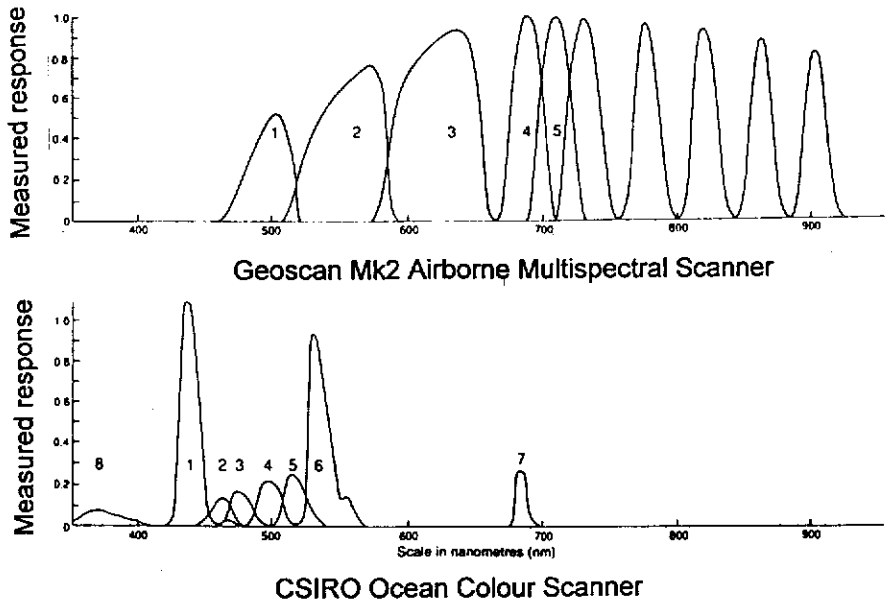

Figure 4.2: Filter functions for both scanners

than 1. The Geoscan instrument records the instrument noise by reference to an internal dark target prior to setting gains and offsets for each channel and stores this information in the header. In this study the method used to calculate and compare S/N was to extract identical areas from each scene for bright and dark uniform targets and determine means and variance.

4.2.2.4 Data acquisition

The OCS data were acquired from 1030 hrs on 20 October 1990 when solar elevation was 62 degrees, at a magnetic heading of 014 degrees. The Geoscan data run commenced 40 minutes later when solar elevation was 66 degrees and corrected track heading was 020 degrees. Surface winds during the acquisition period were 10 km/hr from 230 degrees. The location of the two sites from which data were extracted for S/N calculations had similar image geometry when displayed.

An operational problem and approaching cloud shortened a transect over Gage Roads, outside Fremantle Harbour, and data were not acquired by the trailing Geoscan scanner. In this case that incomplete data set was omitted from the comparison.

4.2.3 Results

4.2.3.1 Spectral band comparison

Figure 4.2 illustrates the waveband overlap between the two scanners. The wavelength-dependant measured responses, or filter-functions, for each band show no corresponding Geoscan bands with the OCS bands 1 and 8. Geoscan band 1 corresponds approximately with OCS bands 2, 3 and 4; Geoscan band 2 with OCS bands 5 and 6; and Geoscan band 4 with OCS band 7. Table 4.1 shows the correlation of the bands of each instrument to each other.

Chemical analysis of the water samples show the total chlorophyll-related pigments principally comprise Chlorophyll *a b c* and phaeophytin. Absolute photosynthetic response peaks occur at 447 and 670 nm for chlorophyll *a*, 647 nm for chlorophyll *b*, 630 nm for chlorophyll *c* and 440 and 665 nm for phaeophytin. Total chlorophyll concentrations (Table 4.2) have strong spectral upwelling radiance and useful diagnostic information especially in the 450-650 nm regions. This relates to Geoscan bands 1, 2 and 3 (460-660 nm) and OCS bands 1 to 6 (430-570 nm).

Chemical analysis of the water samples show the total chlorophyll-related pigments principally comprise Chlorophyll *a b c* and phaeophytin. Absolute photosynthetic

Table 4.1: Correlation matrix for all scanner bands against chlorophyll

	G1	G2	G3	G4	G5	OCS1	OCS2	OCS3	OCS4	OCS5	OCS6	OCS7	OCS8
G1	1												
G2	.815	1											
G3	.867	.949	1										
G4	.016	235	.189	1									
G5	.417	.653	.684	.385	1								
OCS1	.525	.522	.678	.116	.605	1							
OCS2	.576	.561	.712	.111	.564	.993	1						
OCS3	.576	.592	.733	.143	.631	.994	.994	1					
OCS4	.535	.625	.746	.195	.664	.98	.979	.991	1				
OCS5	.473	.65	.744	.256	.715	.942	.936	.958	.986	1			
OCS6	.458	.708	.767	.284	.714	.884	.883	.908	.953	.986	1		
OCS7	.36	.586	.68	.282	.804	.858	.831	.871	.905	.943	.936	1	
OCS8	.292	.157	.344	-.014	.368	.894	.87	.849	.805	.732	.634	.636	1
CHLA	-.555	-.296	-.429	.117	-.093	-.35	-.376	-.363	-.31	-.239	-.192	-.191	-254

response peaks occur at 447 and 670 nm for chlorophyll *a*, 647 nm for chlorophyll *b*, 630 nm for chlorophyll *c* and 440 and 665 nm for phaeophytin. Total chlorophyll concentrations (Table 4.2) have strong spectral upwelling radiance and useful diagnostic information especially in the 450-650 nm regions. This relates to Geoscan bands 1, 2 and 3 (460-660 nm) and OCS bands 1 to 6 (430-570 nm).

Table 4.2: Sites and total chlorophyll used in analysis

Site No.	Location	Total Chloro	Site No.	Location	Total Chloro
1	Gage Roads	0.48	17	Squadron	2.13
2	Gage Roads	0.71	18	Centre	1.37
3	Gage Roads	0.85	19	Applecross	1.07
4	Gage Roads	0.63	20	Monger Lake	4.45
5	Gage Roads	0.58	21	Monger Lake	7.84
6	Gage Roads	0.47	22	Herdsman	2.03
7	Gage Roads	0.55	23	North Lake	3.36
8	Gage Roads	0.48	24	Jackadder Lake	3.74
9	Rottnest	0.08	25	Shenton Lake	0.31
10	Rottnest	0.16	26	Bibra Lake	1.56
11	Rottnest	0.23	27	Barker Swamp	1.25
12	Rottnest	0.15	28	Salmon Swamp	0.02
13	Rottnest	0.12	29	Geordie Bay	0.08
14	Rottnest	0.26	30	Longreach Bay	0.20
15	Rottnest	0.12	31	Timperley Lake	1.52
16	Rottnest	0.12	32	Garden Lake	0.99
			33	Vincent Lake	0.92
			34	Herschell Lake	0.15
			35	Govt House Lake	0.25

Individual band correlations to total chlorophyll for both instruments, presented in Table 4.1, were used to determine the best and the least correlated band ratios to remove the effect of "across-track" illumination, or brightness effects. In both cases the reflected infrared bands in the 700 nm region were used in the ratio, as at this wavelength any upwelling radiance must come from the water surface or the atmosphere, and is crudely assumed to be uniform. The ratio is plotted against the Log of total chlorophyll (Log C), and the result is shown in Figures 4.3 and 4.4.

Figure 4.3 shows regression of Geoscan band 1/5 ratio and Log C, giving r = -0.685, even with the inclusion of the outlying site 28, Salmon Swamp on Rottnest Island, which is a small atypical saline swamp. Significantly, the best band correlations from the OCS data were in the same spectral regions as the Geoscan data.

Figure 4.4 shows regression of OCS bands 2/7 with Log C for all sites (r = -0.596). However, the OCS has three bands (2, 3 and 4) that cover the Geoscan band 1, and all three narrow bands plotted independently gave r values of, -0.448, -0.467 and -0.467 when ratioed with band 7.

Geoscan band 4 more closely aligns with OCS band 7 which is included to measure the second reflectance peak of chlorophyll *a*. The better r value is also sustained when the Geoscan band 4 is used in the ratio, r = -0.667.

The narrow OCS bands were selected by the instrument designer to attempt to characterise the pigment species in the ocean. However, the best relationship of

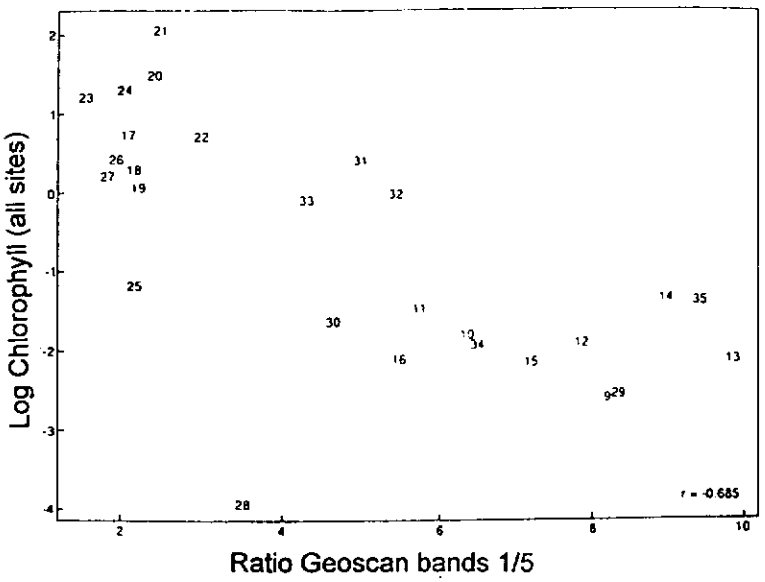

Figure 4.3: Plot of Geoscan band 1/5 ratio and Log C

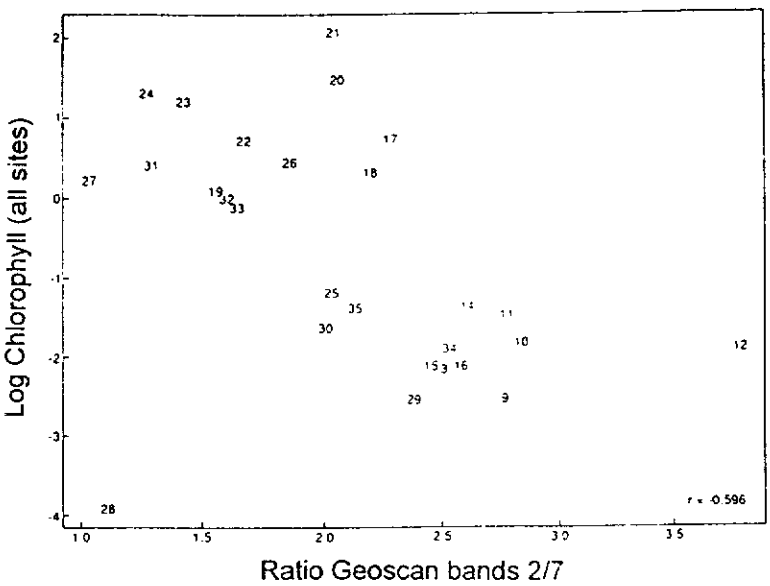

Figure 4.4: Plot of OCS bands 2/7 against Log C for all sites

bands to a limited number, but a broad range, of chlorophyll concentrations and species came from combined OCS bands 2, 3 and 4. A more objective comparison is provided when the three bands are summed.

When the ranges of chlorophyll values were divided into "case one" and "case two" waters representing the low chlorophyll oceanic group (up to 50 µg/l) and the higher pigment content group including the lakes and river, the comparable performance of the two scanners changed significantly. The Geoscan data did not correlate as well in the oceanic case one sites with r value of 0.338 using the best ratio combination (band 1/band 4), although band 4 on its own gave r = -0.46. In the case two sites the same band ratio gave r = 0.669. A contrary result was obtained from the OCS with its performance in the case one oceanic sites as high as r = -0.803 from a band ratio 5/7, but its performance in the case two sites was poor with r = -0.281 from bands 2/8.

4.2.3.2 Signal to noise comparison

To enable comparison of S/N, the raw digital data were extracted from each file for uniform identical areas for dark (deep ocean) and bright (dune sand) targets flown near-simultaneously by both instruments on 20 October 1990. The areas were 15 x 15 (225) pixels. Table 4.3 shows that the mean standard deviation indicates S/N ratios of 10-50:1 could be expected with the performance of the photomultiplier-type detectors in the narrow bands of the OCS being the same, or better, in all bands than the silicon-type detectors in the wider bandwidth Geoscan system.

4.2.4 Conclusions

All these analyses were performed on uncalibrated data. The raw radiances, when used as ratios, are a fair comparison of the relative merits of each system. Simultaneous ground reference data were collected to enable comparison of subsequent acquisitions. This study indicates that a simple universal model will not

Table 4.3: Calculation of signal to noise ratios

Geoscan Airborne Multispectral-Scanner

	Dark Target (Ocean)			Bright Target (Sand)			
Bands	DC	SD	S/N	DC	SD	S/N	Mean S/N
1	80.96	6.9	12	245.69	8.5	29	(20)
2	41.84	2.8	15	252.92	6.1	41	(28)
3	56.24	1.9	30	248.67	7.6	33	(32)
4	14.14	0.9	16	249.04	7.1	35	(25)
5	9.78	1.4	7	221.39	6.4	35	(21)

COSSA Ocean Colour Scanner

	Dark Target (Ocean)			Bright Target (Sand)			
Bands	DC	SD	S/N	DC	SD	S/N	Mean S/N
1	2777	64.2	43	6962	130.2	53	(48)
2	2957	99.1	30	8108	321.3	25	(28)
3	2697	83.1	32	7999	219.9	37	(35)
4	2383	83.4	29	8809	350.1	25	(27)
5	2066	98.6	21	10191	473.7	22	(22)
6	1904	90.1	21	7420	-	*	(21)
7	1070	93.7	11	10313	-	*	(11)
8	2651	38.1	70	3936	96.3	41	(55)

accurately determine chlorophyll over a wide range of concentrations. Variation in predicting chlorophyll levels comes from the physical and chemical nature of the waterbodies. The reflectance from these water bodies is a composite of surface, column and bottom materials. This composition may be resolved in some cases as a function of wavelength.

Both instruments performed well when concentrations were grouped at levels that would occur in the independent biophysical systems. The relationship of the chlorophyll to reflectance for high chlorophyll systems, such as the coastal wetlands with values about 50-800 µg/l, is different from the low level systems such as the ocean which recorded levels from 0-50 µg/l. The OCS, as its name implies,

performed well in the oceanic levels of pigment concentrations. However, its ability to predict concentrations at higher levels could not be sustained. The Geoscan instrument, with its broader bands, performed reasonably consistently in both high and low concentration waters.

Determination of speciation of chlorophyll pigments is unlikely with the Geoscan scanner. However, the OCS with its narrow bands in the 400-600 nm regions showed that it may be possible to quantitatively determine pigments. Signal to noise characteristics of the OCS were better than the Geoscan scanner and both instruments appeared to have a higher noise level than specified. Despite this, the image quality was entirely acceptable considering the maximum gain settings that were selected to maximise the low radiances from water bodies.

4.3 Swan River Study: CASI Experiment

4.3.1 Background and Aims

The second experiment was designed to characterise the spatial and temporal variation of the spectral properties of the water column and the major algal bloom species in the Swan River, and to develop spatial and temporal acquisition parameters and image analysis techniques for improved discrimination and early warning of algal blooms. The majority of algal problems in the eastern states of Australia are caused by cyanobacteria (blue-green algae). The Swan River in Western Australia experiences phytoplankton blooms of green algae, diatom and dinoflagellates.

The ability to spectrally discriminate between types of blooms was a major objective of the study. The use of airborne instruments was also evaluated as a low cost, operational supplement to traditional boat-based sampling for assessing the spatial and temporal extent of algal blooms. Field studies of in-water reflectance, using multi-band radiometers, supported by laboratory studies, indicated that significant spectral differences between cyanobacterial and green algae and diatom/dinoflagellates were measurable.

The Compact Airborne Spectrographic Imager used in the experiment has 288 bands in imaging-spectrometer mode and 14 bands in spatial-imaging mode. It therefore has high spectral resolution but has the disadvantage of producing very large data sets that require significant time to process and analyse.

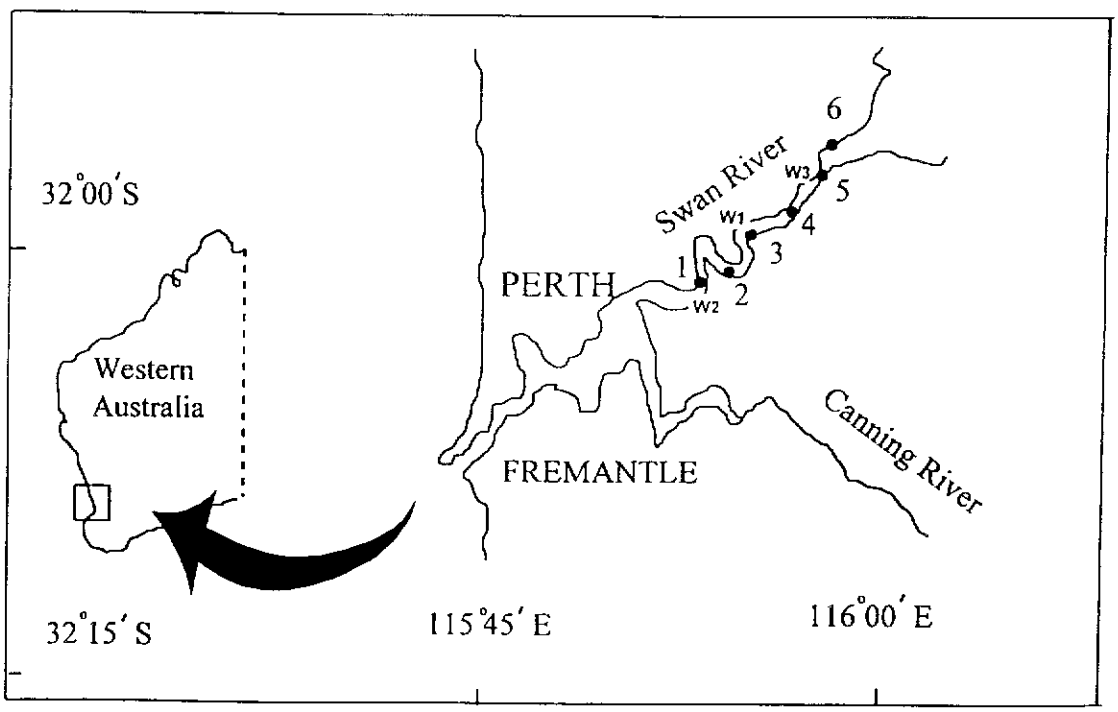

Figure 4.5: Location map of Swan River showing wetlands and six monitoring sites

4.3.1.1 Study area

The Swan River which flows through Perth has a catchment of 124 000 sq km, of which about 70 percent has been cleared for dryland agriculture, with the remaining area being native eucalypt forest. A large proportion of the metropolitan area and the near-urban intensive agriculture drains into the estuaries of the Swan/Canning system (Figure 4.5), around which live about 1 million people

The input of nutrients to the river (principally agricultural-derived phosphate and nitrate from the predominantly winter rainfall and humic-rich groundwater) has resulted in the frequent occurrence of algal blooms of increasing intensity, and toxic severity. The distribution of phytoplankton in the Swan River estuary is controlled by dynamic environmental factors, but is predominantly composed of diatoms and phytoflagellates (John, 1987). Diatom blooms occur during the winter in the lower estuary and throughout the estuary in summer and autumn, while massive phytoflagellate blooms are initiated in the spring. An incursion of clear marine saline water progresses up the river system during the summer, replacing the humic-dominated, less saline, winter river flow.

4.3.1.2 In-water spectral data

Laboratory studies of bloom types, and mixtures, have shown the additive nature of the spectral response of phytoplankton and the diagnostic potential of spectral signatures for the determination of those blooms (Johnsen *et al.*, 1994). The objective of field measurements of algal spectra was to determine whether algal groups (green algae, diatoms, dinoflagellates) could be distinguished on the basis of

their spectral characteristics within the matrix of other water constituents such as humics and sediments. Also, whether the water-leaving radiance could be reliably measured by an airborne sensor.

Spectral measurements of algal blooms were made initially using the DSIR meter, and subsequently the Irricrop radiometer, of a range of sites in the summers of 1992/3 and 1993/4. These measurements were made, where possible, simultaneously with aircraft missions and with biological, physical and chemical sampling.

Figures 4.6 (a), (b) and (c) are examples of 10 replicates of "in-water" spectral measurements (the ratios of the downward/upward) at the Ron Courtney Island site on 15 March 1994. The top graph (a) was measured with the radiometer suspended 1 m above the water surface (Lw) but does not take account of atmospheric radiance (Law) that would be scattered into the path of an airborne sensor. The middle graph (b) was measured with the radiometer located with the downward (radiance) sensors just beneath the surface of the water and the diffuse upward (irradiance) sensors above the water surface. This provides an estimate of the surface reflectance (Lw-Lsw) or the combined contribution of column materials and substrate (Lmw+Lbw). As mentioned earlier, no contribution is assumed from the bottom (confirmed by Secchi and light extinction measurements) and is basically the spectra of dissolved and suspended material in the water column.

In an attempt to separate between column components a third set of readings was made with the radiometer set at varying depths below the surface. The lower graph

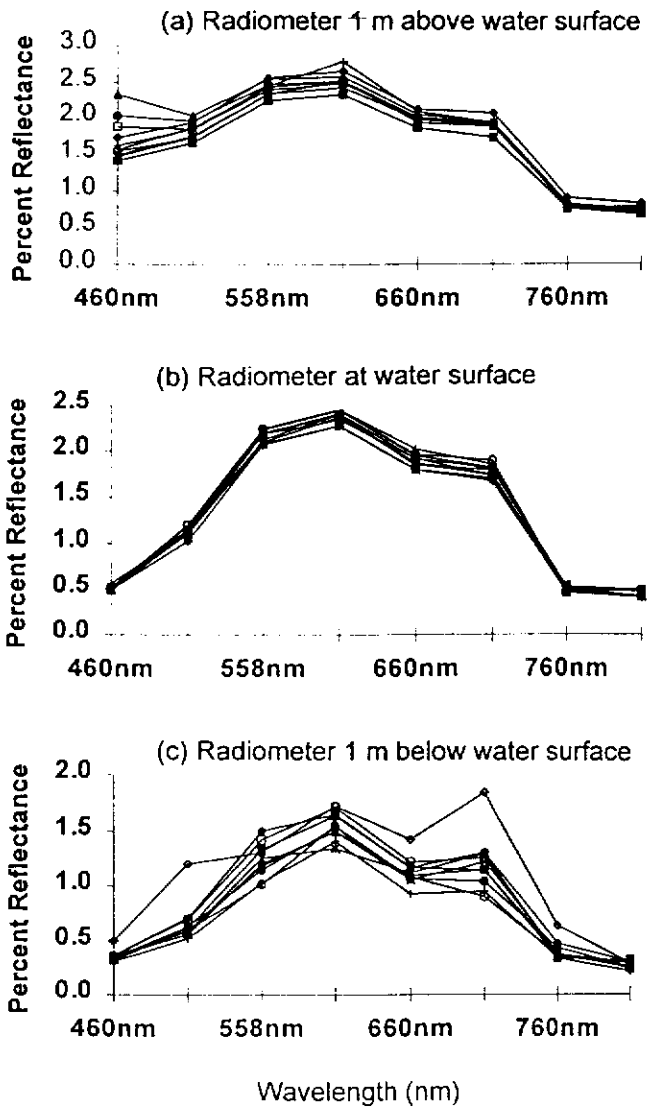

Figure 4.6: In-water spectral measurements from Irricrop radiometer

(c) is in effect a ratio of the transmission through 25 cm of water between the surface and the upward diffuse sensors and the radiance from the deeper water. This was an attempt to quantify the proportions of "forward-scatter" and "back-scatter" by particles in the column. In most cases these values cancelled each other out at depths beyond 50-100 cm (usual Secchi extinction depths for the Swan River).

The points of note in these spectra are the removal of the surface scattered (blue-end) effects of the atmosphere between graphs (a) and (b). Also note the absolute reflectance values and the decline, but consistent band-relationships throughout, even in graph (c) which shows more variability.

Comparisons were thus possible of the spectral contributions of specific column constituents. Figure 4.7 is such a comparison of three bloom types that appeared in the Swan river system during the summer of 1993/4. The cyanobacteria (*Anabaena sp.*) bloomed in the Canning and the green (*Chlamydomonas sp.*) was measured during an extensive bloom in the Bassendean area (near site 5) of the Swan River. The dinoflagellate (*Gymnodinium sp.*) bloomed in the Ascot area (near site 3). Significant spectral differences occur in these bloom types and, on the basis of this analysis, a range of narrow band-pass spectral filters within the range of 480-700 nm was planned for use in the airborne video system in an attempt to translate the "in-water" results to airborne imagery.

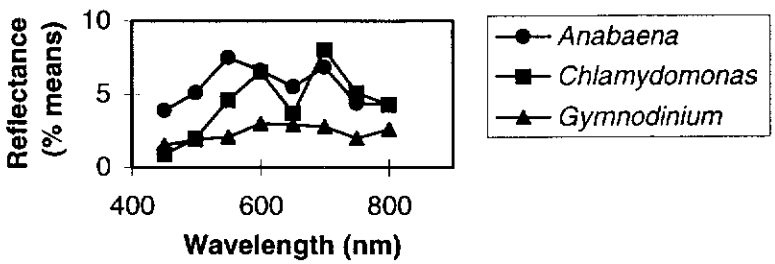

Figure 4.7: In-water spectral measurements from Swan/Canning River system

Recent developments in miniature fibre-optic spectrometers offer have the potential to identify bloom types in the field based on characteristic spectra. A prototype instrument was coupled directly to a portable computer to display and record both

target and reference spectra. A range of optical fibre diameters and collecting optics was developed to provide the opportunity to resolve either absorption or reflectance spectra to 2 nm from a narrow or diffuse field-of-view. Spectral data from the Ocean Optics are used to show concentrations of the algae *Gymnodinium simplex* (from near site 4) later in this thesis.

4.3.2 Methodology

The opportunity to evaluate data from the Compact Airborne Spectrographic Imager was offered to coincide with the anticipated Spring blooms of 1992. The CASI eventually arrived in February 1993 and was flown in both spectral (288 bands x 39 lines) and spatial (14 bands x 512 lines) modes to address four generic objectives. These were to:

(i) Compare the controlled in-water field spectral measurements, taken with submerged radiometers, with the high-resolution CASI spectral-mode measurements, taken from the aircraft;

(ii) Compare the biological measurements with the high-resolution CASI spectral-mode measurements in order to determine diagnostic wavebands;

(iii) Compare the physical and biological measurements with spatial-mode CASI data in order to test the selection of aggregated bands; and

(iv) Simulate the data produced from low-cost, video-based systems that could be used operationally for this type of work.

The limited availability of CASI meant that it was not flown during a major bloom event in the Swan River. However, a reasonable range (5,000 to 31,000 cells/ml) of

concentrations was present and, in wetlands associated with the river, significant cyanobacterial and green algal blooms were occurring. The wetland sites were not sampled simultaneously with the over-flight, but subsequent inspection and anecdotal evidence confirmed the presence of these bloom types (probably *Anabaena sp.* at an excess of 100 000 cells/ml.- W. Hosja. Waterways Commission, pers. comm).

4.3.2.1 CASI instrument

The CASI is based on an f/4 reflection grating spectrograph coupled to a CCD array of 578 spatial pixels which are dispersed over 288 bands (Babey and Anger, 1989). To handle the high data rates, the CASI can be flown in one of two modes. In spatial-mode, up to 15 full-image bands between 423 and 946 nm can be acquired across a field of view of 35 degrees; in spectral-mode 288 contiguous bands of 39 evenly-spaced picture elements or "rakes" chosen within the same field of view can be acquired. The flight lines need to be repeated to capture data in both modes.

The CASI instrument was brought to Western Australia for evaluation in February 1993 and was installed in a Britten-Norman Islander aircraft. A gyroscope, to record aircraft roll, a GPS and a drift-site for site location, were also fitted.

A series of flight lines was flown over the Swan River on 18 February 1993. Weather conditions were acceptable, although cloud which formed shortly afterwards limited some of the field spectral measurement program. Meteorological data and atmospheric profiles and site data were obtained from the Perth Bureau of Meteorology. The flight lines were flown in both spectral and spatial modes. The

"Scene Recovery Channel", which is included to view the area covered for the spectral-mode was selected at band 210 (750 nm) to give good land/water comparisons. The spatial mode was selected to have 14 bands (Table 4.4).

.

Advice, given by D.L.B. Jupp (CSIRO Div. Water Resources, Canberra, pers. comm) was that the analysis should only be performed on bands beyond 500 nm because of low signal to noise ratio below that wavelength. This appeared to be sound advice, as high variability in the shorter wavelengths was shown in the early analyses.

Calibration of the CASI spatial-mode data to reflectances was done using a "flat-field" correction, interpolating a reflectance line between a dark target, assumed zero, and a measured invariant target that was included in each flightline (Jernakoff and Hick, 1994). In this study, a large area of a clear bitumen carpark was used and compared with a $BaSO_4$ standard plate. Pre-delivery calibration of the spectral-mode was considered adequate at the time for the purposes of the analysis.

Table 4.4: Wavebands of CASI, DMSV and DSIR spectrometer

No	CASI	DMSV	DSIR	Purpose
1	446-453	438-462	440	Water penetration
2	477-484		480	Chlorophyll
3	497-504			Ocean Chloro Ref.
4	527-534		520	Scattering
5	547-554	538-562		Green Ref.
			560	
6	564-572			Pigment (p/erythrin)
7	597-604			Yellow Ref.
8	622-629		620	Pigment (p/cyanin)
9	647-654	638-662		Red Ref.
10	674-683		670	Pigment (chloro-a)
11	708-715			Red edge 1
12	746-755			Red edge 2
		758-782	780	
13	800-808			Near-infrared
14	844-851		860	Near-infrared

4.3.2.2 Site sampling methods

Sampling of the water column was done at the surface, 50 cm and 1 m and then at 1 m intervals to the bottom using a submersible pump. Phytoplankton identification was done on the same day and the cell densities were determined from lugol iodine preserved samples, using a 1 ml Sedgewick-Rafter counting chamber and an Olympus B-H-2 microscope at X125 magnification. Salinity and temperature were measured using a Yeokal 602 meter (Hanon, Autolab. Sydney). Dissolved oxygen was measured in-situ with salinity compensation using a Yeokal 603. Secchi disc depths were estimated on the sunlit side of the boat, using a 200 mm diameter Secchi disc.

Chlorophyll was determined on phytoplankton cells filtered onto Whatman GF/C filter paper, stored frozen, and extracted by acetone after crushing. The spectrophotometric determination was done according to standard methods of the Chemistry Centre of Western Australia.

For the in-water spectral measurements, a water-tight radiometer housing with a clear perspex viewing window was mounted astern of the boat in a suspension frame. This enabled the DSIR radiometer within the housing to be pointed upward, with a diffuse filter, or downward for calculation of radiance or irradiance. The radiometer was lowered from a boom, clear of the stationary boat, to reduce the effect of shadowing or reflectance from the boat hull.

Spectral measurements were made just above the surface, with the radiometer housing centred at 1 and 2 m below the surface. This was done at times that were as close as logistically practical to the flight using the Mk2, DSIR Eight Channel Radiometer. The DSIR meter (Table 4.4) has narrow bands (bandwidths bracketed) centred at 440 (12.5), 480 (9.5), 520 (10.5), 560 (9.5), 620 (10.8), 670 (11.5), 780 (11.7) and 860 (10.7) nm and a field of view of 20 degrees. From these eight channels, an interpolation of a reflectance curve is possible.

4.3.2.3 Analysis methods for CASI data

A canonical variate analysis (CVA) was performed on all the data extracted from the CASI spatial image files for polygons (comprising between 50 and 200 pixels). Briefly, a canonical variate analysis finds the linear combinations of the original variables (spectral bands) that maximise the differences between reference classes relative to the variation within the classes. Mathematically, this corresponds to finding linear combinations (canonical vectors) that maximise the ratio of the resulting between-groups to within groups sum of squares for the resulting linear combinations. The canonical vectors give the directions of maximum class separability and the canonical roots give a measure of class separation in these directions. For a detailed description see, for example, Campbell and Atchely (1981) and Campbell (1984).

The polygons were selected as close as could be identified to the monitoring sites, although site 6 was missed from one flight line through a navigation error and site 3 was repeated with a second overlapping sampling site.

The classification of the river and wetland types was done with a "maximum-likelihood" technique. This used the combination of a predetermined number of bands that the CVA showed to provide maximum separation between all of the training sets (in this case all of the sampling sites), and allocates pixels to classes that are most like those known sites. Pixels in the image that fell outside class groups were not allocated.

These statistical analyses were done to:

(i) Establish the relationship of the CASI data to the monitoring sites for which cell concentration data and water quality data were available;

(ii) Determine if the CASI spatial data could discriminate between major bloom types that may bloom in the Swan/Canning system;

(iii) Determine which wavelengths, and how many, are required to describe water column constituents, in particular, how well the existing bands in the DMSV perform compared with the full CASI data; and

(iv) Classify the river and nearby wetlands based on the above analyses.

4.3.3 Results

4.3.3.1 DSIR radiometer

The first objective was to compare the relationship of the in-water spectral measurements to the CASI spectral-mode (288-band) data. Unfortunately, because the time taken for field measurements was significantly longer than the flights, simultaneous spectral measurements were possible for only two of the monitoring

sites. During the morning of the overflight of CASI, cloud formed over the area and curtailed further measurement.

Figures 4.8 and 4.9 are DSIR meter spectra for sites 1 and 2 respectively. The relative reflectance was calculated from the ratio of the upward (forward scatter) to the downward (back-scatter) position for each depth. The surface spectra (the unbroken line with Standard Error bars) show low relative reflectance (less than two percent) below 500 nm and probably include a proportion of surface-skin scattering of sky radiance. At depth, the first two channels fall to zero. This is possibly explained by absorption by the humic-rich (coffee-coloured) nature of the Swan River. A maximum peak occurs at 550 nm (greater than three percent) and the reflectance declines to near zero by 780 nm. Site 1 had significantly lower cell counts of both dinophytes and cryptophytes (covered in the next section and Table 4.5) than site 2 which responded with a relative increase at 550 nm and a decrease at 670 nm. The relevance of the low reflectance below 500 nm, and the maximum slope change beyond the red (650-750 nm) is shown later in the analysis of the CASI data.

The apparent increase in relative reflectance with depth is a function of the subsurface upward-to-downward ratio. This occurs as the irradiance (forward-scatter) becomes less, relative to the subsurface upwelling radiance (back-scatter). However, of importance to note is the preservation of the spectral-shape components. It is also important to note that the Secchi extinction occurs at about 1-1.5 m (Table 4.5) which indicates that total upwelling radiance is coming from within that range.

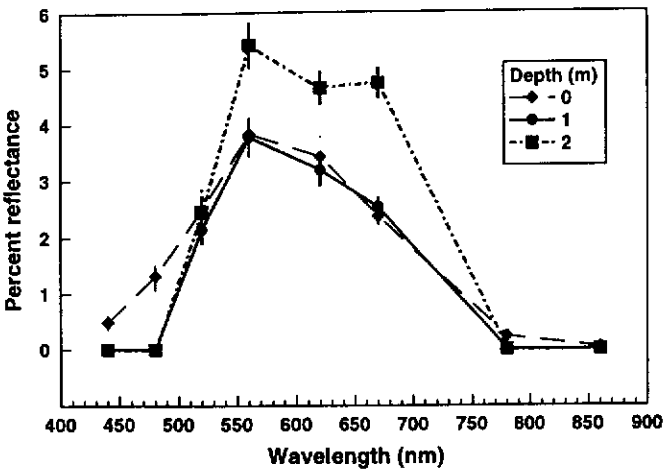

Figure 4.8: DSIR meter spectra for site 1

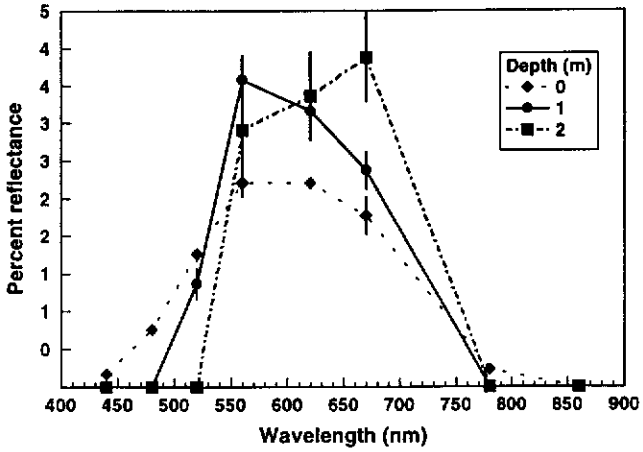

Figure 4.9: DSIR meter spectra for site 2

Table 4.5: Chemical and biological measurements, 18/2/1993

Site	Secchi (m)	Salt (Mg/l)	Chlor.a (Mg/l)	Chloro-phyta	Dyno-phyta	Crypto-phyta	Diatoms	Total Cells
1. Causeway	1.5	20.7	0.014	364	3569	72	34.3	5536
2. St Johns	1.3	17.2	0.025	533	5370	1506	41.1	10880
3. Maylands	-	16.7	0.006	-	1108	1918	73.0	-
4. White Rk	0.9	13.4	0.049	728	15445	12239	13.3	30599
5. Kingsley	1.0	11.5	0.046	582	11656	12676	5.2	26518
6. Success	0.8	9.3	0.048	777	6977	20043	1.4	30421
r^2 @ 750 nm	0.87	0.95	0.77	0.70	0.44	0.95	0.59	0.94

4.3.3.2 Comparison of biological and spectral-mode CASI data

The second objective was to measure the correlation of the biological measurements with the high-resolution CASI spectral measurements. Table 4.5 shows that the in-water measurements appear ranked in a one-dimensional direction upstream and many of the properties are highly correlated. This feature is caused by the incursion of saline marine water during the low-flow summer period.

Figure 4.10 shows the mean CASI spectral curves, extracted from the spectral-mode data, for the six monitoring sites in the Swan River. As mentioned earlier the spectral response is dominated by the contribution of the atmosphere and instrument noise at the shorter blue (400-500 nm) wavelengths. However, a gradual decrease from the green (500-600 nm) region through the red (600-700 nm) and a strong overall absorption into the reflected infrared is comparable up to about 750 nm.

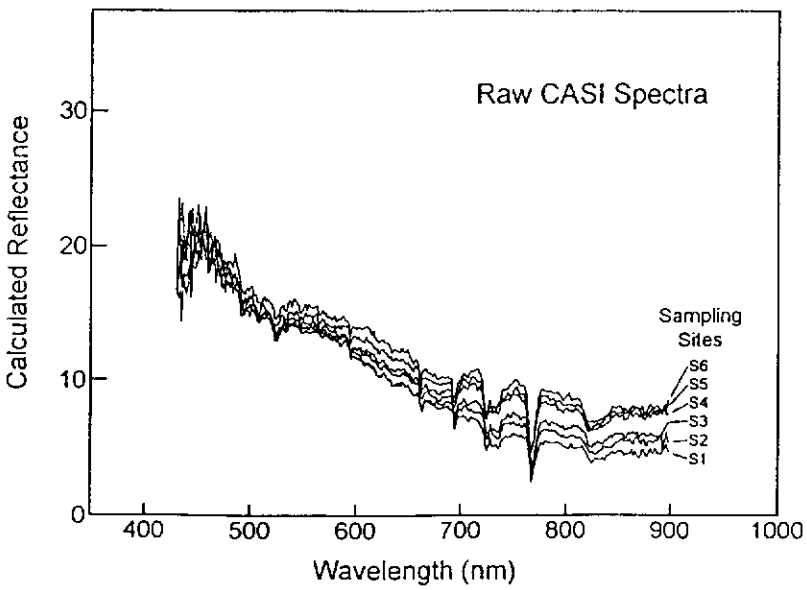

Figure 4.10: CASI spectral curves extracted from spectral-mode data

Beyond that wavelength the DSIR instrument provided no appreciable signal but the CASI data contained the maximum spectral information for the separation of the sites.

The spectral feature of specific interest is the slight but well ordered increase in red/infrared response corresponding with the increasing total cell counts and decrease in Secchi and salinity for the upstream sites. Table 4.5 summarises the surface to 0.5 m values for phytoplankton and pigments. This relationship of the CASI spectral data to the biological data was tested at 750 nm.

Secchi disk readings and salinity were negatively related but both showed a very close relationship (r^2 = 0.87 and 0.95 respectively) to the spectral response and may reflect the saline incursion progressing upstream. The strong relationship of total cells was shown for the dominant cryptophyte *Cryptomonas sp.* However, the strong relationship was not supported by the dinoflagellates, with the main species *Gymnodinium cf. simplex.* The importance of this early result becomes significant in the next phase of the study.

The poor relationship of the dinophytes may be explained in part by the large variation of the biomass of the cryptophyte cells, which are of the order of three to four times larger that the dinoflagellates, thus producing biomass disparity of that order for the same cell count (Vas Hosja, Swan River Trust, pers comm.) Also these highly mobile organisms have huge variability especially in the earlier parts of the day.

Figure 4.11 shows the plot of one of the monitoring sites, site 2, and an adjacent wetland that at the time had a severe (probably *Anabaena sp.* - Vas Hosja, Swan River Trust, pers comm.) cyanobacterial bloom. The strong green peak (550-560 nm) and a secondary chlorophyll peak closer to the infrared region are characteristic of pigments in cyanobacterial algae which can occur at the low salinity extremes that occur in the upper Canning River and in the wetlands associated with the Swan River system.

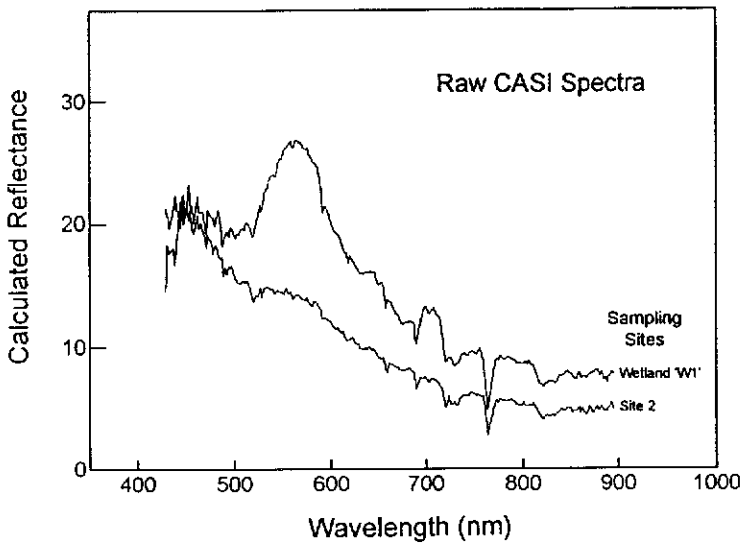

Figure 4.11: CASI spectra for site 2 and an adjacent wetlands site

4.3.3.3 Comparison of biological data with spatial-mode CASI data

The third objective was to compare the Spatial-Mode (14-band) CASI data with the biological and physical measurements from the monitoring sites and with other known areas of specific algal bloom types using canonical variate analysis techniques. The purpose of this analysis was to determine which spectral regions, expressed as wavebands, can provide maximum separation between sites.

The first analysis was performed on training polygons selected close to the river monitoring sites. Site 6 was not included in the spatial-mode image because of a navigational error. Site 3 is represented by two training samples. Table 4.6 summarises the analysis and Figure 4.12 is the canonical variate means plot. The size of the canonical roots indicate that the sites are very different spectrally. The first canonical vector, explained 95 percent of the variability in the training data.

Table 4.6: Canonical Variate Analysis of CASI spatial-mode data using bands 3-14 for river sites

Canonical roots (1-5)					Sum of roots
127.6	4.601	1.812	0.621	0.091	134.763
Canonical Vectors for CVA 1 and 2 for the 12 bands.					
-0.5330E-02	-0.688E-02	-0.9677E-02	-0.6007E-02	0.1843E-02	0.6533E-02
0.8545E-02	0.6894E-02	0.7496E-02	0.1079E0-01	0.7746E-02	0.2091E-02
0.1623E-01	0.3929E-02	-0.6082E-03	-0.1010E-01	-0.4104E-02	-0.9043E-02
-0.5041E-02	-0.1312E-02	0.3826E-02	0.3418E-02	0.2514E-02	0.3684E-04

The second analysis includes an additional three training sites (plotted as W1, W2, W3) selected from the wetlands to represent cyanobacterial and green algal blooms.

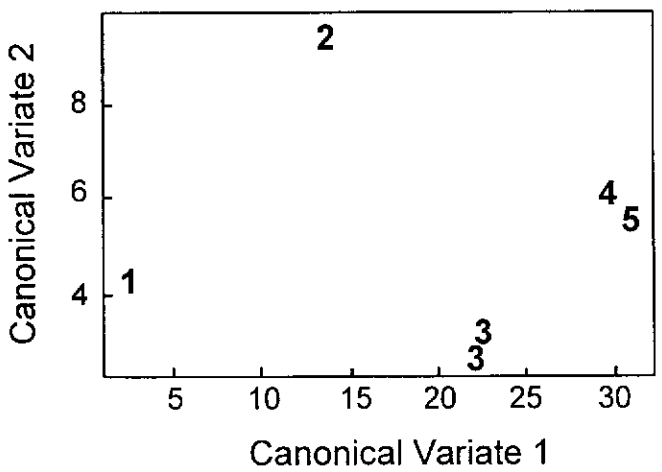

Figure 4.12: Canonical variate analysis for river sites using bands 3-14

Table 4.7 summarise the analysis and Figure 4.13 plots the canonical vectors. They show that the algal sites are very different spectrally from the river sites.

Table 4.7: CVA of CASI spatial-mode data, bands 3-14 for river and wetland sites

Canonical roots (1-5)					Sum of roots
544.1	72.23	13.37	1.842	0.221	679.829
Canonical Vectors for CVA 1 and 2 for the 12 bands.					
-0.2244E-02	0.1603E-02	0.1266E-01	0.1954E-01	0.2345E-02	-0.3871E-02
-0.7422E-03	-0.1430E-01	0.2114E-02	-0.2928E-02	-0.1337E-02	-0.1664E-02
-0.2663E-02	-0.3171E-02	-0.5866E-02	-0.4353E-02	-0.2448E-02	0.4591E-02
0.5424E-02	0.6037E-02	0.2098E-02	0.1091E-01	0.8324E-02	0.2471E-02

The first canonical vector discriminates between the algal and river sites. The second canonical vector maintains the ordination of the river sites. Referring back to Figure 4.11, which is CASI spectra from site 2 and an adjacent highly eutrophic wetland that drains into the river, the spectra show the characteristic green peak near 550 nm and a secondary peak near 700 nm, which is consistent with a green algal bloom.

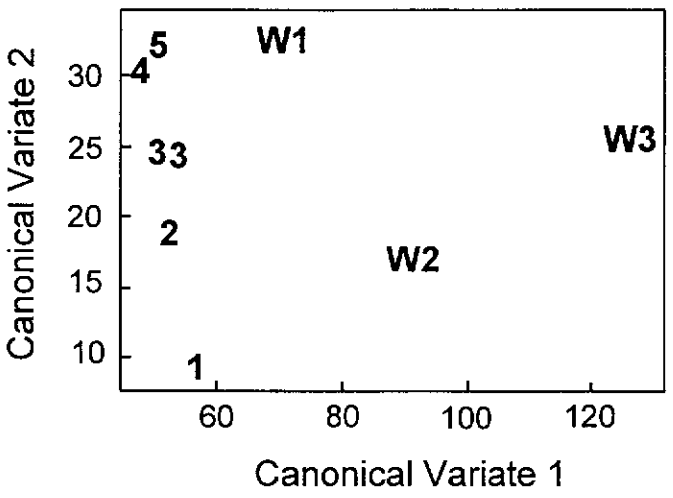

Figure 4.13: Canonical variate analysis for river and wetlands using bands 3-14

Comparison with Figure 4.10 shows that the difference between the spectra from the wetland and the river site is much greater than the variation in the spectra for the six

river sites. This difference is reflected in the large first canonical root in the analysis with the second canonical variate maintaining the separation of the "river-only" sites.

4.3.3.4 Variable band selection results

In order to determine and rank spectral bands, a variable selection procedure was applied to the data as shown in Tables 4.8 and 4.9 which are a summary of the results when applied to the river-only and wetland sites. It shows that few bands can maintain the separation of the training samples. These bands are 3 (497-504 nm), a chlorophyll band, 6 (564-572 nm), the pigment phycoethrin and, as shown in the spectral-mode data analysis, band 12 (746-755 nm), the infrared.

Table 4.8: Optimum separation using a variable selection procedure and cumulative percentage for 12 bands for river sites only

Size of Band Subset	Best Band Combination	log (det (W)/ det W+B)	percent
1	12	3.98	48.5
2	3,12	5.23	64.8
3	3,6,12	6.20	75.6
4	3,6,11,12	6.78	82.7
5	3,6,10-12	7.19	87.1
6	3,6,7,10-12	7.50	91.5
7	3,6,7,10-13	7.67	93.5
8	3,4,6,7,10-13	7.84	95.6
9	3-7,10-13	7.97	97.2
10	3-7,9-13	8.08	98.5
11	3-13	8.14	99.3
12	3-14	8.20	100

Table 4.9: Optimum separation using variable selection procedure and cumulative percentage for 12 bands for river sites and wetland sites

Size of Band Subset	Best Band Combination	log (det (W)/ det W+B)	percent
1	6	2.37	66.0
2	6,10	2.83	78.8
3*	5,6,10	3.40	94.7
4	5,6,8,10	3.45	96.1
5	5,6,8,10,14	3.51	97.8
6	3,5,6,8,10,14	3.53	98.3
7	3,5,6,8,10,11,14	3.56	99.2
8	3-6,8,10,11,14	3.57	99.4
9	3-6,8,10-12,14	3.59	100
10	3-6,8-13,14	3.59	100
11	3-12,14	3.59	100
12	3-14	3.59	100

4.3.3.5 Image classification

Maximum likelihood classification (Figure 4.14) was used to match the rest of the image pixels to the training samples which represented the river and wetland sites. A subset of the spectral bands was chosen for use in the calculations. Bands 3, 5, 6, 7, 10, 11 and 12 were selected in the previous analysis as the best bands to both discriminate between the river sites (six bands 3, 6, 7, 10, 11 and 12) and to separate the wetland algal bloom sites (three bands 5, 6 10) from the river sites.

Figure 4.14 is the CASI image with the classification overlain. The colours are class labels based on the correlation to total cell count from the sampling points. The image has been corrected for aircraft roll and calibrated to reflectances. The river pixels that have not been assigned to one of the classes are affected by sunglint. No attempt has been made to remove this effect, although the qualitatively-effective technique of Ong *et al.* (1994), referred to in Chapter 3, could have been applied, but its effect on the classification may have created misclasses.

4.3.3.6 Simulation of simple multi-band video system

A simulation of the four-band SpecTerra DMSV system was done using the CASI data. The bands of the DMSV were specifically chosen by the manufacturer for terrestrial vegetation purposes, although significant information on the pigments in the Swan River was clearly evident on available imagery. To assess the usefulness of the standard band configuration, canonical variate analyses were performed to determine the spectral separability of both the river monitoring sites and the wetland algal bloom sites using the CASI bands that most closely represent the DMSV bands.

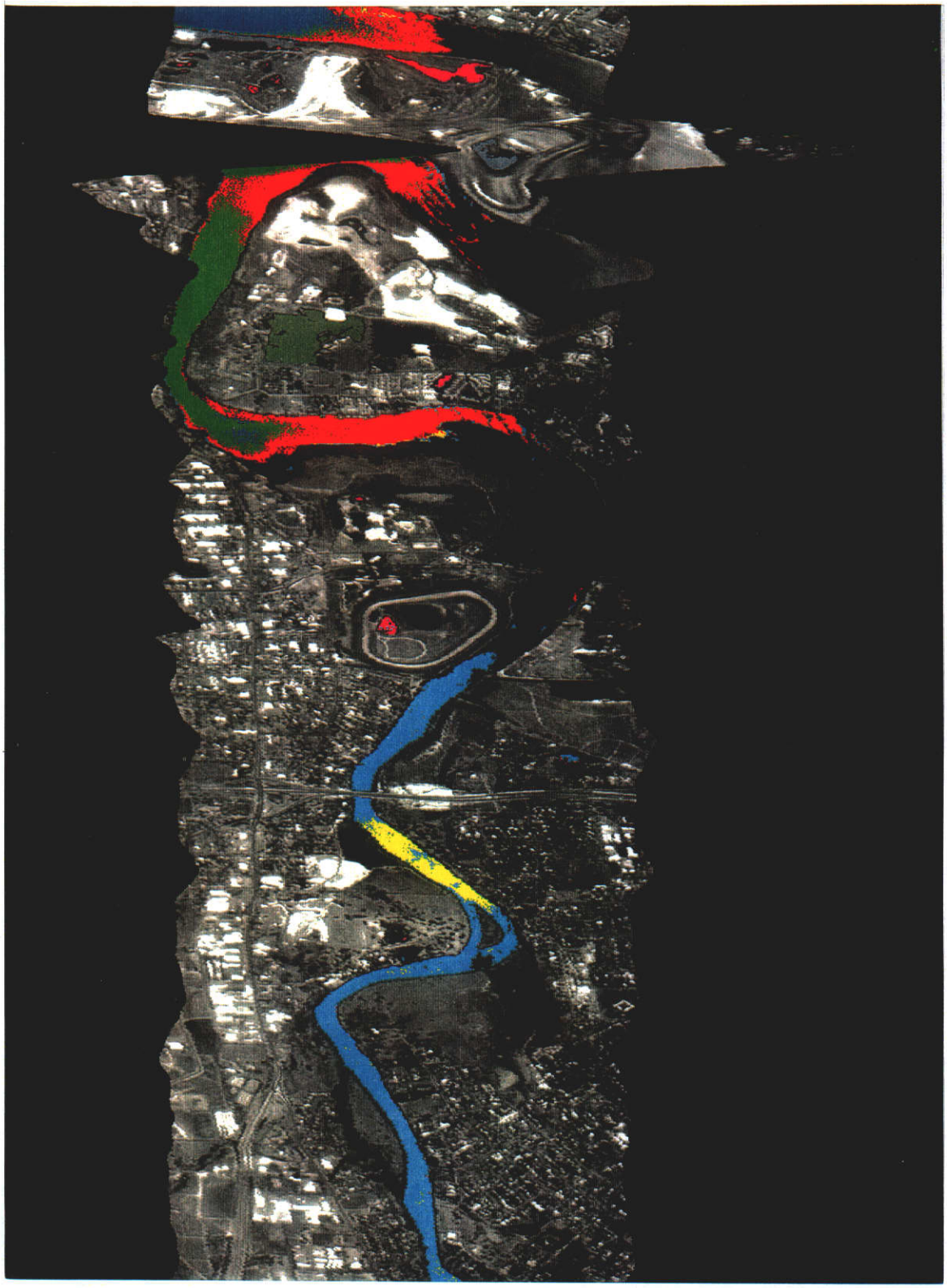

Figure 4.14: CASI classification of Swan River using best-possible-subset bands

The colours represent a scaled range of total cells from low being dark blue, through red, green, cyan and yellow being 20,000 cells/ml. The pink, grey and green represent cyanobacteria in the adjacent wetlands.

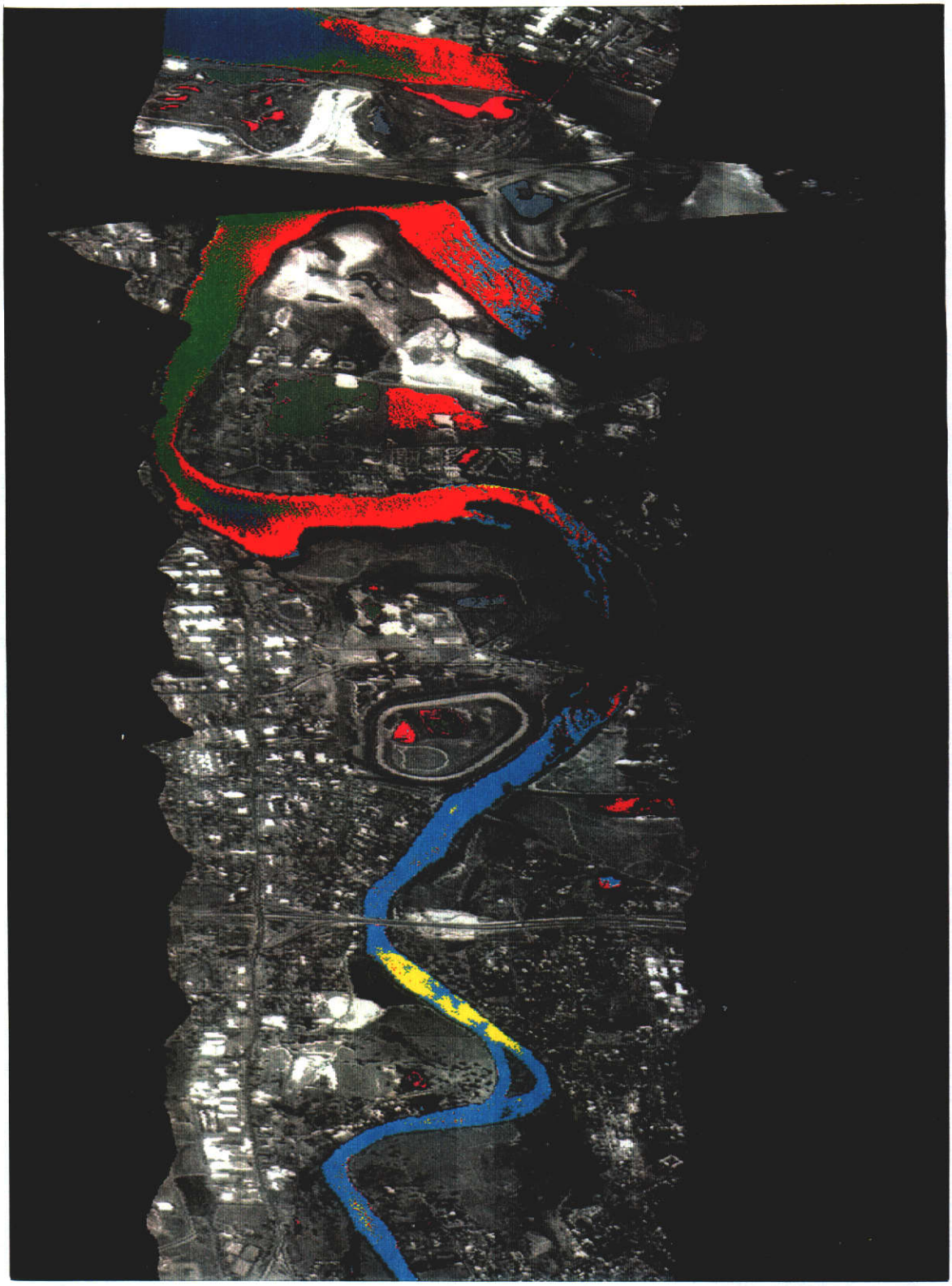

Figure 4.15: CASI classification using only three simulated DMSV spectral bands

The colours represent a scaled range of total cells from low being dark blue, through red, green, cyan and yellow being 20,000 cells/ml. The pink, grey and green represent cyanobacteria in the adjacent wetlands.

The analysis was performed as follows. Firstly, bands 1,5,9,12 were compared with 1,5,9,13, because the DMSV band 4 lies between CASI bands 12 and 13. The sum of roots varied only slightly and the band combination accounted for 57 percent and 52 percent respectively of the total separation provided when all bands were used.

Therefore band 12 was chosen as it is spectrally closer to band four and also gave the higher value. Secondly, to be consistent with the analysis of the CASI data (omission of data below 500 nm), the CVA was re-run omitting band 1, thus leaving the three remaining bands 5, 9, 12, which then accounted for 55 percent of the maximum possible separation achieved using 12 CASI bands.

The classification was supervised by the use of the six sampling sites for which biological data had been recorded. Training of the classifier used pixel values for the area of the river closest to the sampling site.

Figure 4.15 is the same CASI image used in Figure 4.14 but in this example the classes were obtained by processing only the three CASI bands that correspond with the existing DMSV (ie. CASI bands 5, 9, 12). The differences between the class-label images are summarised in Table 4.10 which compares the site by site totals of the allocated pixels.

In effect, if a pixel that was allocated to site *n* using the best subset of CASI bands was also allocated to site *n* using the best subset of DMSV-equivalent bands it is said to concur. If the allocation moved to the adjacent site or sites it is considered as drift.

For example, 666 pixels were allocated to site W2 (Figure 4.5) by the CASI subset, and all those pixels were correctly allocated by the best subset of DMSV-equivalent bands. In contrast, 19404 pixels were correctly allocated to site 5 and about 1000 drifted to the adjacent sites 3, 4 and W1, therefore giving about five percent drift.

Table 4.10: Concurrence of classes between best seven CASI bands and three CASI bands corresponding to DMSV

Three DMSV bands	site1	site2	site3	site4	site5	W1	W2	W3	Uncl
site1	11215	969	439	0	0	0	0	0	251
site2	811	10820	3276	4	0	3	0	0	71
site3	18	1877	15924	153	787	12	0	0	7460
site4	0	0	76	2160	282	0	0	0	1
site5	0	9	37	750	19404	2	0	0	7811
W1	0	0	4	0	33	1642	0	8	2531
W2	0	0	0	0	0	0	666	0	1082
W3	0	0	0	0	0	0	0	3797	2971
Uncl	0	0	0	0	0	0	0	0	1903656

Seven CASI bands

The separation of the six sample sites by the best subset of all CASI bands is good (bands 3, 6, 7, 10, 11 and 12 giving 91.5 percent of separation) and a three-band combination of DMSV-equivalent bands (bands 5, 9 and 12 that accounted for only 55 percent of that separation) is giving a highly comparable result. The cross-aggregation shows that the three DMSV equivalent bands are also able to separate the algal blooms in the wetlands. Drift to other adjacent river classes is on average less than 15 percent. When the comparison of the likely separation of the best-subset and the DMSV-equivalent bands is made with the cyanobacterial algal blooms (W1, W2 and W3) there is concurrence in better than 99 percent of pixels.

From this analysis it is reasonable to assume that the next stage is to test the best-bands selection from the CASI analysis in the DMSV. The choice of the four best

bands would be to use the combination of CASI bands 5, 6, 8 and 10. This relates to using narrow wavebands centred on about 550, 570, 625 and 670 nm.

4.3.4 Conclusions

The examples in this study clearly show what the CASI instrument does well. It is sensitive to spectral features of low to moderate concentrations of algal bloom types and other co-varying parameters. The very high spectral resolution will undoubtedly give great confidence to the selection of diagnostic wavelengths for the remote sensing of water quality parameters. This study also emphasises the difficulty of obtaining spectral measurements of the water column using conventional field methods, and this very important aspect requires further research and instrument development.

However, the real issue to address is: how few bands and how broad can these bands be, to still retain reliable diagnostic information. Recent laboratory studies by Johnsen *et al.* (1994) concluded that, for the 10 main classes of phytoplankton covering 31 algal bloom species that they studied (most of which are in the Swan River system), a set of only three to five specific wavebands yields near-optimum classification success. The challenge is to transfer that success to field operational remote sensing systems for a predictable suite of bloom types.

This study shows that, within the range covered for six river monitoring sites, the classification of water bodies having low to moderate concentrations of phytoplankton is possible, but is probably influenced by co-varying parameters, e.g.

salinity and turbidity. Correlations to cell counts of better than $r^2 = 0.9$ are presented for the limited extent of this study. The domination of the spectral response by the humic component needs to be considered if low concentrations of bloom types are to be sensed. In circumstances where major blooms are likely, this analysis demonstrates that spectral separation is possible. To discriminate between bloom types in the major groups of chlorophytes, cryptophytes and diatoms may also be possible with a limited number of bands.

When the comparison of the separation of the best-subset of all CASI bands and the DMSV-like bands is made only with cyanobacteria in the wetland sites, there is concurrence in better than 99 percent of cases. The cross-aggregation shows that the three DMSV-like bands are able to separate the algae in the wetlands from the river sites with very high reliability, and drifts to other adjacent river-only classes is small.

Delays in the arrival of the CASI instrument unfortunately meant that by February the most severe algal blooms that occur in the Swan River in the spring and early summer were finished, as the river had increased salinities from marine incursions. However, for monitoring the widely scattered water bodies in Western Australia it is likely that a simple low-cost airborne system with as few as three or four well-chosen bands could provide the spectral requirements for detection of blooms, if supported with some in-water calibration. It then becomes an economic question as to the temporal frequency that is preferred for monitoring those bloom occurrences.

4.4 Swan River Study: DMSV Experiment

4.4.1 Aims

The third experiment was to assess and demonstrate the short-term spatial and temporal variation in bloom dynamics and its implication for the timing of field referencing of airborne acquisition using digital multispectral video.

The work with CASI and other baseline spectral sampling highlighted the logistical difficulties of gathering spectral and other in-water information, that cover sufficient spatial area, within the duration of airborne data collection.

The range of potentially confounding factors makes collection of ground truth data essential to calibrate remotely sensed images and algorithms applied to them (Jupp *et al.*, 1994). While these data can be used to calibrate models, the highly dynamic nature of algal blooms and variability in space and time implies that field referencing data collection times should be as close as possible to the remote sensing flight. This may not always be practical and validation sampling to confirm the reliability of image processing algorithms as they apply to other locations and/or times may be necessary.

4.4.1.1 Background

Perth experienced its driest spring, summer and autumn during 1994/5 for over 100 years. Consequently far fewer nutrients were washed into the river and blooms were much smaller, compared with other years. Despite the lack of rain and catchment-

related nutrient input into the Swan River during the summer of 1995, a small bloom of the dinoflagellate *Gymnodinium cf. simplex* occurred in mid-January.

Each year *Gymnodinium* usually forms large monospecific blooms, generally between January and April. *Gymnodinium* is a mobile alga with flagella that allow it to alter its vertical distribution in the water column, presumably in response to environmental parameters such as nutrients and light.

4.4.1.2 Study area

Because of the routine monitoring undertaken by the Waterways Commission and the relative success of the CASI experiment in the Swan river upstream from Perth it was decided to concentrate on that section of the river again (see Figure 4.5).

4.4.2 Methodology

4.4.2.1 Field reference data collection

Sampling locations were recorded automatically by a GPS logged to a laptop computer. The location of each sampling site was further fixed by the sighting of three landward bearings from the boat, and the location of the boat with respect to land features was recorded on an aerial photograph of the section of river to ensure an accurate location of each sampling site. Data collected are shown in Table 4.11

(a) Chlorophyll fluorescence

A Turner fluorometer, logged by a laptop computer recorded *in vivo* fluorescence. Samples were pumped on-board the boat and through the fluorometer from a

darkened intake tube that could be moved vertically in the water column to sample at different depths. Samples were taken at 0.25 m during transit and at 0.25 m, 0.5 m and 1 m depths at each field reference site. Sampling sites were chosen that had approximately 20, 40, 60, 80 and 100 percent (log scale) of the maximum chlorophyll concentration for each day and these were selected to provide a range of chlorophyll values from which to calibrate airborne data. A minimum of five replicates of each sample were taken for each bloom concentration.

Table 4.11: Field reference data collected during the study

Data collected during field trips (Parameter)	Depth	No. reps	Times per day
In vivo fluorescence calibrated to yield chlorophyll a in $\mu g\ l^{-1}$	< 0.25 m	5	3-4
In vivo fluorescence calibrated to yield chlorophyll a in $\mu g\ l^{-1}$	0.5 m	5	3-4
In vivo fluorescence calibrated to yield chlorophyll a in $\mu g\ l^{-1}$	1.0 m	5	3-4
Total suspended solids ($\mu g\ l^{-1}$)	< 0.25	5	3-4
Secchi (m)	variable	1	3-4
Current speed & direction ($m\ s^{-1}$)	1.0 m	1	3-4
Wind speed & direction (knots)	-	1	3-4
Chlorophyll a, b, c & phaeophytin ($\mu g\ l^{-1}$)	< 0.25 m	5	1
Spectral transmission of unfiltered water	< 0.25 m	5	1
Spectral transmission of GFC filtered water ($\approx 1\mu m$)	< 0.25 m	5	1
Spectral transmission of 0.2 μm membrane filtered water	< 0.25 m	5	1
Phytoplankton ID	< 0.25 m	5	1
Cell count (cells ml^{-1})	< 0.25 m	5	1

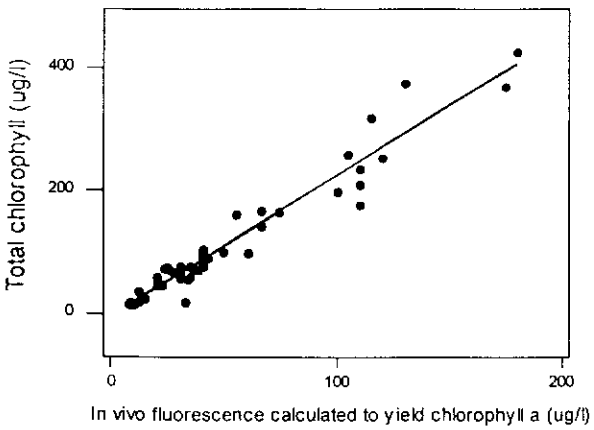

Figure 4.16: Relationship between total chlorophyll and *in vivo* fluorescence

(b) Chlorophyll determinations from filtered samples

Samples for chlorophyll *a*, *b* and *c*, and phaeophytin analysis taken from the surface sample were filtered through a 0.8-1.2 micron GFC filter, and the filter paper, with filtered material, was stored on ice in a completely darkened, insulated container until the samples were taken to the laboratory within one hour of collection of the last sample for that overflight. Data from the first and last day of the study (i.e. 18 and 20 January 1995) were used to calibrate the fluorescence samples from the Turner fluorometer. There was a very good linear relationship between total chlorophyll and fluorescence. Figure 4.16 shows an $R^2 = 0.94$, $N = 50$; $P < 0.001$ (with N = number of observations and P = probability) indicating that more rapid measurement of fluorometry could reliably be used to estimate chlorophyll of the algal bloom.

(c) Spectral measurements

Reflectance spectra of *Gymnodinium* at cell concentrations of 7,300, 28,000 and 47,700 cells ml^{-1} were measured on filter papers using an Ocean Optics miniature field spectrometer covering 360-860 nm. Water samples, also collected for spectral scans, were stored in an iced-chilled container until transportation to the laboratory. Unfiltered samples and samples filtered through both a 0.0.8-1.2 micron GFC filter and a 0.2 micron membrane filter were scanned between 300 and 900 nm for transmission spectra using a Varian laboratory spectrophotometer.

(d) Water clarity

Water clarity was measured using a Secchi disk at each field reference station and the total suspended solids were determined from samples taken at the same time.

Analysis of the total suspended solids (greater than 0.45 micron) were carried out on 1 litre samples.

(e) Water movement

River current speed and direction were estimated by measuring the distance that a subsurface, 1 m diameter-ballasted drogue, set at 1 m depth (with a small surface float) travelled over a set interval of time from the anchored boat.

(f) Biological samples

The species and density of phytoplankton cells were measured each day in the Swan River Trust laboratory from samples collected in the field to which a Lugol preservative had been added.

4.4.2.2 Airborne data collection

The DMSV was installed in a light aircraft and flight plans were lodged for three days of missions over the Swan River in the metropolitan area of Perth. The part of the river that was reported to have shown evidence of the bloom was divided into eight flightlines comprising about 50 DMSV frames each covering about 1 km^2. Spatial resolution was set at a nominal pixel size of 1.5 m x 1.5 m (flying height 2,200 m above ground) and frames were taken with a 50 percent overlap; only the portions of the image unaffected by sunglint were used.

Waypoints for navigation were recorded into a GPS prior to the flights. Flight times were scheduled for 10.00, 12.00, 14.00 and 16.00 hrs with simultaneous in-water sampling planned to coincide with each flight (approximately 45 minute duration).

The flight lines were adjusted to give optimum coverage of the bloom range in the river by communications between the air crew and the boat crew.

As covered more fully in Chapter 2, the Digital Multi-Spectral Video is a four-camera (CCD-array) which frame-grabs and digitises images. Narrow band interference filters at the waveband-centres of 450 nm, 550 nm, 650 nm and 770 nm are attached to each camera. The spatial resolution, as a function of flying height, was chosen to be 1.5 m. The capability of filter interchange, to provide choice of optimum wavelengths for different bloom types was not possible to test, because of a logistical difficulty during this study.

4.4.2.3 Calibration of DMSV data to reflectance

To enable comparison of data from each flight time, and to compare imagery from previous missions, it is essential to calibrate DMSV data. Illumination conditions may vary, and gains and offsets are normally set at the beginning of each flight to optimise the dynamic range of the 8-bit data, but are not changed during the flight.

The method of calibration used to transform raw data to reflectance was a modified "flat-field" correction (Hick *et al.*, 1994). The range of reflectances that are of interest in algal bloom studies in the river is between one and eight percent (Hick and Jernakoff, 1994), and fringing vegetation is of the order of 30 percent in the reflected infrared regions. A target at each end of this range was used to estimate the calibration line. The invariant standard target on the apron and runway of Perth International Airport was approximately 20 percent reflectance. The shadow of bridges and other fixed structures were assumed to have the lowest reflectance value

in the range of interest. The zero value was estimated at 0.9 of these values (Hick and Ong 1995).

4.4.2.4 Image rectification

DMSV images were georeferenced to a SPOT panchromatic satellite image. The usual spatial resolution, or pixel size, chosen for DMSV data is of the order of 1 to 2 m while SPOT panchromatic data have a nominal resolution of 10 m. The linear fit of the DMSV data to the SPOT image is based on a minimum number of ground control points that will give subpixel precision of panchromatic data, selected where possible in each corner of each frame. Each DMSV frame is then "stitched" into the image.

4.4.2.5 Image analysis

The position of each in-water sampling site was located on the image and the calibrated four-band digital data for that site were extracted for analysis. Sites that were sampled more than 20 to 25 minutes before or after the flight times were omitted from the analysis. River current and wind conditions were accounted for during the selection of data polygons and, where possible, the selected areas were in close concurrence to the sampled position. The analysis included linear regressions of the fluorometer data with individual bands and various combinations of band ratios. This was done for all sites grouped as a whole, for all sites on each day, and for the combined sites flown in the mornings and afternoons.

4.4.3 Results

4.4.3.1 Composition of algal bloom types

The algal bloom was virtually monospecific and consisted of the dinoflagellate, *Gymnodinium cf. simplex*. There were small levels of cryptophytes and chlorophytes but these were less than 15 percent of the total cells in the bloom (Figure 4.17).

4.4.3.2 Composition of bloom pigments

The proportion of bloom pigments was relatively constant throughout the study indicating that no major life-cycle changes happened during the study, e.g. bloom death, which would be indicated by an increase in phaeophytin. Over the three days, the percent of the total pigment concentration was 77.3 percent (± 0.9 percent) for chlorophyll *a*, 1.9 percent (± 0.2 percent) for chlorophyll *b*, 18.2 percent (± 0.7 percent) for chlorophyll *c*, and 2.6 percent (± 0.4 percent) for phaeophytin levels.

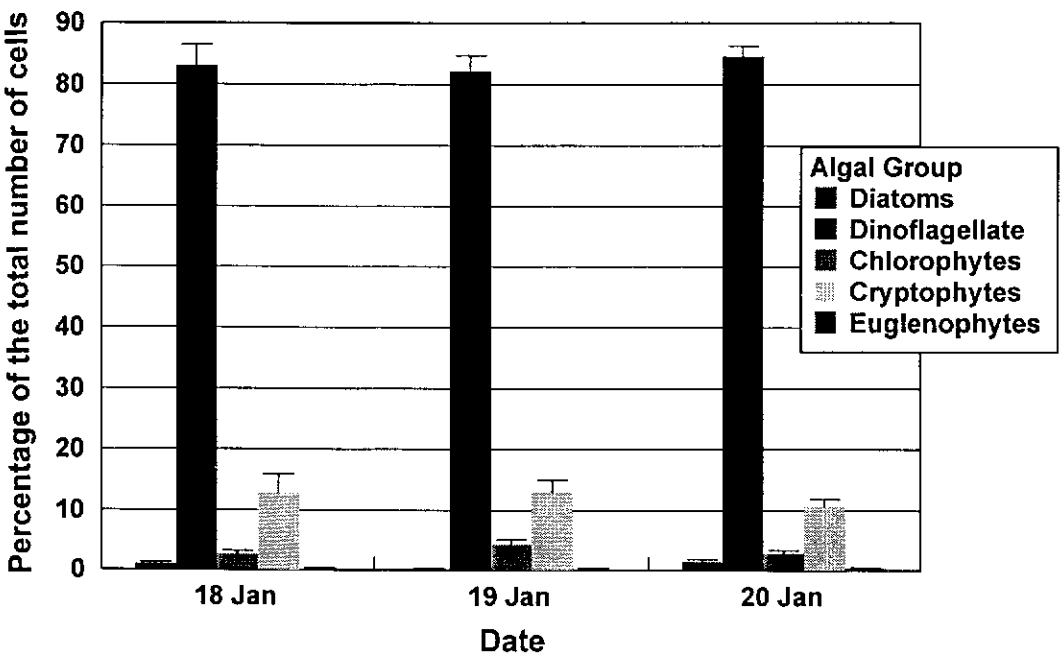

Figure 4.17: Composition (± SE) of algal groups within the bloom

4.4.3.3 Spatial, temporal and depth variability in algal bloom chlorophyll

The distribution of the bloom at the study site, as measured by fluorescence, varied within and between days, and depths within the water column (Figure 4.18). In general, the distribution of phytoplankton in surface waters was greatest in the mid to late afternoon. Data (pooled within and between days) indicated that at the water surface values ranged from 7.5 μg l^{-1} to 340.0 μg l^{-1} while at 0.5 m they ranged from 8.5 μg l^{-1} to 270.0 μg l^{-1} and at 1 m depth they ranged from 12.0 μg l^{-1} to 125.0 μg l^{-1}.

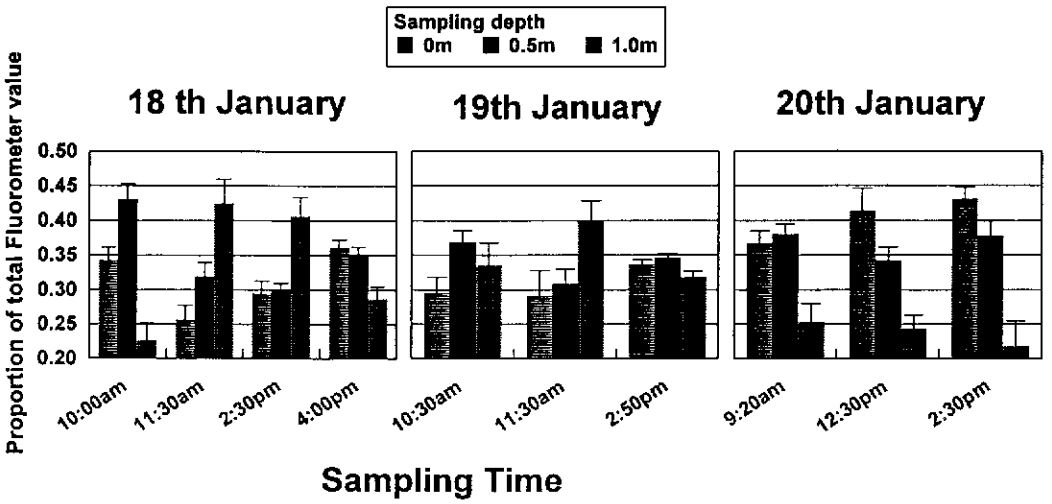

Figure 4.18: Proportion (±) SE of total bloom concentrations

The series of DMSV images provide qualitative information on the dynamics of water column constituents. Figure 4.19 is an example of six single calibrated DMSV frames that show the spatial and temporal variation in bloom dynamics taken at 11.26 a.m., 3.03 p.m. and 3.36 p.m. on Thursday, 19 January and at 10.21 a.m., 11.26 a.m., and 2.20 p.m. on Friday, 20 January 1995, for an area near site 6 (Ron Courtney

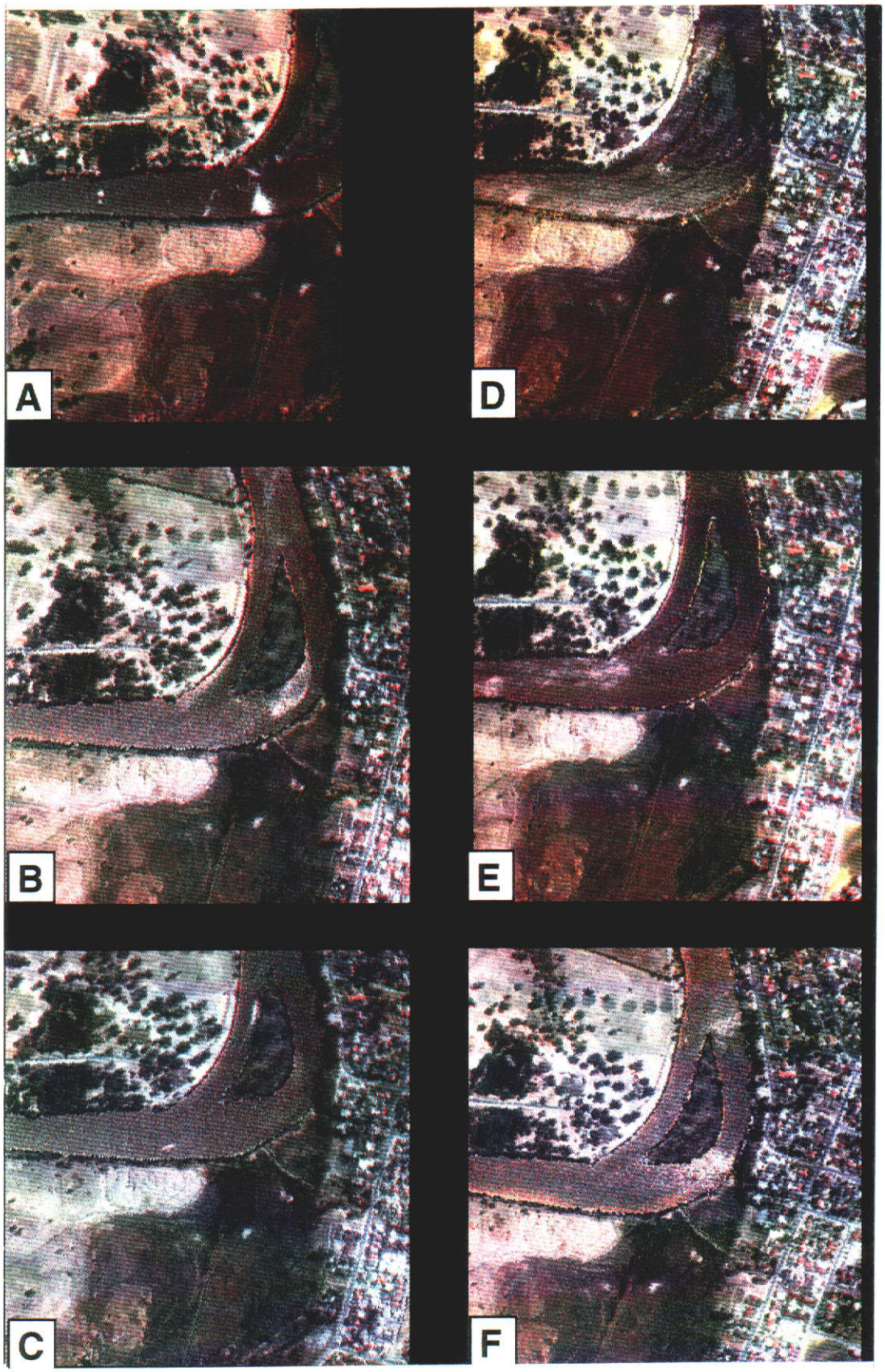

Figure 4.19: Six calibrated DMSV frames, 19, 20 January near Ron Courtney Is

Island). Spatial and temporal variation in bloom concentration and distribution is evident as white patches on the images.

The effects of surface scatter (caused by winds gusting to greater than 20 km/hr causing wave-facets) have been removed from the images, using the techniques developed in the Peel Inlet Experiment described in Section 3.3, before the mosaic was produced. The areas for which in-water data are available lie within these images. The areas where visible and fluorometrically-measurable blooms occurred appear as lighter areas in these enhancements (11.26 a.m., 19 January). These images show that the patterns of algal bloom distribution within the same area of the river vary substantially within a day and between days. These images show also that the areas suspected of having the highest concentrations do not persist for long periods (11.26 a.m., 19 January). However, in images B and C (33 minutes apart, 19 January) this is apparent with the bloom disappearing although the bloom appears in the same place, at about the same time, on the next day (2.20pm., 20 January). Overturn of water caused by the passage of a boat can be seen in some images, and this feature was readily observed by the boat crew.

4.4.3.4 Secchi disk index of light penetration

While secchi depth limits were from a minimum of 0.2 m to a maximum of 1.0 m the overall average Secchi depth was 0.48 m ($\pm$ 0.02 m) during the study. This indicated that it was unlikely that the DMSV could detect phytoplankton below 0.5 m depth. More specifically, Secchi readings were relatively consistent between sampling times on 18 January, but on 19 and 20 January there was a marked decrease in light

penetration in the afternoon sampling period (Figure 4.20) which corresponded with the increase levels of chlorophyll in the upper water column.

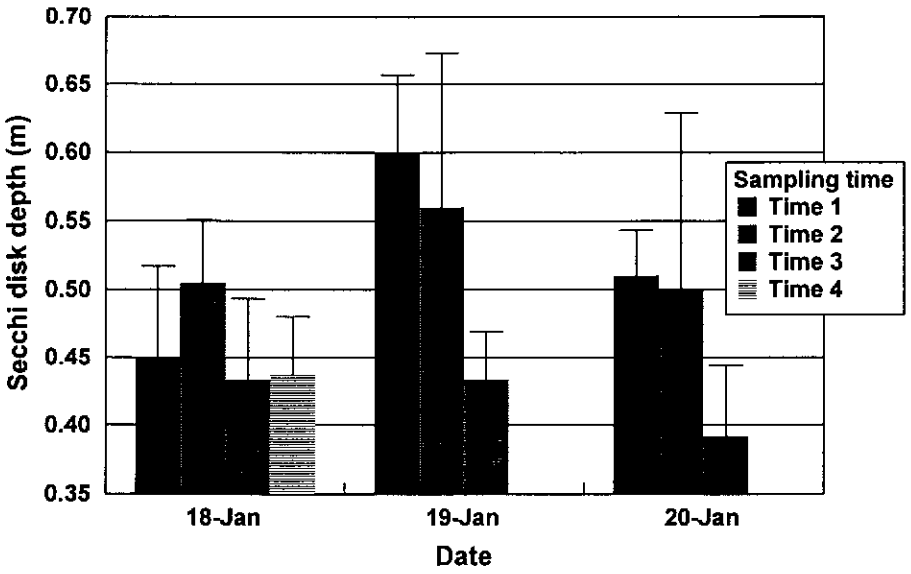

Figure 4.20: Secchi depth penetration

4.4.3.5 Total suspended solids

The level of total suspended solids was significantly higher on 20 January (33.28 mg l^{-1} $\pm$ 0.60 mg l^{-1}) compared with either 18 January (27.24 mg l^{-1} $\pm$ 0.92 mg l^{-1}) or 19 January (26.83 mg l^{-1} $\pm$ 0.91 mg l^{-1}). This difference was believed to be caused by wind-generated water column disturbance and the resuspension of sediments (average wind over the study sites was estimated to be 8 km/hr on 18 and 19 January and 20 km/hr, with gusts significantly stronger, on 20 January).

4.4.3.6 Relationship between chlorophyll, Secchi depth and total suspended solids

The influence of chlorophyll content and total suspended solids within the top 0.5 m, on light levels as measured by Secchi depth penetration, was variable between days.

On 18 January, chlorophyll alone showed a significant negative relationship with Secchi depth ($R^2 = 0.81$, N = 25; $P < 0.001$). This relationship was improved by the inclusion of the total suspended solids in a multiple regression ($R^2 = 0.89$, N = 25, $P < 0.001$): Secchi = 0.657 - 1.03 x Log (Chlorophyll) + 0.00001 x Total Suspended Solids. The contribution of chlorophyll explained 91 percent (of the total sum of squares) of the significant regression, whereas only nine percent was explained by the level of total suspended solids. This suggested that, for this particular day, bloom cells were the major water column constituent that was influencing light levels in the river.

On 19 January some Secchi data were identified as being incorrectly recorded and were removed from the subsequent analyses. Chlorophyll alone showed a significant negative relationship with Secchi depth ($R^2 = 0.41$, N = 18; $P < 0.001$). Once again, this relationship was improved by the addition of the total suspended solids in a multiple regression ($R^2 = 0.75$, N = 18, $P < 0.001$); Secchi = 0.632 - 0.141 Log (Chlorophyll) + 0.000017 x Total Suspended Solids. The contribution of chlorophyll explained 55 percent of the significant regression while 45 percent was explained by the total suspended solids.

On 20 January chlorophyll alone showed a significant positive relationship with Secchi ($R^2 = 0.71$, N = 25, $P < 0.001$) which was only slightly improved by the addition to the multiple regression of the total suspended solids ($R^2 = 0.79$, N = 25, $P < 0.001$); Secchi = 0.351 + 0.0967 x Log (Chlorophyll) - 0.000006 x Total Suspended Solids. This indicates that the contribution of chlorophyll explained 90

percent (of the total sum of squares) of the significant regression with Secchi values, whereas only 10 percent was contributed by the total suspended solids. It is of interest to note that, while there was a negative relationship between Secchi and chlorophyll on the 18 and 19 January, the relationship on 20 January was positive. Furthermore, the only occasion where the amount of chlorophyll was correlated with the level of total suspended solids was on 20 January (correlation coefficient = - 0.676; N = 25, $P < 0.01$). These relationships highlight the highly dynamic and complex nature of the water column constituents within the Swan River.

4.4.3.7 Spectral characteristics of Gymnodinium

These spectra in Figure 4.21 are dominated (98 percent of cells) by the dinoflagellate *Gymnodinium cf. simplex,* which has a mixture of pigments resulting in a brown-orange colour, and characteristic spectral features of chlorophyll *a* generally below 500 nm with a tail of *B*-carotene above 500 nm and other chlorophyll pigments contributing to the shape of the reflectance curve between 660 and 700 nm.

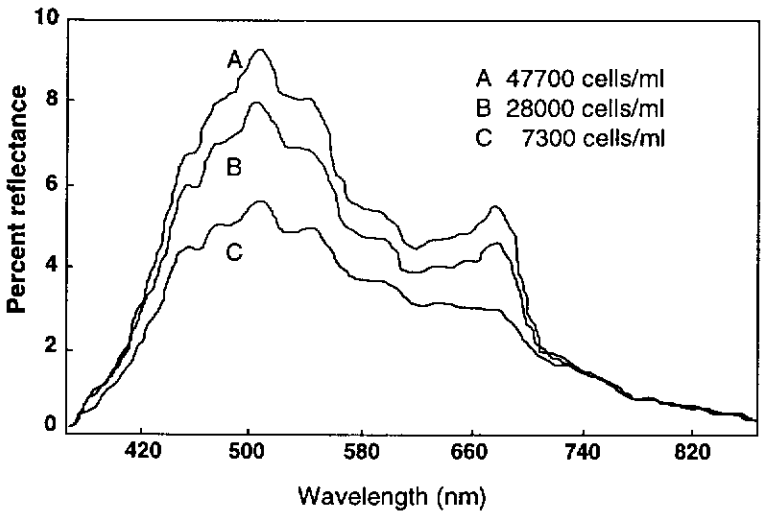

Figure 4.21: Reflectance spectra of *Gymnodinium* at three concentrations

4.4.3.8 DMSV data compared with algal bloom concentration

A serious hardware malfunction in the DMSV on 18 January resulted in the loss of most of the video data collected for that day. However, on that and the other two days, a total of 27 sites had data from in-water samples at coincident times (within 45 minutes) of the overpasses of the DMSV. The analysis was performed on those 27 data sets.

There was no combination of bands, or a single band, that gave a consistently good relationship to fluorometer measurements across all times and days. The best regression was against band ratios of b1/b2 (R^2 = 0.58, N = 13, P = 0.002) on 19 January, but this good relationship of b1/b2 was not consistent on the other two days (R^2 = 0.36, N = 6, P = 0.211) and (R^2 = 0.11, N = 5, P = 0.594). The best band combination on 18 January was b2/b3 (R^2 = 0.47, N = 6, P = 0.135) and b2/b4 (R^2 = 0.37, N = 5, P = 0.274) on 20 January. There was a poorer relationship when all the days were combined and when the mornings and afternoons were compared. The best relationship for fluorescence for morning data was for the ratio of band b2/b3 (R^2 =0.801, N = 17, P = 0.004). Using the afternoon data the best relationship was obtained using the ratio of band 1/3 (R^2 = 0.54, N = 10, P = 0.015). Thus, a significant regression was only apparent using the afternoon data (which was also when more phytoplankton tended to be in surface waters).

4.4.4 Conclusions

Algal blooms such as *Gymnodinium* are very dynamic in space and time. Although this study was unable to determine whether the bloom's temporal and spatial

patchiness was caused by horizontal advection or vertical migration of the phytoplankton cells (or a combination of both), it has highlighted the need to take account of this variability during in-water sampling for calibration and validation of remote sensing data.

Regardless of the reason for the bloom patchiness, the study indicates the need to ensure in-water sampling is carried out within a short time of overflight. It also highlights the problems of collecting enough in-water samples within that restricted time period. The small number of samples at some sites and times within the overflight period may be the reason why several anticipated trends in the data, based on the boat observations, were so poor. A better approach that would obtain more samples within a short time period would be to use several fluorometers simultaneously.

In the present study, the 1.5 m x 1.5 m pixel size provided good discrimination of bloom distribution within the Swan River. It also allowed several replicate pixels within the images to be measured for analyses and interpretation, and it was possible to sample at a similar spatial scale during in-water sampling.

In this study the DMSV did not, with its existing band combinations, show any satisfactory relationship with in-situ measurements. This suggests that, for blooms like *Gymnodinium*, the system as currently configured could not reliably be used to quantify the bloom concentrations. The lack of characteristic diagnostic features, specific to the bloom or the river humics, and the dynamic movement of the bloom

over time suggests that, even if clear diagnostic bands are available, it may not be possible to estimate *Gymnodinium* concentrations in the river from the air.

Issues of water-clarity and the biology of the particular phytoplankton species may also affect the ability of remote sensing platforms such as DMSV to describe accurately a bloom's distribution and abundance within the water column. This may not be a problem for surface forming blooms (e.g. cyanobacteria, Jupp *et al.*, 1994) that are easily detectable remotely. However, for those blooms such as *Gymnodinium*, which can alter their distribution within the water column, it is essential that the timing of remote sensing flights be coincident with maximum daily abundance at the water surface if the bloom's magnitude and extent is to be determined.

In conclusion, at the time of the design of the experiment it was not possible to adequately anticipate the abnormal lack of bloom diversity or the logistical limitations. This is a point that should not be lost on others planning such coordinated studies. The problems in quantifying in-water data on algal blooms, with data from remote sensing, requires ground sampling to be done simultaneously or within a very short period of the remote sensing flight. For accurate assessment of bloom distribution, flights must coincide with the biological activity of the phytoplankton (i.e. daily afternoon migration of cells to the surface waters) and at times of the day that will minimise sunglint. If flights are not so timed, the relationships between bloom distribution and abundance, and remotely sensed images will be poor. A good relationship between the ground data and the images is

obviously necessary for detection and estimation of bloom concentrations. However, in situations where blooms are rapidly changing, remote sensing provides an effective tool for describing in a qualitative sense, the dynamic nature of the bloom at a particular moment over large spatial scales.

4.5 Summary

The chronological sequence of these three studies represent an evolving theoretical and applied understanding of the problems that face managers with the responsibility for maintaining a high standard for our rivers and coastal systems. The apparent simplicity of identifying, and even quantifying a toxic bloom, such as cyanobacteria, creates enthusiasm that is difficult to match in reality.

The opening preface of this chapter that *"It is widely accepted that the spatial extent of visible effects of phytoplankton and chlorophyllous materials can only be measured practically using an appropriate form of remotely sensed data"* is commonly believed but the words *"practically"* and *"appropriate"* are often forgotten.

The use of remote sensing to detect and quantify algal blooms requires that a relationship exist between in-water data and the remotely sensed image. Although the detection of, for example, cyanobacterial algal blooms in this and other studies has been highly successful because of the algae's distinctive spectral pigments (Jupp *et al.*, 1994), detection of the brown-pigmented dinoflagellates is more difficult, especially in humic dominated water such as in the Swan River.

Earlier work, reported in this study, compared different algal blooms using CASI and this indicated a variable relationship between spectral bands and the type of phytoplankton. While there was a strong relationship between spectral bands and cell count for the dominant cryptophyte, *Cryptomonas sp.*, that was occurring in the river at that time, the relationship for dinoflagellates with the main species *Gymnodinium* was low ($R^2 = 0.44$). A synthesis of the DMSV using the CASI data indicated that even the existing DMSV bands (centred at 450, 550, 650 and 770 nm) would provide a diagnostic capability for most bloom types in the river system. However, for blooms with spectral characteristics such as *Gymnodinium*, this relationship would not be expected to be strong.

The initial studies using the Geoscan and the OCS would "blow the budgets" of even well-funded environmental managers, but in a research study these implications are secondary. The CASI instrument, unfortunately, also falls into the same category, especially as most applications require rapid answers in frequent repeat cycles. The trend to low-cost video-based systems could not be shown, albeit for serendipitous reasons, to provide a perfect solution to the problems associated with quantifying the characteristics of the water column.

Chapter 5

DETERMINATION OF BOTTOM CHARACTERISTICS

5.1 Introduction

Local studies performed by, or associated with, the CSIRO WA Remote Sensing Group (Lyons, 1976; Hick, 1978; Honey and Byrne, 1978) indicated that the full potential of remotely-sensed data for water penetration had not been achieved. However, many examples of aquatic habitat mapping, using aerial photography, produced satisfactory results. These photos were often acquired using non-standard specification such as yellow (wratten 12) filters and slight over-exposure (Honey and Hick, 1976b). The benefits of satellite data over aerial photography showed that a narrower field of view reduces the solar-flaring effects, and multiband digital data can mathematically remove the effects of pathlength and surface scatter (Lyzenga, 1978). Satellite data also usually have fewer geometric rectification problems. Simple water reflectance models, which account for most of the signal received for a given band over clear shallow water, are considered in this chapter and examples given have been chosen to illustrate the potential practical applications.

Landsat TM data have been used to great advantage in the delineation and mapping of substrate features in shallow coastal waters. The position of TM band 1 (450-520 nm) is ideally situated to avoid atmospheric absorption and permit maximum measurement of water-leaving upwelling radiance. The other water-penetrating band of some use in the TM instrument, band 2, can provide information on water column

characteristics, and any of the infrared bands can help to delineate the dry land/water interface. However, the uncertainty when purchasing what appears on the microfiche quick-look to be a cloud-free and clear-day image has left many disappointed potential users. Further disappointment can occur with the realisation that some mathematically elegant algorithm, that was supposed to deliver contoured bathymetry, is unsuccessful.

These outcomes led the direction of the research to investigate the advantages, in terms of timing flexibility and spectral selection, of airborne-based digital scanning systems for bathymetric purposes. This chapter covers the progress of the research that addressed the shortfalls experienced with satellite-based acquisition, with the results of studies that were designed to produce useful information on benthic habitat, using both the Geoscan Multi-Spectral Scanner and the Compact Airborne Spectrographic Imager.

The problems and expectations of "in-water" spectral measurement of benthic habitat discrimination are also covered and the use that can be made of such data are summarised in Chapter 6. These examples serve to enforce the determination and industry requirement for specific and spatially-coherent information about the near-shore bottom habitats and the need to monitor change to these environments over time.

5.1.1 Upwelling radiance from a waterbody

A simple water reflectance model which accounts for most of the signal received for

a given band over clear shallow water but combines the effects of scattering in the column and at the water surface as given by Jupp (1988) is:

$$Li = Lsi+ki\ rbi\ \exp(-Ki\ f\ z) \qquad (5.1)$$

where for band i:

si is the radiance of deep water,

ki is a constant for solar irradiance, atmospheric transmittance and surface refraction,

rbi is bottom radiance,

Ki is the attenuation coefficient of the water,

f is the geometric factor for pathlength, and

z is depth.

5.1.1.1 Substrate radiance

Lyzenga (1981), offered a single index for substrate radiance based on a log ratio of two bands (xi/xj) plotted on an axis with variability of substrate being a function of distance from the axis. Bierwirth *et al.,* (1993) used another approach to derive substrate reflectance and depth in the same algorithm. They used the multispectral data and water attenuation coefficients to produce images of bottom reflectance and depth.

As discussed in Chapter 1, and briefly restated here, basic models for radiance, R, the measured energy recorded at the sensor, at waveband, i, may be resolved into components involving the atmosphere and radiation leaving the water surface such that:

$$R = ti\ (Li + Lsi) + Lai \qquad (5.2)$$

where:

R is radiance recorded at the sensor,

ti is total atmospheric transmittance,

Li is radiance from the water column,

Lsi is radiance returning from the water surface, and

Lai is radiance scattered into the sensor field of view by the atmosphere.

Radiation emerging from the water column Li includes effects of depth, sea floor type and particulates in the water column. In cloud-free imagery, of the type usually selected for this work, assumptions may have to be made that ti, Lai and the reflected component of Lsi are uniform across the image. If this is not the case where sun angles produce "sun glint", and solar azimuth and elevation give across-track illumination variation, correction may need to be applied to Li and Lsi for some scenes. Corrections to Lai, the atmospheric component, may be possible by using other wavebands of Landsat TM.

Li has constituent components which need further consideration. These may be suspended sediments, dissolved substances or chlorophyll-based material in the water column or the textural components of the sea floor. Li can be measured with a radiometer at the sea-surface, and calibrated against a Lambertian standard. Lsi can then be derived, in a crude form, by radiometric samples above and below the ocean surface skin.

The next consideration, which is vitally important for studies that focus on substrate stratigraphy and habitat mapping, is to separate from the total water-leaving radiance Li, the bottom component rbi from the scattering and absorption of materials in the water column. This can be done with the use of in-water spectral measurements.

A very good general approximation suggested by Jupp (1988) is based on Equations 5.1 and 5.2, and describes the way water properties, substrate reflectance and water depth affect resultant signal. This is:

$$Li = \exp(-2\, ki\, D) \qquad (5.3)$$

where:

ki is the effective attenuation coefficient of the water mass, and

D is depth below the water surface.

Li and Lsi are affected by solar elevation. Illumination increases with solar altitude but so does the surface backscatter and sunglint component Lsi. Surface roughness or spatial reflecting facets can significantly reduce the usefulness of the image data. Methods and techniques with specific relevance to removal or correction of this component are covered in Chapter 3. Resampling high-resolution data to a lower order of spatial resolution can also be used to smooth the data and therefore appears to remove some of the effects of facet scattering.

5.1.1.2 Bathymetric determination

The bathymetric determinations based on some linear relationship of shallow ocean depth and reflected solar energy from the ocean bottom were defined by Doak *et al.*

(1980) and the model is given in Chapter 2. Subsequent site-specific variations, Jupp (1988) and Bierwirth *et al.* (1993), have covered this topic well.

5.1.1.3 Signal to noise considerations

Signal-to-noise ratios are not generally a problem with conventional applications of satellite data. However, for in-water related image processing, where Dn values between target materials are small (differences are often of the order of a few digital counts within a range of 0 to 255), processing is aimed at the maximum information retrieval. The enhancement is limited by the radiometric resolution of the sensors, and the SNR can introduce image degradation which would be unacceptable for most terrestrial applications. However, for qualitative interpretation of linear or reasonably homogeneous pattern edges a lower than normal SNR is often acceptable.

Airborne digital systems usually offer the capability to set instrument gains and offsets, based on the pre-acquisition analysis of the signal range for a test run over the target area, which enables the maximum dynamic range selection to suit the sensitivity of the instrument. The Thematic Mapper detector arrays have across-track, multi-line mirror systems coupled to the detectors which have fixed gains and offsets that may not be identically calibrated. These can produce horizontal striping in the data which is often most evident in TM band 1. Algorithms which sample entire rows or columns and then apply a mean-average correction can remove much of the striping caused by detector arrays without significant data degradation.

5.2 Broome Project

5.2.1 Background

TM data have been used at scales compatible with nominal 30 m spatial resolution for the delineation of mapping substrate features in shallow coastal waters. A research project in the La Grange area, south of Broome W.A. (Hick and Scoones, 1988; Scoones and Hick, 1990), surveyed the distribution of habitat for pearl oysters and prawns using both Landsat and SPOT data.

As stated earlier the blue-blue/green TM band 1 (450-520 nm) is ideally situated to avoid atmospheric absorption and permit maximum measurement of water-leaving upwelling radiance. The other bands of some use in the TM instrument are: the green/yellow band 2 (520-600 nm), that can provide information on water column characteristics; the red band 3 (600-700 nm) that can in some cases provide information on quantity and nature of turbid particulates; and the infrared bands, as they do not penetrate water at all, can help to delineate the land/water interface. Reflected infrared wavelengths are also useful to separate the effects of organic (floating) and physical (wave scattering) surface components of an image.

Possibly the earliest use of TM data for commercial fishing in Australia was for the pearling industry in Broome. Figure 5.1 is a location diagram of the study area. However, prior to the inclusion of the details here, that report was kept in commercial confidence, which enabled the funding company to reap the extensive benefit that the outcomes of this research provided. Parts of the original restricted

report, "Satellite Data Use for Studies of Benthic and Bathymetric Characteristics of Sub-Sea Stratigraphy in the Eighty-Mile Beach Region of Western Australia. (Hick and Scoones, 1988)" was later presented to the wider fishing industry as "Bathymetric imagery and its relevance to fisheries in the tropical regions of Western Australia" (Scoones and Hick, 1990).

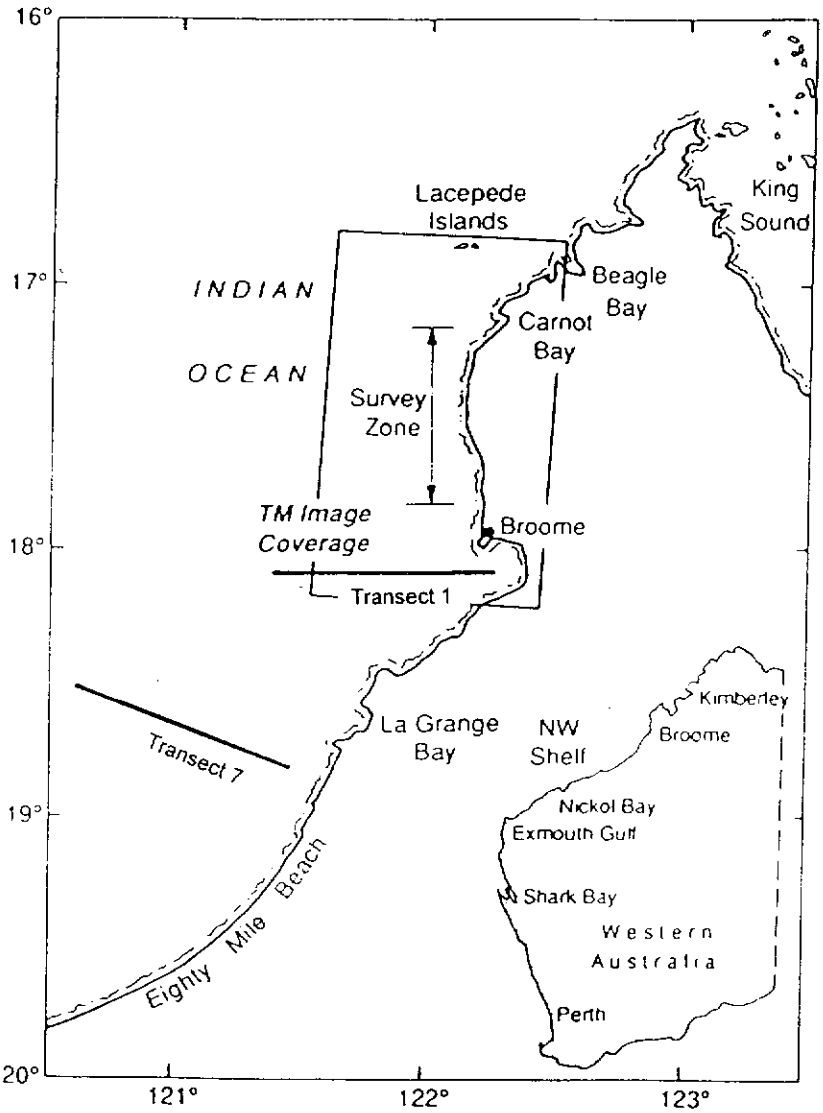

Figure 5.1: Location diagram of Broome study area

5.2.2 Aims

The experimental aims of the project were to:

(i) Determine the quantitative relationship between reflectance and depth as a basis for bathymetric mapping using passive sensors;

(ii) Determine spectral reflectance characteristics of the benthic habitats of pearl oyster *(Pinctada maxima)* and Western King Prawn (*Penaeus latisulcatus*) in relation to the catch records from the "R.V. Flinders" cruise;

(iii) Map sub-sea stratigraphy, and subsequently interpret the positions of, and modification to, the ancient coastline sequences; and

(iv) Evaluate existing remote sensing systems and image enhancement techniques for water penetration, and select optimum multi-temporal and multi-spectral wavebands within the physical constraints of:

- wavelength
- sun angle and surface reflectance
- atmospheric absorption and scattering
- turbidity, and sea state
- phyto/zoo planktonic blooms, and
- ocean floor reflectivity.

Broome Pearls Pty Ltd requested CSIRO to evaluate the recently developed processing techniques for satellite data for their applications. The Hick and Scoones (1988) study compared Landsat TM and SPOT images and the choice of TM was based on that information. No similar work to date had been performed in Western Australia.

Following that research project in the La Grange area an extension of that study was funded, in part, by the Western Australian Fisheries Department. This study was to correlate the data gathered from the 1987 Flinders cruise (Penn and Dybdahl, 1988) with the satellite-based techniques. Their report had the specific objective of surveying the distribution of pearl oysters and prawns in the Broome area between 17 and 18 degrees South latitude. This had been prompted by reports that prawn trawlers were interfering with the established pearl oyster grounds. (The Commonwealth Government subsequently closed the area to prawning).

5.2.3 Methodology

The two Landsat TM images that were acquired for comparison with the Flinders data were for Path/Row 111/072 on 30 September 1986 and 11 December 1987. Tides for the 0930 local acquisition times were high (5.7 m at 0918 hr) for the 1986 image and were incoming (low 1.6 m at 0742 hr, high 6.8 m at 1353 hr) for the 1987 image. The images were rectified to a geocoded map base and resampled to a 50 m pixel size. These two images were merged with a vector file compiled from the hydrographic information extracted from chart AUS 324 (1987) and the sample location points supplied from the Flinders survey. Image processing techniques were used to enhance subtle edge-effects based on the filtering convolution kernels that were devised to highlight features resulting from orientation or heterogeneity.

Radiance measurements were made with a specially modified Exotech radiometer and reflectance was derived by comparison with a $BaSO_4$ standard target. This instrument is a 4-band, Landsat MSS-equivalent radiometer that had been modified

with a 25 nm band, centred at 485 nm, to replace the infrared band. This modification creates a narrower but similar band to TM band 1.

5.2.4 Results

5.2.4.1 Ocean reflectance

Radiance from the ocean floor is limited by atmospheric scattering, surface reflectance and column absorption. However, a relationship between the thickness of the water column and radiance may be interpreted as bathymetry where the nature of the bottom materials are reasonably uniform. An example of this relationship is shown in Figure 5.2, which shows data extracted from a transect running roughly west from Broome out to the 30 m bathymetric contour (Transect 1, Figure 5.1). The data were extracted from areas which could be identified on the charts and which on the image showed to be uniform with a reasonably flat, clear bottom.

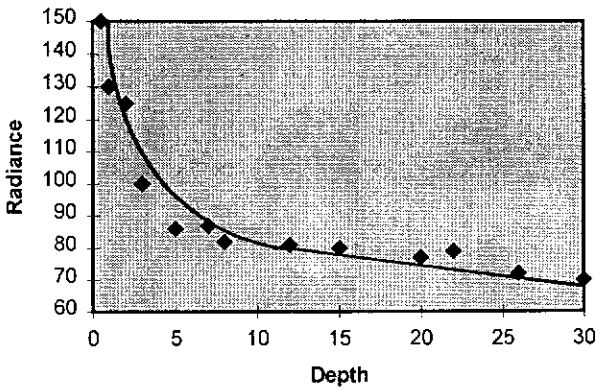

Figure 5.2: Satellite-measured radiance and its relationship to depth

Another transect (Transect 7, Figure 5.1), chosen to sample reflectance from the ocean bottom, is shown in Figure 5.3 and was taken from the cruise records of the

"Pacific Lady". This transect ranges between about 20 and 30 m in depth, which is probably the critical depth for which additional penetration is provided by TM band 1. Analysis from four stations show that the reflectance levels from the modified TM band 1 equivalent are of the order of 1.19 percent at position RI (29.9 m), 1.75 percent at R2 (23 m), 2.28 percent at R3 (23 m) over rough bottom, and 2.00 percent at R4 (22 m) on the smooth bottom types. This reflectance difference of approximately one percent between depths of the order of 20-30 m is of the same order as the digital counts of reflectance measured by the satellite.

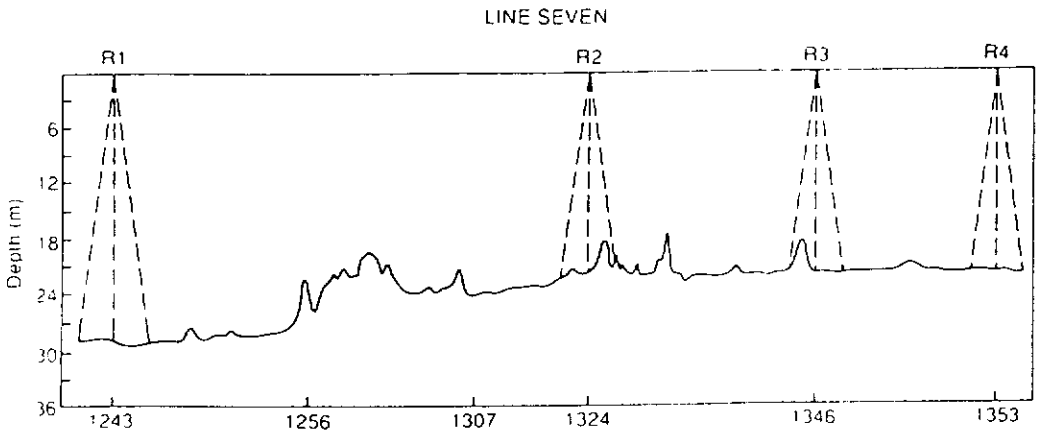

Figure 5.3: Transect line seven from Pacific Lady cruise

The 8 bit quantisation (0 to 255) of TM data translates to about 2.5 digital counts for each one percent brightness or reflectance. The digital enhancement of the data confirmed these levels of reflectance. The ship-board reflectance measurements were taken between 1200 and 1400 hrs on the 19 August, 1988 which gave solar altitude maxima of 50 degrees at noon to 44 degrees at 1400 hrs. The solar elevation of the imagery was 50 and 55 degrees respectively. Both the September and December acquisitions were recorded near 0930 hrs local time.

Figure 5.4 shows solar elevations plotted from Kodak R10 Computations for 20 degrees South latitude at 0930 hr local times. Figure 5.4 also includes the SPOT acquisition which was used in Hick and Scoones (1988) and the reason for its rejection is quite clear on the basis of sun angle (approximately 45 degrees). What is not so clear is how useful SPOT might be with the additional sun elevation because of its later acquisition time (1045 hr local time). This would permit summer solstice solar elevations of up to 75 degrees (i.e. 20 degrees higher than TM). This additional illumination would have some trade-off due to SPOT's less appropriate band 1 (500-590 nm) compared with TM's band 1 (450 - 520 nm). The Japanese MOS-1 satellite has comparable bands and acquisition times with SPOT.

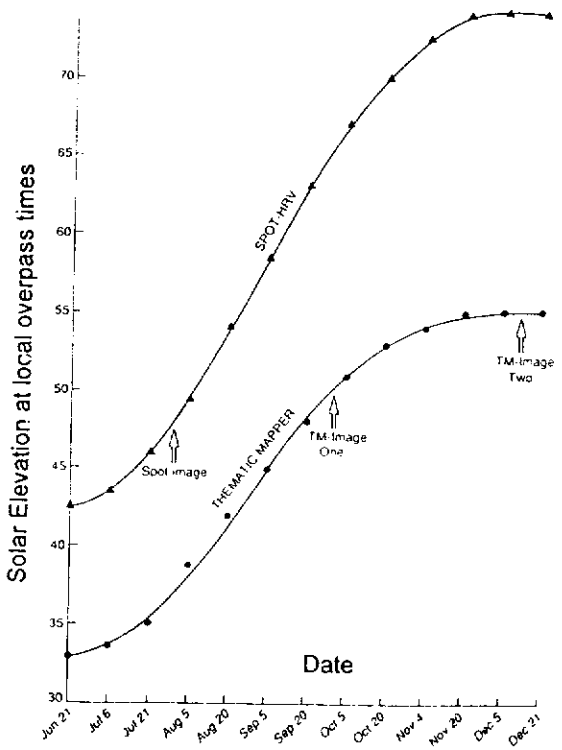

Figure 5.4: Graphs of solar elevation from winter to summer solstice at 20°S

5.2.4.2 Data filtering

Digital filters, described earlier in Chapter 3, are a very useful means of altering the appearance of image data for various purposes. The filter kernels displayed in Figures 5.5 and 5.6 were used to derive Figures 5.7 and 5.8 respectively, and show the effect of varying the weightings of directional filters. . Figure 5.7 (a) shows enhanced raw data, (b) has centre pixel value of -2, (c) has -3 and (d) has -4.

1	1	1	1	1	-1	1	1	-1	1	1	-1
1	1	1	1	-2	-1	1	-3	-1	1	-4	-1
1	1	1	1	1	-1	1	1	-1	1	1	-1
	(a)			(b)			(c)			(d)	

Figure 5.5: Effect of varying weightings of an "east" directional filter.

Kernels were also tested to provide directional filtering to the north-east, south-east, and south to complete the major directions and test the effects of this image processing on the physical orientation of linear features. This technique is often used by structural geologists to map geological lineaments. These kernels were as follows:

1	-1	-1	1	1	-1	1	1	1	1	1	1
1	-2	-1	1	-2	-1	1	-2	1	1	-2	-1
1	1	1	1	1	-1	-1	-1	-1	1	-1	-1
(a) n-east			(b) east			(c) south			(d) s-east		

Figure 5.6: Kernels designed to provide directional filtering

All of these treatments have subtle variations in data presentation but none appeared to significantly improve the image over the raw data. The reasons for this relate to the signal-to-noise ratio of the raw data. The subtle north-south trending features in

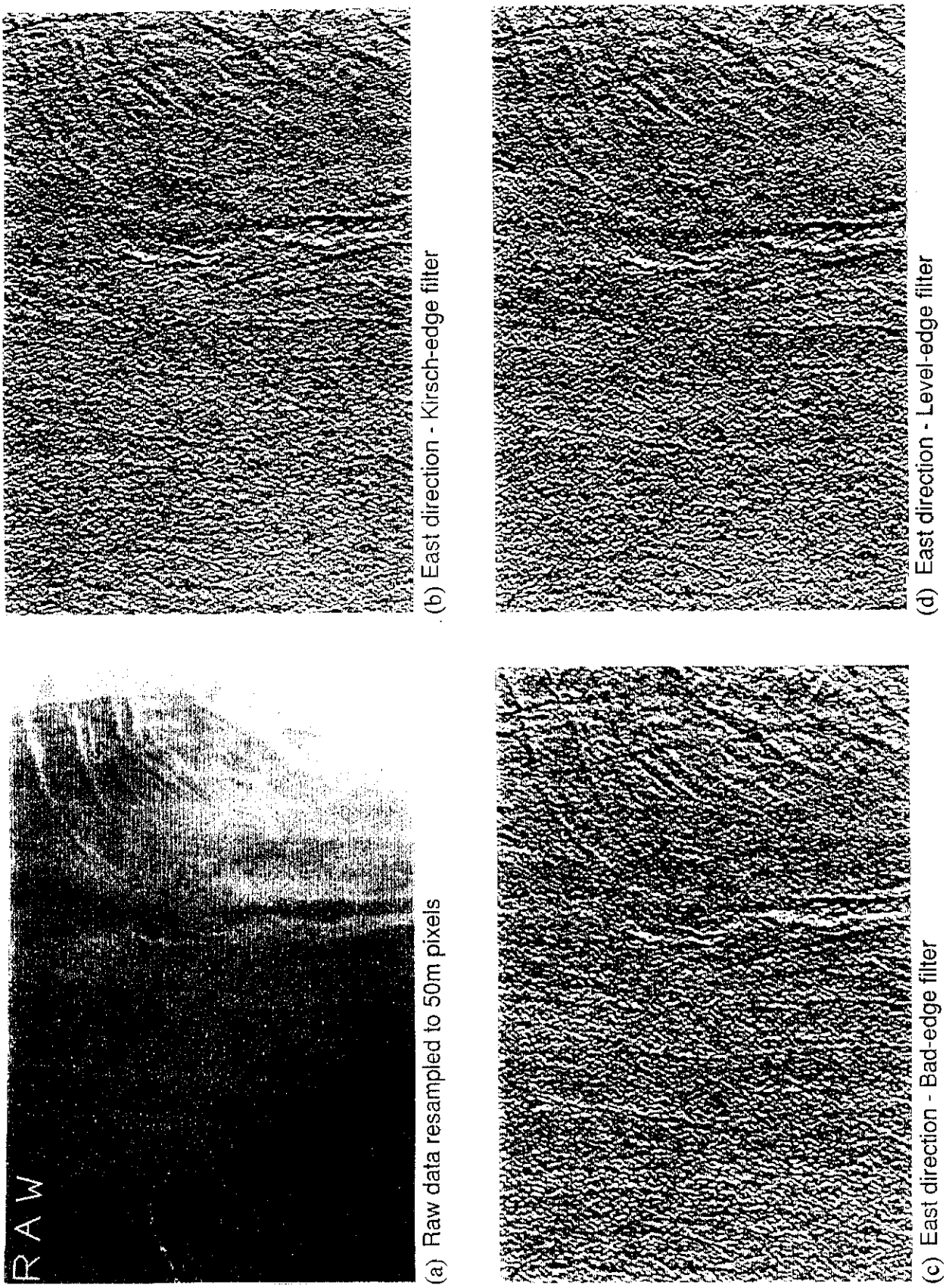

Figure 5.7: Band 1 enhancement (a), weighted edge filters in (b), (c) (d)

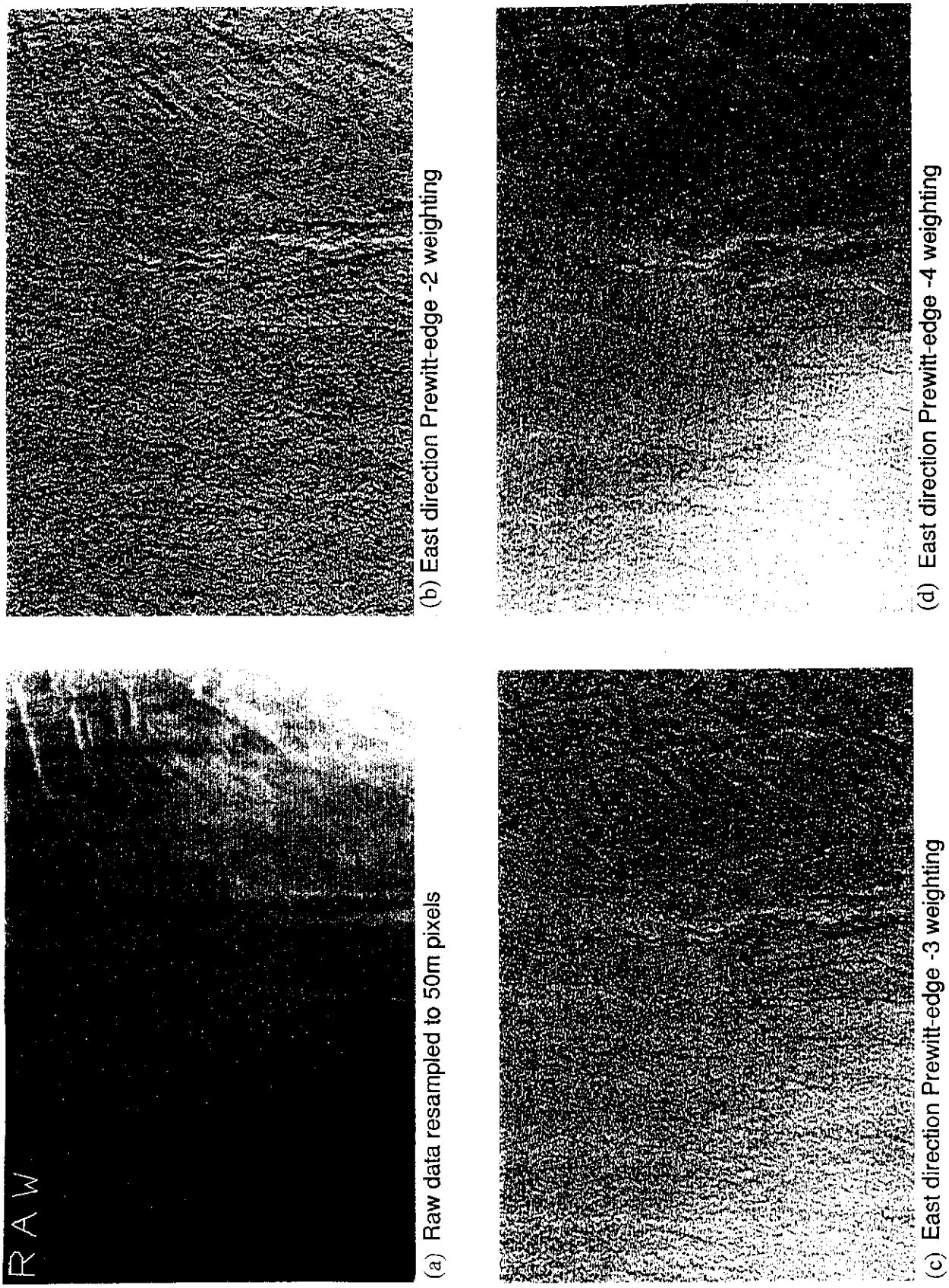

Figure 5.8: Direction filters to highlight discontinuities and heterogeneity

Figure 5.8a, and displayed with varying clarity in Figure 5.8 (b), (c) and (d) are based on filtering convolutions which highlight direction or heterogeneity. The features on the raw image have north-south trends although other trends are clearly visible in shallower depths.

5.2.4.3 Atmospheric effects

Water vapour in the atmosphere causes scattering especially at the TM band 1 wavelength (450-500 nm). The high signal-to-noise ratio of band 1 can be a function of this non-visible atmospheric water content. Figure 5.9 shows examples of an area between Carnot Bay and the Lacipede Islands. Top left (a) is produced from TM band 4 (760-900 nm), which shows the land/sea boundaries very clearly, and also shows an apparently clear atmosphere (since any cloud should be evident at these wavelengths). Top-right (b) is an enhancement of TM band 1 which, as well as showing good water penetration, also shows patterns which are attributed to atmospheric water vapour.

Indications of this water vapour variability comes from (c), bottom-left, which is an enhancement of the Thermal TM band (10,400-12,500 nm). This band is detecting the effects of cold (atmospheric) water vapour, showing as black, which has not yet formed into visible clouds.

The bottom-right frame (d) is a composite of TM bands 1 (blue), 4 (green) and 6 (red). The effect of this water vapour, now showing in red, results in loss of visible light penetration into the water column. Reference back to (b) shows bottom features

(a) Band 4 showing no visible cloud

(b) Band 1 showing water vapour effect

(c) Band 6 (Thermal) showing water vapour

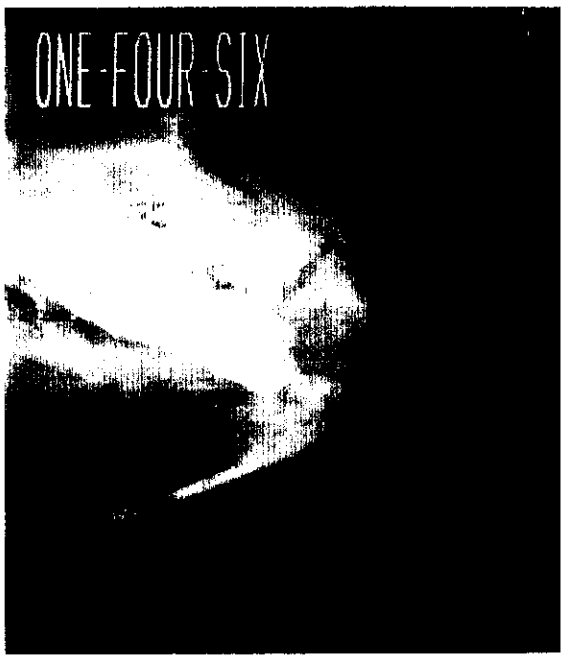

(d) Composite bands 1,4 and 6

Figure 5.9: Landsat TM band displays for part of Broome Study Area

clearly away from the areas of heaviest concentrations of water vapour. Crude calibration of the entire scene, or specific parts of interest, is therefore possible by correcting band 1 in response to the levels in band 6.

5.2.4.4 Ocean floor features

The evidence of strandline features both on imagery and on the bathymetric transects (Hick and Scoones, 1988) relates well to the accepted Holocene marine transgressions which show stillstands (or periods of stable sea level sufficient to develop persistent shoreline evidence) at about 30 and 15 m below present sea levels. These features indicate that the coastline in this area has been relatively stable tectonically during the Recent geological record (Hick, 1978).

Figure 5.10 has been extracted from Bird (1976) and combines in part earlier work of Fairbridge (1961). The sequences of "stillstands" in the generally accepted "Flandrian Transgression" seem to be reasonably well supported by the data from Figure 5.3. The sea level "highs" at 30 m and 15 m below present on Figure 5.10 probably represent those two shore-paralleling features.

The shore-paralleling features in the region of the 15-30 m bathymetric contours can be traced along much of the Western Australian Eocene coastline (Hick, 1978). The deeper features, beyond 30 m, which do not follow present day shoreline alignment, are probably remnants of an even earlier eustatic adjustment and are less well understood. These features have great significance for this study and for the location of commercial quantities of the pearl oyster *Pinctada maxima*.

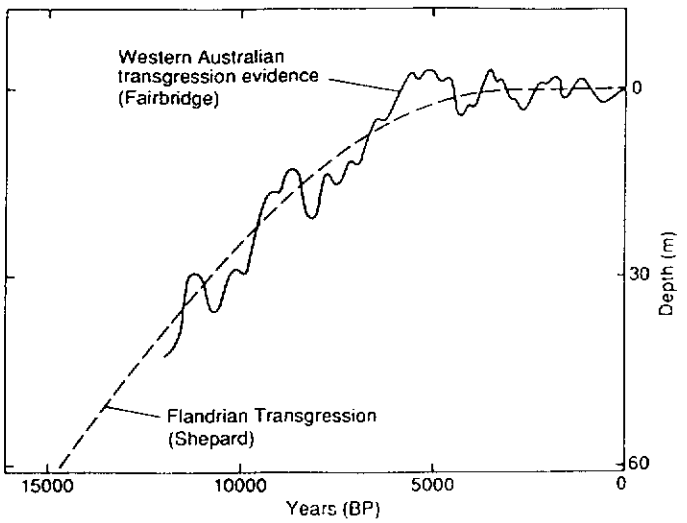

Figure 5.10: Holocene global marine transgression based on Fairbridge (1961)

5.2.4.5 Pearl-catch relationship results

An enhanced (saw-toothed stretched) image was produced to show maximum information of submarine features at a matching scale to the Flinders data sheets (Penn and Dybdahl, 1988). A novel approach to image analysis was undertaken using an independent assessment of bottom condition (by the report co-author Scoones, an experienced marine biologist and diver) on the basis of the textural features on the image. Its inclusion here illustrates the type of validation that is readily accepted by the industry and user community.

This assessment was influenced only by features such as proximity to reef, sand ripples and weed growth which were visible on the imagery, and from knowledge gained from dive/image assessments from the La Grange survey (Hick and Scoones, 1988). Each assessment was made at the published location of the dive sites from an assessment of bottom type against Catch Per Unit Effort (CPUE) of both "culture" and "mother of pearl" shell as recorded by the Flinders cruise (Penn and Dybdahl, 1988).

Each site was ranked as either "good" or "poor" bottom type for pearl shells. Table 5.1 summarises the data extracted from the dive information and shows the relationship between diver assessment and image assessment of good bottom type to be strong with CPUE. Thirty-four observations, with a CPUE of 673 (average 19.8 per observation) concurred. Five observations, where diver assessment indicated

Table 5.1: Diver versus image assessment of bottom type

	Rankings	CPUE	DIVER SITES	No. of Observations	TOTAL CPUE	AVE
	GG	>40	(8a,35b,53)	3	154	
	GG	>30	(13b,20c,25,38e,51,52)	6	210	
Diver 'good' Image 'good'	GG	>20	(5,35c,35d,38a,38d,54)	6	150	
	GG	>10	(4,13a,20a,20b,33,35a,35e, 35f,38b)	9	140	
	GG	>0	(8b,24,38c)	3	19	
	GG =	0	(9,18,19,32,35g,35h,36)	7		
				34	673	19.8
	GP	>10	(23)	1	12	
Diver 'good' Image 'poor'	GP	>0	(34)	1	5	
	GP =	0	(6,11,15)	3		
				5	17	3.4
	PG	>10	(28,29)	2	31	
Diver 'poor' Image 'good'	PG	>0	(30)	1	5	
	PG =	0	(1,21,26,27,31,42)	6		
				9	36	4.0
	PP	>30	(41)	1	32	
	PP	>10	(22,40)	2	31	
Diver 'poor' Image 'poor'	PP	>0	(16,17,37)	3	18	
	PP =	0	(2,3,7,10,12,16,43,44)	7		
				13	81	6.2

good bottom type and where image assessment was poor produced a CPUE of 17 (average 3.4 per observation). Conversely, nine observations, producing a CPUE of 36 (average 4.0 per observation), occurred where diver assessment was poor, and image assessment was good. Thirteen concurring poor assessments produced a CPUE of 81 (average 6.2 per observation)

A similar visual assessment was also made of the prawn trawl locations whereby the image was evaluated at each trawl site. In shallow water locations, occasional turbidity problems due to tidal flow made interpretation of some of the sites not possible. Conversely, in deeper water some trawl sites could not be reliably interpreted. Sites were also rejected when close to features that could not be located within the 300 m accuracy of the, now superseded, SATNAV system.

Penn and Dybdahl (1988) reported that within the survey zone, a considerable proportion of the ground, particularly inshore (less that 18 m) was considered unsafe for trawling both from echo sounder observation and trawl results. In contrast, the two areas where the prawns were concentrated were found to have relatively barren sand substrates. These were judged by the divers to be poor pearl oyster habitat and to an extent appear atypical of the general 19-37 m zone. Also, on the basis of the survey information, it appears that most of the shallow water areas (less than 18 m) off Broome would be unsafe for prawn trawling because of the isolated patches of hard corals. In deeper waters, where fewer hard corals occur, the substrates appear to be more generally suitable for trawling.

Therefore, the assessment of the 38 trawl sites included in the study (Table 5.2) is a reasonable representation of the range of trawl sites and includes a range of "smooth" and "rough" bottoms. Concurrence of ship assessment and image assessment as "smooth-sandy" bottom occurred at 21 sites and concurrence of rough bottom sites agreed at another nine sites. Only on eight occurrences did the ship data not concur with the image data and these errors were evenly spread, ie. four sites of rough-bottom assessed as smooth and four smooth sites assessed as rough.

Table 5.2: Trawl data versus image assessment

Trawl Sites	Ship	Image	Trawl Sites	Ship	Image	Trawl Sites	Ship	Image
1	R	S	25	S	S	49	-	-
2	S	S	26	R	S	50	S	S
3	S	S	27	-	-	51	S	S
4	-	-	28	-	-	52	S	S
5	-	-	29	-	-	53	-	-
6	-	-	30	-	-	54	-	-
7	-	-	31	-	-	55	-	-
8	S	S	32	-	-	56	-	-
9	R	S	33	-	-	57	-	-
10	-	-	34	S	S	58	R	R
11	-	-	35	S	S	59	-	-
12	-	-	36	S	S	60	-	-
13	-	-	37	S	R	61	-	-
14	R	R	38	S	R	62	-	-
15	S	S	39	S	R	63	S	S
16	S	S	40	R	S	64	S	S
17	-	-	41	S	S	65	R	R
18	-	-	42	-	-	66	R	R
19	-	-	43	-	-	67	S	S
20	-	-	44	-	-	68	S	S
21	-	-	45	R	R	69	R	R
22	S	S	46	-	-	70	S	R
23	-	-	47	S	S	71	R	R
24	S	S	48	-	-	72	R	R
						73	R	R

RR =	9	Uninterpretable - 29
RS =	4	Unlocatable - 6
SR =	4	
SS =	21	
Total	38	"R" Rough "S" Smooth

Tests of significance (χ^2) were used to show relationships between "pearl-bottom" assessment, prawn catch and image assessment (Table 5.3). These data show a

highly significant relationship between the suitability of bottom type for pearl shell lodgement and growth and the image interpretation by a skilled interpreter. The success rate of the order of 80 percent with the χ^2 of 12.3 (degree of freedom, df = 1, probability, p less than 0.001) for pearl bottom assessment was almost matched with a less significant, but still acceptable, score for the suitability for prawn trawling. Here χ^2 of 8.5 (df = 1, p less than 0.01) with some of the confusion reasonably explained by uncertainty in interpretation.

Table 5.3: Tests of significance (χ^2) between pearl-bottom, prawn catch and image

		Pearls Diver log		
		G	P	
Image	G	34	9	43
	P	5	13	18
		39	22	61

χ^2 = 12.3 on 1 df
** p < .001

G = Good; P = Poor

		Prawns Trawl log		
		R	S	
Image	R	9	4	13
	S	4	21	25
		13	25	38

χ^2 = 8.5 on 1 df
** p < .01

R = Rough, S = Smooth

5.2.5 Conclusions

The relationship between radiance and depth can be sustained only when the ocean bottom is uniform and principally sandy. Radiometric measurement over different bottom types did support a linear absorption with depth, especially when radiance was converted to reflectance. Ship-borne reflectance measurements were also of a similar dynamic-range as the radiance measured by the satellite. The conversion of

an image to a "pseudo-bathymetric" chart from the imagery was not derived, but useful relationships and additional information were evident on the image when the bathymetric data from the latest hydrographic charts were embedded.

Significant relationships were established between the diver assessment of bottom type from the Flinders data for pearl oyster habitat and the information contained in the image. Similarly rough and smooth trawling ground could reliably be identified on the imagery.

The SATNAV position-fixing system on the survey vessel Flinders had an accuracy of approximately 300 m, or six pixels on the resampled TM Image. This holds inherent inaccuracies with reference to the predictions of bottom-type, made both from the hard copy image and the image on the computer screen, and underlines the benefits of using GPS technology. This, coupled with the limited dive-time, on some occasions only 30 seconds bottom-time, and the normal visibility of less than 4 m experienced in the survey area, may have introduced errors into the results. The interpretation of bottom-type relating to its suitability for trawling or for pearl oyster habitat is based on textural characteristics, sometimes over very limited areas, and the survey methods used may not have had the precision required for this technique.

This survey technique was designed to identify areas of seafloor with different textural characteristics, each of which may, or may not, be associated with target species. The result of identifying a set of characteristics which is significantly correlated with the presence/absence of a target species is a saving of significant

amounts of unproductive vessel time, with a commensurate increase in the efficiency of a fishing vessel.

The test of data significance (χ^2) results for trawling indicate a 79 percent success rate in identifying trawlable and non-trawlable bottom. The results for pearl oyster bottom-type indicate 80 percent success. This means that elimination of unproductive steaming and/or fishing time can be achieved at the expense of missing only a small percentage of potentially productive grounds. This opportunity-cost can be justified in a fishery where the identified productive grounds support economic catches. This method has the greatest potential benefit in the exploration and development of a new fishery, where the distribution of target species is unknown, and in many instances where the bathymetry is uncharted.

Evidence of drowned shoreline features as remnants of stillstands during the Eocene transgression can be extended from the La Grange image data, used in an earlier study, northward to the Lacipede Islands. Propositions of some explorers as to the likely exit point of an older course of the Fitzroy River through the Roebuck Deep south of Broome may account for the broad sedimentary nature of the areas west of Broome. Exploration trawling for sedimentary diamonds has commenced. This work has contributed significantly to submarine geomorphic and sedimentological studies (Tapley, 1990), with these techniques being used on five separate study areas in Western Australia.

The study also indicates the importance of careful data selection and processing. High sun angle imagery is of critical importance, but to obtain maximum benefit it must be coupled with an incoming tide and low wind conditions. For tropical environments, where phytoplankton blooms, coral spawning and spat release are evident at certain times of the year, local information is also required. The waveband characteristics of Landsat TM band 1 appear to be ideal. However, the usefulness of the SPOT data should not be discounted despite the longer wavelength band, as the higher sun angles, due to the later acquisition time, can still retain good water penetrating characteristics.

5.3 Geographe Bay Project

5.3.1 Aims

In the light of the conclusions from the Broome studies and the need to obtain a better understanding of the distribution of seagrass habitat along the entire coast of Western Australia, a small research project was initiated using the Geographe Bay area because of the competing interests of the fishing (potential trawling) and mining (potential mineral sand dredging).

The Western Australian Fisheries Department had a specific interest in the Bay as pressure was being applied for the area to be released for commercial pelagic fish trawling. The recreation and conservation values, and the potential for sub-marine dredge mining of heavy metal deposits associated with quaternary strandlines, had also indicated that information on the bottom characteristics would be important.

Geographe Bay, at latitude 33 degrees South longitude 115-116 degrees East, is south of Perth on the coast of Western Australia near the towns of Bunbury and Busselton (Figure 5.11). Anecdotal evidence of great water clarity and seagrass meadows at depths of more than 40 m indicated that tongues of oceanic water from the Leeuwin Current (Pearce and Griffiths, 1991) could provide conditions that might support the detection of bottom features at depths approaching 50 m.

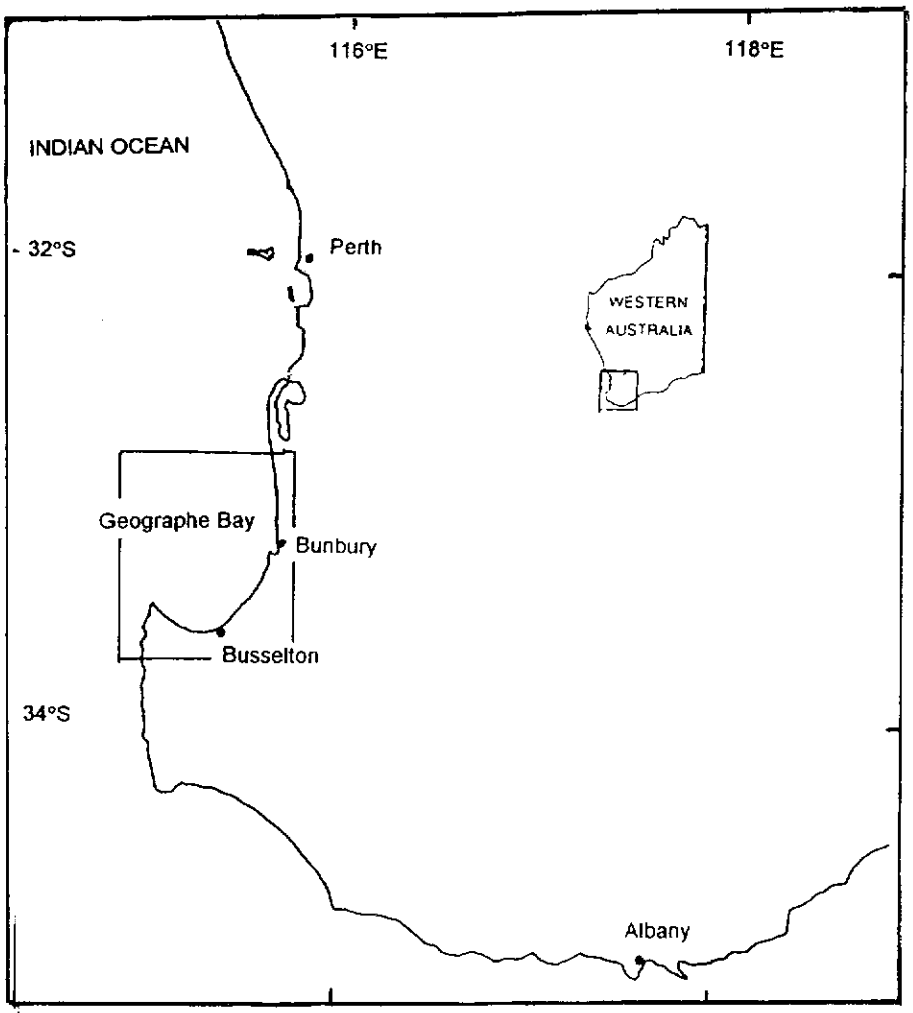

Figure 5.11: Geographe Bay study area

This author noted features in the ocean in Geographe Bay on a Landsat TM image in 1986, but as they appeared to be at charted depths greater than had been thought possible from the experience gained using Landsat MSS data, they were believed at that time to be probably surface or turbidity effects. Inspection of a subsequent image showed the same features, in the same geographic locations, confirming that they may in fact be bottom materials or seagrass beds. The main species in the seagrass meadows are *Posidonia sinuosa*, *Amphibolis antarctica* and *griffithii,* and *Heterozostera tasmanica.* It is substrate-type and photosynthetically available radiation-dependence that regulate density and occurrence of these species.

Reflectance is influenced by many factors both above and below the surface of the water (Zibordi *et al.,* 1990). Underwater these include absorbance/transmittance of light by pigments within the plants. A leaf within a plant receives two kinds of radiation, incident solar radiation directly through the water column onto that leaf, and also intercepted radiation scattered within the canopy, either through transmission through other leaves or reflectance from other surfaces. The sensor also measures two kinds of fluxes, the flux measured from the surface of an illuminated leaf (single scattering) and the flux measured from the composite of many interceptions of that radiation (multiple scattering).

Marine plants have developed specific canopy architecture that optimises the use of all available light energy and the reduced illumination is compensated by the location of chloroplasts on either side of leaves and other adaptations to maximise the absorption of light during the wave-induced forward and backward motions.

5.3.2 Methodology

The TM image 112/083, 26 October 1991, was chosen for several reasons besides the fact that significant substrate information was visible. The weather conditions at the time of acquisition were clear sky with SE winds at 19 km/hr. This offshore wind would at that time of the year be relatively dry and insufficient to cause strong wave action. The more important fact was that for the previous two days the wind had been calm, or light easterlies, and low swell conditions normally result from such a pattern. Solar elevation at acquisition was 55 degrees, which is only 8 degrees less than the maximum at solstice of 63 degrees.

Therefore with reference to the model for radiance (Equation 5.2, Section 5.1.1.1) the assessment was that atmospheric conditions were suitable (Lai), surface water condition was calm (low Lsi), low swell condition would indicate low turbidity and particulates in the water column (Li), and solar elevation was high (positively effecting rbi and negatively effecting Lsi).

5.3.3 Results

Figure 5.12 is the resultant image with the overlay of part of the Admiralty Chart AUS 334. The image confirms the depth determination and supports the proposition that there is a decline in biomass of the meadows with increasing depth. Multiple scattering, caused by the leaf structure of the canopy of the meadow, absorbs light at the wavelength of TM band.1 The crescentic-shaped scours, known as "blowouts" are characteristic of rare storm events on seagrass meadows (Patriquin, 1975; Cambridge, 1975). These blowouts have a scarp edge about 0.7 m deep and a lee

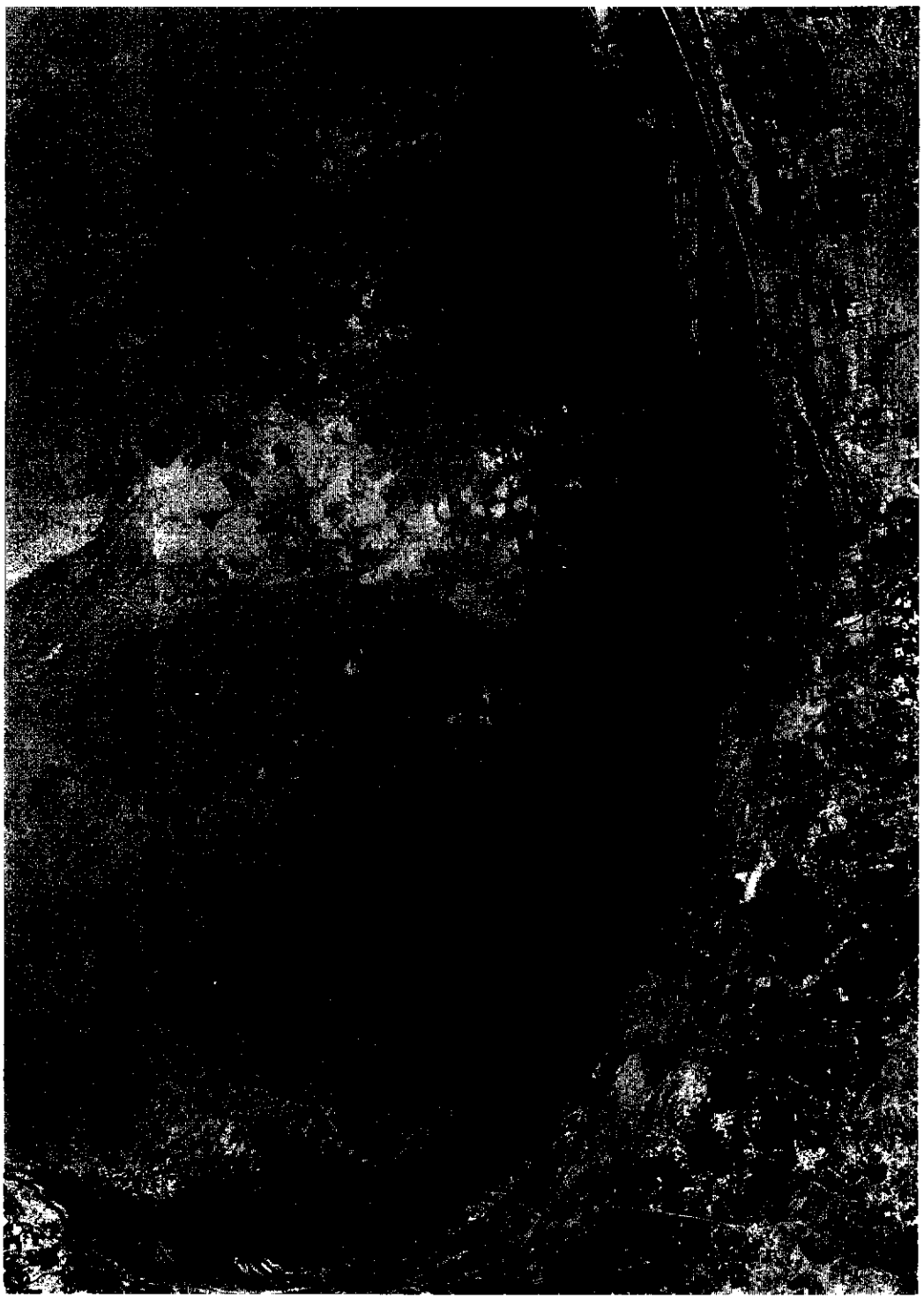

Figure 5.12: TM image and Admiralty Chart AUS 334 (depth in fathoms)

edge that slopes into the seagrass meadow. They are often colonised by smaller species of seagrass which are more easily scoured out by storms than the surrounding meadow. A diving programme and a towed video camera from the Research Vessel Flinders confirmed the interpretation of the images and verified the location, depth, condition and species of seagrasses, as was reported in Hick *et al.* (1994).

5.3.4 Conclusions

This study indicates that, if consideration is given to the selection of data at optimum environmental conditions, systems such as Landsat TM are capable of producing diagnostic data for habitat mapping at depths of the order of 40-50 m.

The anecdotal evidence from local fishermen, divers and the crew of the Flinders, of great water clarity in Geographe Bay, is supported by the recent identification of the Capes Current by Pearce and Griffiths (1991). This current runs counter to the Leeuwin Current and the suggestion is that it may bring deep oceanic water into the Bay. Water circulation through the Bay is from the Leeuwin Current, which is a poleward-flowing, low density, low-productivity saline tropical current, and probably also from this high-density Capes Current, which may introduce water into the Geographe Bay area from southern oceanic sources.

This could explain, firstly, why seagrasses occur at these depths in Geographe Bay, and, secondly, why they are detectable when the surface conditions are suitable. Also of interest is the apparent reduction of biomass of seagrass (reduction of multiple scattering) in the image, if the observer notes the change that occurs at most places in

transects normal to the coast, giving an increased reflected response with increasing depth. This is at variance with the findings of the Broome study.

5.4 Coastal Waters Project

5.4.1 Aims

The importance of the metropolitan coastline to Perth, Western Australia, has been discussed in Section 3.2.1. In 1991, the State Government initiated complementary studies into the cumulative impacts of waste inputs, particularly nutrients, to Perth's coastal waters (Simpson *et al.*, 1993).

Protection of the coastal waters off Perth requires information on key habitats. Inventory and baseline surveys of some of these key areas were required, which included a need to accurately map the main benthic habitats as a reference for quantifying future habitat changes.

5.4.1.1 Study area

The coastal waters off the southern metropolitan area of Perth comprise a series of semi-enclosed nearshore basins that are separated from the offshore waters by an extensive system of limestone reefs and islands parallel to, and within a few kilometres of, the coastline (Figure 5.13). This chain of reefs can be found on much of the tectonically-stable Western Australian coast and represents old shorelines of Late Pleistocene emergence and subsequent post-glacial submergence. Of interest to this study was the area extending from Mandurah to Fremantle including Penguin Island, Cape Peron, Garden Island and Stragglers Rocks.

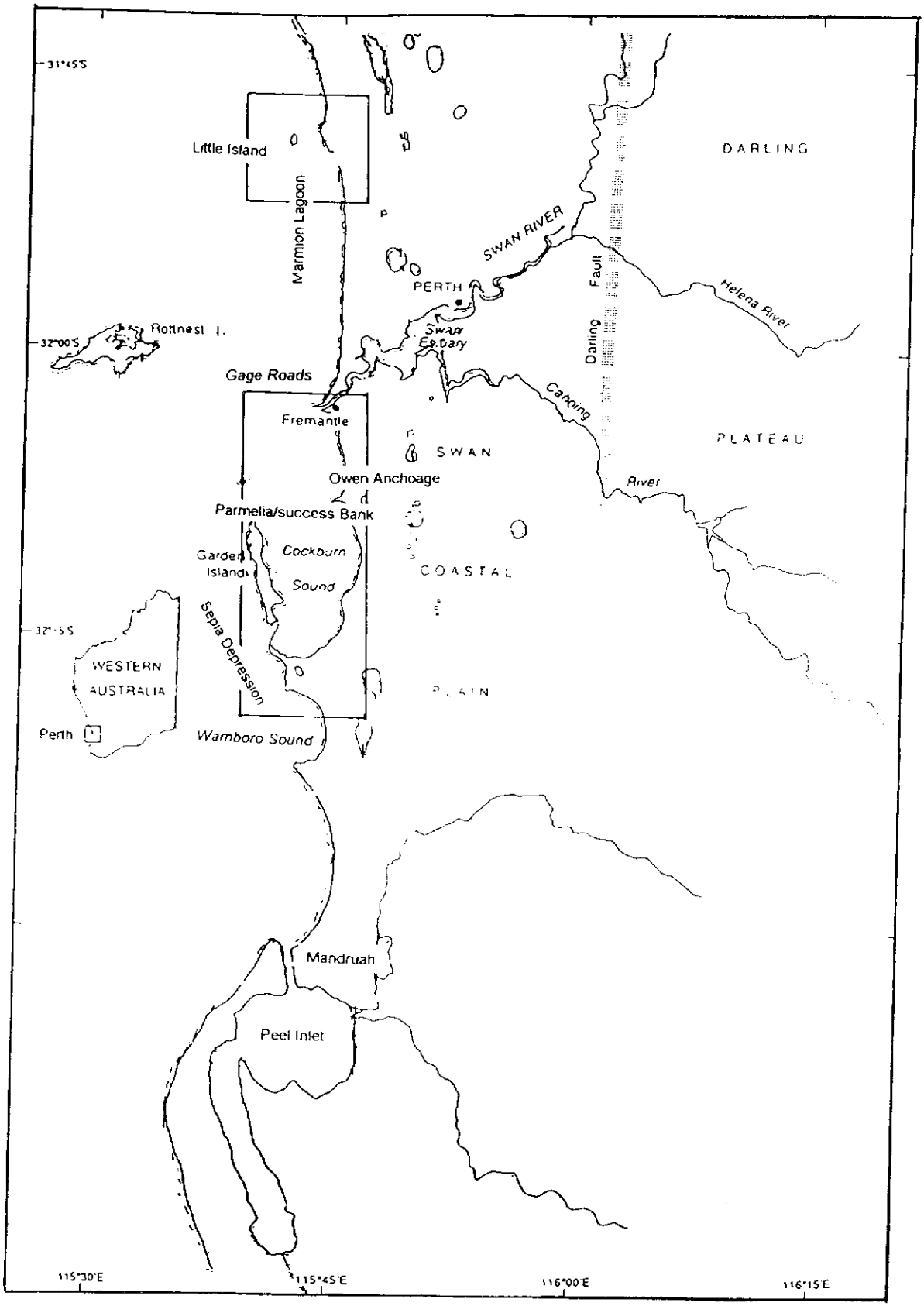

Figure 5.13: Location map for the Coastal Waters Project

A similar ridge, Five Fathom Bank, occurs further offshore to the west of Sepia Depression and extends from Cape Bouvard, 22 km south of Mandurah, to the west end of Rottnest Island. Between these ridges is the deep trough (24 m) of Sepia Depression. These islands and reefs form a barrier which protects the coastline from offshore swell, creating low energy coastal lagoons and embayments. In the lagoons, water depths are typically less than 10 m whereas in the central basins of Warnbro Sound and Cockburn Sound depths are approximately 20 m.

5.4.1.2 Benthic habitats

The study area comprises seven main benthic habitats and these have been summarised in Ong *et al.* (1994) and more extensively in a joint report of this work by Mr J Burt of the WA Department of Environmental Protection. These are silts, fine sands and silts, sand including sparse seagrasses, coarse sands, seagrass meadows, subtidal reefs, and intertidal reefs.

(a) Silt

The silty-sediment that occurs in the central deep basins (over 10 m depth) of Warnbro and Cockburn Sounds is unique on the central west coast of Western Australia (Collins, 1988). The plant communities of these deep basins are impoverished and restricted to a few species of green and red algae. In general these soft-sediments contain high diversity of fauna with an abundance of some species, such as the detritus feeding sea-star *Stellaster inspinosus*, in some localities. Filter feeders and some sponge species and sea anemones are also common.

(b) Fine sand and silt

The area classified as fine sand and silt occurs in the deeper (about 12 m) western part of Owen Anchorage, between the relatively shallow sills (4-5 m) of Parmelia and Success banks and inshore of the shipping channel. Protection of these areas from offshore waves has created a relatively low-energy depositional environment. The sediments consist of unconsolidated fine carbonate sands and silt with a relatively high organic content (about six percent). This habitat contains a low abundance and diversity of plants, because the water depth and the often relatively high turbidity of these waters limits the amount of light available to benthic plants. The benthic fauna is sparse and again dominated by invertebrates both on the seabed (echinoderms) and in the surface sediments (polycheates and molluscs).

(c) Sand including sparse seagrass

Bare sand with areas of sparse seagrass primarily occur in the relatively shallow waters (less than 5 m depth) of sandy lagoons and embayments on the eastern side of the Garden Island reef chain. However, patches of bare sand are also found within these reefs and the offshore reefs on Five Fathom Bank. The sediments of this habitat are coarser with less silt and organic material compared to the deep basins. The biota of bare sandy sea-floors are dominated by burrowing invertebrates. Sparse patches of seagrass are sometimes found in areas of bare sand adjacent to seagrass meadows or within seagrass meadows, where the physical or biological conditions for meadow development are sub-optimal.

(d) Coarse sand

This habitat occurs in offshore areas in the relatively deep (more than 20 m) exposed waters to the west of the Garden Island reef chain. The sediments in these areas consist of coarse carbonate sands and fragments of rock, shell and coral rubble, with relatively low silt and organic content. Considerable sediment movement occurs in these offshore waters which is unfavourable for colonisation by plants. Consequently, the biota of these areas are dominated by fish and burrowing invertebrates, especially molluscs with seasonally high abundances of echinoderms and crustaceans.

(e) Seagrass meadow

Seagrass meadows (predominantly *Posidonia sp.*) generally occur on the sandy seafloor of the protected waters inside the coastal reef chain. Seagrasses occur to a depth of about 18 m in Warnbro Sound and about 12 m in Owen Anchorage. However, meadows of greatest extent and density occur in waters less than 10 m, particularly on Parmelia and Success Banks. Ten species of seagrass have been recorded in the study area and the dominant species are *Posidonia sinuosa, P. australis, Amphibolis antarctica* and *A. griffithii*. Seagrass meadows usually occur as a mixture of *P. sinuosa* and *Amphibolis sp.* Monospecific stands of *P. sinuosa* occur on the leeward side of Penguin Island. Seagrass meadows provide a source of food and shelter to many different animals, including a number of important commercial and recreational species (Bell and Pollard, 1989). Studies have also shown that seagrass meadows are important nursery grounds for a variety of juvenile fish and crustaceans. The leaves and stems of seagrasses provide a substrate for a

diversity of epiphytic plants (Burt *et al.*, 1995) and animals which form an important part of this community.

(f) Subtidal reef

There is a high diversity and abundance of plants and animals associated with subtidal reefs. Large attached macroalgae, such as the kelp, *Ecklonia radiata* and *Sargassum sp.*, dominate the flora of reefs with an under-story of red coralline algae and non-calcareous foliose and filamentous algae. The diversity of the plant community combined with the reef structure provides habitat for a variety of sessile invertebrates, such as ascidians, sponges and soft corals. Mobile invertebrates include crustaceans, echinoderms, molluscs and burrowing in-fauna.

(g) Intertidal reef

Intertidal reefs, forming platforms close to mean sea level, occur onshore at Cape Peron. However, they are principally found offshore along the Garden Island Ridge system as fringing reefs adjacent to islands. Species dominance, diversity and abundance on reef platforms is principally determined by the frequency of tidal submergence giving rise to a zonation of community types (Benjamin, 1985). Seasonal factors such as summer desiccation and irregular sand-scouring result in significant seasonal changes in the biota, particularly the plant assemblages.

The biota of the upper intertidal zone is relatively impoverished although some species of blue-green algae *Calothrix confervicola*, rock crabs, littorinid snails and welks are relatively common. Species of green *Ulva rigida* and red algae *Gelidium pusillum* are abundant during winter. The lower levels of the reef platforms are less

exposed and hence more stable and are generally dominated by small red and green turf algae sometimes with an over-story of larger brown algae, such as *Ecklonia radiata* and *Sargassum sp.*, particularly around the raised rim on the seaward edge of these platforms. The dominant animals include the commercially important abalone, *Haliotis roei*, the common whelk, *Thais orbita*, marine snails such as the chiton, *Rhyssoplax torriana* and the large turban shell, *Turbo torquata*.

5.4.2 Methodology

5.4.? 1 Data acquisition

On 12 February 1993, between 0900 and 1000 hr (Western Standard Time) the Geoscan Airborne Multi-spectral Scanner was flown over the entire study area from well north of Little Island, south to Mandurah, and offshore to the 30 m bathymetric contour, including Rottnest Island. Details of the flight and the instrument have already been discussed in Section 3.3.2. Figure 5.14 is an example of the Geoscan image data, part of which was chosen for the classification and validation experiment.

Four control targets were deployed from vessels during the flight period in areas that were considered to have insufficient features for spatial rectification purposes. These targets were fixed using both differential GPS and traditional survey triangulation from shore-based theodolites. The scanner image was registered to a SPOT panchromatic (10 m) satellite image that was acquired on 22 January 1993, and had been registered to the Australian Map Grid. The tessellation technique of Craig and Green (1987) was used to rectify the Geoscan images to an accuracy of ± 20 m using

a SPOT panchromatic image as a map base. Digital bathymetric data were also incorporated into the image to assist the separation of habitat types.

Divers, equipped with SCUBA gear and an underwater video camera, identified and recorded the habitat types throughout the study area. The areas were mapped as silt, sand with sparse seagrass, seagrass meadows, coarse sand and subtidal reef. The areas of intertidal reef could not be traversed by boat and the fine sand/silt class was not sampled. Vessels were located at sites using GPS.

5.4.2.2 Data processing

This aspect was also covered in detail in Chapter 3, and is briefly summarised here. The flightlines, which followed the general north-south direction of the coast, contained a proportion of sun-glint caused by specular reflection from the sea surface. Specular reflections from long-period swell waves also caused interference on some parts of the image. A two-stage correction procedure was applied to remove across-track illumination and wave facet effects.

Rayleigh scattering resulted in systematic across track effects in the shorter wavelength Geoscan bands, especially bands 1 and 2, where higher digital counts were recorded as the scan angle increased giving longer atmospheric pathlengths. Hick *et al.* (1992) showed that correction of illumination effects is possible by using ratios between visible and near infrared bands. However, this technique was tried but was not able to effectively remove the across track illumination effects on this dataset.

The first stage involved estimating the brightness curve of the combined effects of Rayleigh scattering and specular reflection effects. This curve was smoothed by fitting a moving average filter combined with a cubic polynomial over the area of greatest curvature which was then subtracted from band 1 of the raw image.

The second stage correction assumed that the infrared bands had no water penetration capabilities but had similar wave facet contributions. The removal of wave facet effects was performed by regressing the visible bands 1 and 2 against the infrared band 7, over an area of deep ocean. The resulting image was subtracted from the across-track free image. The residual is an image with all visibly detectable across-track and wave facet effects removed to within the level of instrument noise, and rendered the data acceptable for use in training for classifications (see Figure 5.14).

Unsupervised cluster classification of images was applied on panels (512 x 512 pixels) of the total scene, Figure 5.15. Digital bathymetric data were incorporated into the image to provide a depth threshold to separate habitat types. Classes labels were established then identified in known training areas and with inputs of local knowledge.

5.4.3 Results

5.4.3.1 Validation program

The diving program, using an underwater video camera, identified and recorded the habitat types at 106 sites throughout the study area. The sites included areas of silt, sand with sparse seagrass, seagrass meadows, coarse sand and subtidal reef. The

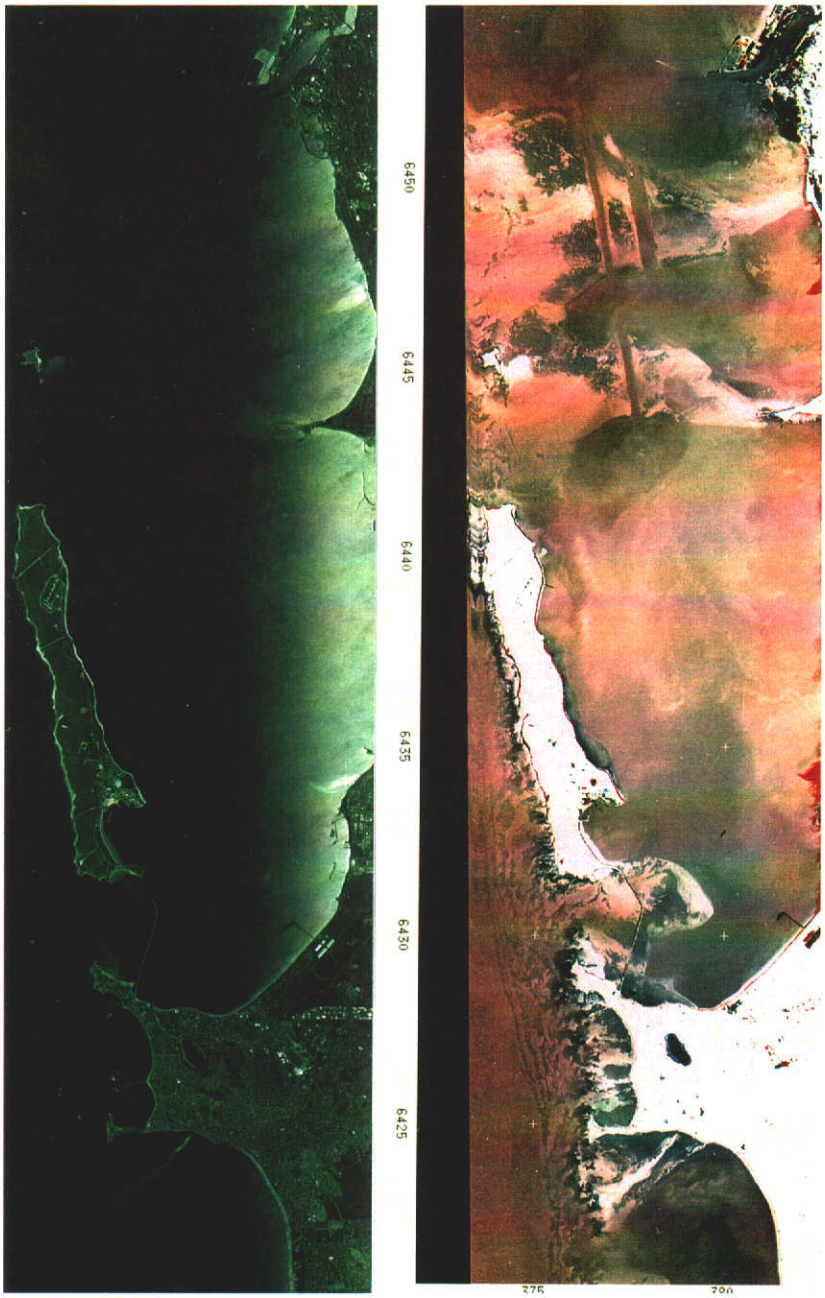

(a) Raw data (b) Processed data

Figure 5.14: Part of Geoscan data for Coastal Waters Project

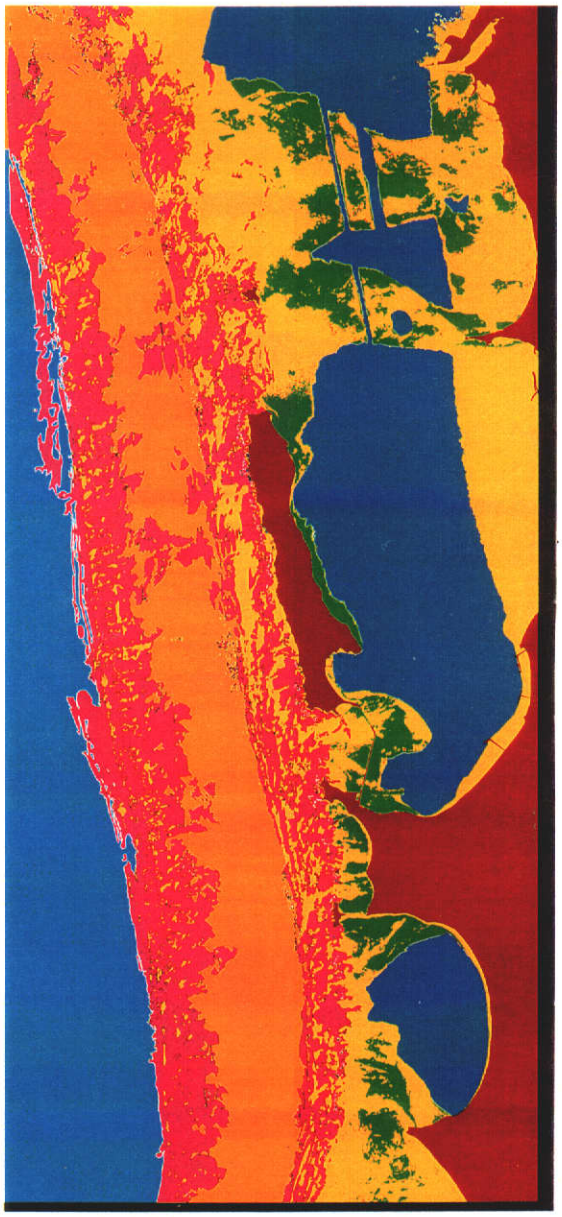

Light Blue	Coarse sand
Red	Subtidal reef
Orange	Seagrass meadows
Yellow	Fine sand and silt
Green	Sand and seagrass
Dark blue	Silt
Brown	Land

Figure 5.15: Part of classified image of Coastal Waters Project

areas of intertidal reef could not be traversed by boat and the fine sand/silt class was not sampled. The boat was accurately located at sites using GPS. Sites were randomly selected within areas that were classified.

The best result from the validation of the classification was produced for the "coarse-sand" areas where for 12 sites 92 percent were correct and for the 57 "sand with sparse seagrass" sites visited, 90 percent were correctly labelled. For the 23 "silt" sites, 83 percent were correct and the more variable "seagrass-meadows" were correct for 71 percent of cases. The worst classification was produced for the highly-variable "subtidal" reef with only 62 percent correct for the 13 visited sites.

The study area which has been classified into the seven main benthic habitats is shown in Figure 5.15 and the area and coverage percentage of each habitat calculated for the entire study area. A summary of the result follows.

5.4.3.2 Habitat distribution

(a) Silt

Overall, for the study area, soft-sediment constitutes only about 10 percent of the benthic habitat. However, in Cockburn Sound it is the dominant habitat type representing more than 60 percent of the area. The silty sediment of the Warnbro Sound basin also occurs over nearly 30 percent of the benthic habitat in the Shoalwater Island Marine Park.

(b) Fine sand and silt

This habitat type covers about 10 percent of the area of Owen Anchorage which is a relatively shallow basin, about 12 m in depth.

(c) Sand, including sparse seagrass

In general, bare sand is a major habitat type in the study area covering more than 38,000 hectares, or 35 percent, of the total area. In the embayments of Cockburn and Warnbro Sounds, bare sand covers about a third of the area compared to shallower lagoons such as Owen Anchorage, where it is the dominant benthic habitat representing more than two-thirds of the seafloor.

(d) Coarse sand

Coarse sand is the dominant offshore benthic habitat and covers 38,600 hectares, or nearly 40 percent, of the total study area.

(e) Seagrass Meadow

Seagrass meadows are not a dominant habitat in these waters covering about five percent of the study area. In Owen Anchorage seagrass meadows represent about 20 percent of the benthic habitat compared to 15 percent in Warnbro Sound and six percent in Cockburn Sound, the latter reflecting the historical loss of seagrass from the Sound since the 1970s.

(f) Subtidal reefs

Subtidal reefs extend along the entire western margin and constitute about 15 percent

of the study area although they comprise between 23 percent of the Shoalwater Island Marine Park to less than two percent of the embayments of Cockburn Sound and Owen Anchorage.

(g) Intertidal reefs

Intertidal reefs, forming platforms close to mean sea level, constitute a small proportion of the habitat in the study area (less than one percent). Although intertidal reefs occur onshore at Cape Peron, they are principally found offshore along the Garden Island Ridge system as fringing reefs adjacent to islands.

5.4.4 Conclusions

Geoscan Airborne Multi-Spectral Scanner data, when used in conjunction with other data sets for classifying marine benthic habitats, provides several significant advantages over other forms of remotely sensed data, such as satellite and aerial photography. These include fine spatial resolution, relatively high water penetration capability and greater logistical discretion to acquire data under optimal environmental conditions.

Satellite data, typically at 20 to 30 m resolution, would not have presented the scattering problems associated with the Geoscan data because of the smaller field of view of the satellite scanners, but the acquisition cycle of satellite systems reduces the probability of achieving the acquisition criteria. Aerial photography, which could have provided higher spatial resolution data, has limited spectral quantisation, which reduces the potential for multi-band image processing to remove solar flaring effects, and geometric rectification is far more complex.

The raw Geoscan imagery was affected by several artefacts, especially sun-glint and specular reflection long-period swell waves. The heuristic approach used to remove these effects from the image relied on the inclusion of a uniform area across the image (eg. deep ocean) in order to separate sun-glint from real features.

Water penetration, spatial rectification and the capacity to remove depth effects from confounding the classification of benthic habitats have been the major obstacles to the broad-scale application of remote sensing technology for mapping the marine environment. The approach adopted in this study suggests that airborne scanners, such as Geoscan, can provide marine managers with a technique that produces an accurate, spatially rectified digital habitat map over large areas of the coastal environment.

5.5 Marmion Lagoon Project

5.5.1 Aims

Coastal seagrass meadows are important as they are nursery areas for many recreational and commercial fishery species (McRoy and Helfferich, 1977) as well as providing habitat and food for other types of fauna (Ackleson and Klemas, 1987). Meadows may be monospecific although in some areas, such as south western Australia, up to 12 species may co-exist, sometimes in a patch-reef environment, together with many species of macro-algae (Kirkman, 1990; Kirkman and Kuo, 1990). They are susceptible to change from human development, through factors such as sand and carbonate mining, siltation and eutrophication (Cambridge and McComb, 1984). The need to map and monitor the distribution, abundance and

diversity of these areas is, therefore, of prime importance in assessing the status of these coastal systems.

5.5.1.1 Background

The methods to map submerged coastal features, such as seagrass meadows, range from intensive field sampling to remote sensing (Jensen *et al.*, 1980; Savastano *et al.*, 1981; Dervieux and Tamisier, 1987; Zibordi *et al.*, 1990). Work reported earlier in this chapter shows satellite remote sensing can reliably map large areas at regional scales. However, as also shown in this chapter, success is dependent on ideal acquisition conditions, such as optimal solar angle, low atmospheric water vapour, calm sea-surface state, few water column particulates, and high contrast substrate composition. The ability to quantify that contrast from a remote sensor is the purpose of the inclusion of this work.

Aerial photography has traditionally been used for marine habitat mapping, and offers some advantages over satellites because of the ability to schedule flights under optimum conditions, at fine spatial resolution, and use of specified film, filter and exposure settings (Honey and Hick, 1976b). Colour photography may provide better water penetration than panchromatic (Kirkman, 1990). The technique is well established as a mapping tool although identifying plant species is extremely difficult (Dervieux and Tamisier, 1987; Sorokin *et al.*, 1988).

5.5.1.2 Study site

The area chosen for the study was at Little Island in the Marmion Lagoon, 20 km north-west of Perth, Western Australia (see Figure 5.13). Figure 5.16 is part of an

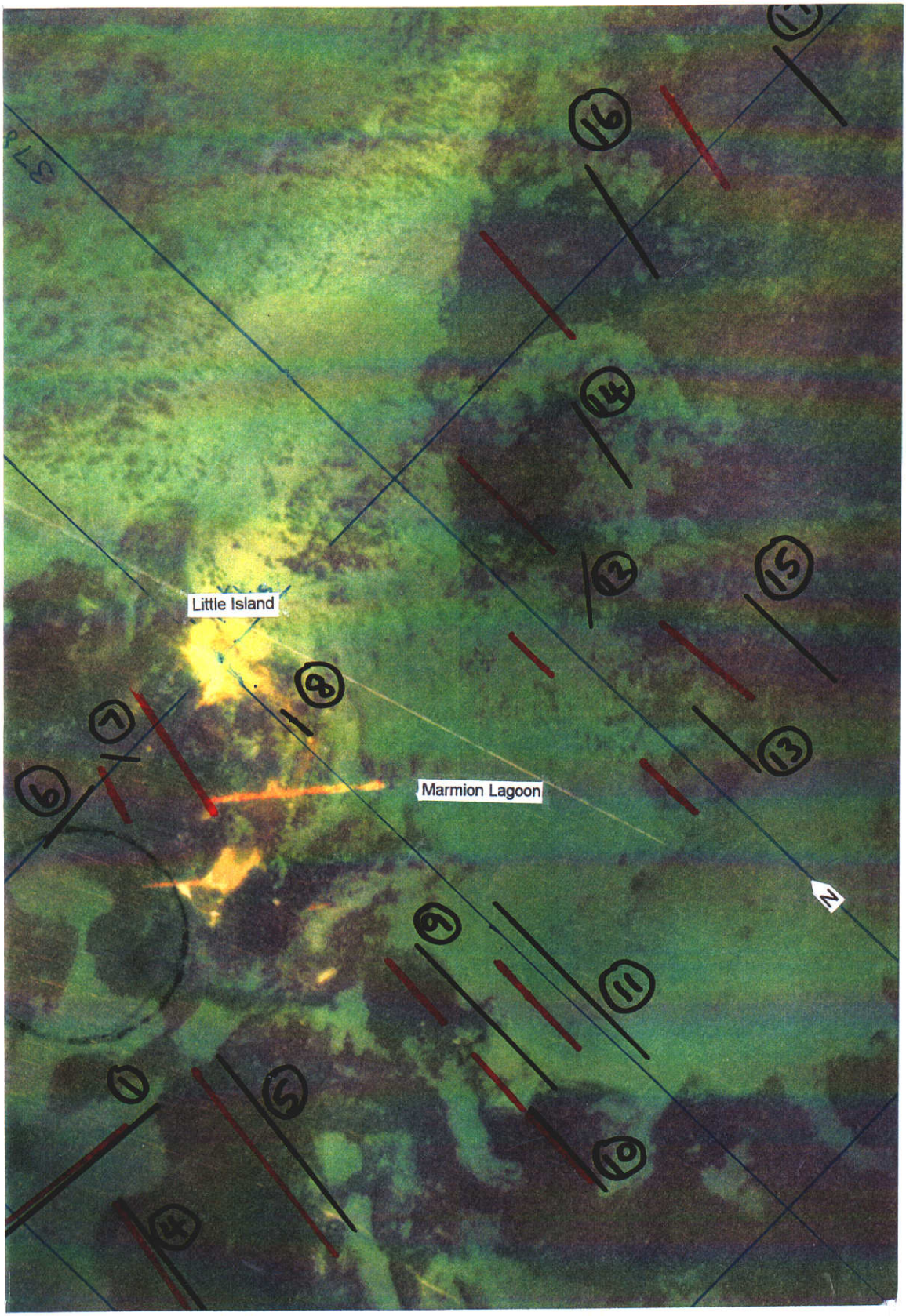

Figure 5.16: Air photo of Little Island with examples of transects

aerial photograph of the area and includes the transects that were used for parts of this study. The seabed around Little Island consists of algae- and seagrass-covered limestone reefs grading to seagrass meadows, predominantly species of either Amphibolis, Posidonia, or Heterozostera and Halophila, and the area is interspersed by patches of sand. The study was restricted to monospecific dense stands of the seagrasses *Amphibolis antarctica* and *Posidonia australis*, the macro-algae *Ecklonia radiata*, and areas of bare sand. The Amphibolis is a seagrass with lignified stems supporting small tufts of leaves. The stems attract many epiphytes and the plants are generally less than 60 cm high. The Posidonia is an important component of the seagrass areas along temperate coasts of Australia. It has no stem and consists of a ribbon-like blade generally less than 40 cm high. The Ecklonia is a brown laminarian algae, approximately 70 cm high when mature, and it grows on limestone reefs.

5.5.2 Methodology

5.5.2.1 Preliminary habitat study

A preliminary study was conducted (unpublished report by this author and Jernakoff) where in-situ radiance from a series of sites around Little Island. Radiance was measured using a 4-band spectral radiometer in a submersible housing, connected via a cable to a recording meter in a boat. The wavelengths in the radiometer were band 1 (470-495 nm), band 2 (500-600 nm), band 3 (600-640 nm) and band 4 (635 and 675 nm), each with a 15 degree FOV.Spectral measurements were made on 9 and 24 April 1992 during periods of cloudless skies, when the sun azimuth was greater than 45 degrees from the horizon. Underwater visibility during these periods was

estimated by a diver at better than 8 m. The radiometer was positioned by a diver 30 cm above the seagrasses, algae and sand, and also over the same targets just below the water surface. This enabled the calculation of upwelling radiance, or the attenuation coefficient of the water column. The water column over Ecklonia at 2 m was not measured, because the plants at this depth occurred as individuals rather than uniform beds, and the field of view of the sensors just below the water surface would have measured the surrounding reef material as well as the Ecklonia.

The radiance of a target was recorded from each of the four bands sequentially and the process was repeated three times to obtain a mean reading, before signalling to the diver to randomly select another of the 10 replicates of each target. The near Lambertian standard white plate of spectralon (Poly Fluoro Tetra Ethylene) was attached to a frame 30 cm away from the sensors, with full sun illumination, just above the target surface or just below the surface of the water, and was measured after every five replicates of each target. The ratio of the radiance of the targets to that of the standard enabled calculation of the percent reflectance.

Reflectance measurements were analysed separately for each depth using multivariate analyses of variance to test whether the spectral bands for each of the targets were significantly different from each other, and canonical variate analyses were carried out to determine the best separation of the targets, based on a linear combination of the spectral bands.

5.5.2.2 CASI habitat study

The second phase of this study was to test the ability to separate the habitat components from a remote platform, and the Compact Imaging Spectrographic Imager was scheduled to be available in Perth during the following summer, 1993/4. Flight lines were positioned to cover Little Island in a series of multiple passes using both the spectral (288-band) and spatial (14-band) modes at two altitudes, and including the invariant calibration targets. These targets were the Marina bitumen car-park and an area of dune sand that were near-simultaneously measured with a field spectrometer.

The area around Little Island is well known for its species diversity and transects have been monitored since the mid-1970s by research scientists of the CSIRO Marine Laboratory (Kirkman,1990). Additional transects were selected to cover a range of habitat types for coverage of the flight lines of CASI. Two divers from the CSIRO Division of Fisheries swam the transects describing the features, and depths were recorded from the Echo-sounder on the dive-boat. These are shown in Figure 5.16 where they were selected, and the slightly different positions where they were actually recorded by the diving team who had used GPS methods that produced positional accuracy within about 40 m.

Spectra were extracted for transects that were covered by the "rake-lines" of the CASI spectral-mode data. These spectra were calibrated by linear adjustment to the reflectances of the invariant targets. Signal to noise problems below 500 nm made analysis of the data suspect in that region.

5.5.3 Results

5.5.3.1 Preliminary habitat study

Spectral reflectances of the sand and its water column at both depths were not included in the statistical analyses because their reflectances were clearly different from the other targets in all four bands. Band one was excluded from the analysis because the values were at or near zero reflectance. The distribution of data the other three bands at both water depths was skewed. They were normalised using a natural logarithm transform. The variances of the raw data were significantly different, with limited degrees of freedom (Bartlett's test at 2 m depth: $\chi^2 = 53.47$, P less than 0.005; and at 4 m depth: $\chi^2 = 255.46$, P less than 0.001), and these could not be stabilised by the log transform.

Sometimes the five replicate readings for each of the two standards for species and spectral bands were very similar or identical, as in the case of Ecklonia for band 3 or the water column over Amphibolis for band 4 at 4 m depth. The mean value of the five replicates under the first standard with zero or near zero variance, compared with a different mean value for the other five replicates, also with zero or near zero variance under the second standard, probably led to the statistically significant Bartlett's variance heterogeneity test. To overcome this problem, the data from the five readings for each standard were averaged and the data reanalysed (now two replicates instead of ten). The raw values of these processed data were normally distributed and variances were not significantly different (Bartlett's test at 2 m depth: $\chi^2 = 10.62$, P greater than 0.05; and at 4 m depth: $\chi^2 = 27.3$, P greater than 0.05).

The results indicated that there were significant differences in the spectral reflectances between targets for both depth ranges (Bartlett's test at 2 m depth; χ^2 = 41.0, P greater than 0.001; and at 4 m depth; χ^2 = 125.6, P greater than 0.001). At both depths, reflectance through the water column was less than the measurements taken 30 cm above all targets in bands 3 and 4 although this was not always the case for band 2. While the order of species with highest mean reflectance at 2 m depth was Ecklonia and Posidonia followed by Amphibolis, this changed at 4 m depth to Amphibolis, then Ecklonia, followed by Posidonia.

The results of the processed data (with two replicates) indicated an identical pattern to that of the raw data based on ten replicates (Bartlett's test at 2 m depth; χ^2 = 7.88, P less than 0.001; and at 4 m depth, χ^2 = 17.49, P less than 0.001). The relationship of the spectral readings for the processed data of bands 2, 3 and 4, were the same as for the raw data. Therefore clear differences in the reflectances of the targets was apparent at the two depths studied (2 m and 4 m), although the pattern of separation between spectral bands for the targets was different for the two depths.

5.5.3.2 CASI habitat study

The results described here are from a limited number of spectra from 10 x 10 m pixels (ranging from 3 pixels up to the mean of 9). Because of the configuration of the rake lines, greater replication was not possible, therefore great care was taken in the selection of the training sites within the transects. Transects that did not have clear homogeneous pixels exactly where the transect was intersected by the rake-line were excluded from the analysis in Table 5.4.

Table 5.4: Transects used in spectral analysis for habitat mapping

Transect No.	Depth range (m)	Habitat type
1	8.0-12.5	Bare sand throughout
4	8.0-9.0	Ecklonia reef - brown/red macroalgae
6	4.5-8.0	Ecklonia reef - brown/red macroalgae
7	3.0-3.5	Ecklonia reef - brown/red macroalgae
8	1.0	Ecklonia reef - brown/red macroalgae
10	4.0	Ecklonia reef - brown/red macroalgae
11	5.0-5.4	Mixed Posidonia/Halophila/Heterozostera
12	4.5-5.0	Mixed /Halophila/Heterozostera
15	7.0-8.5	Posidonia
16	5.0-5.5	Posidonia
17	6.0-6.5	Posidonia

Figure 5.17 is a spectrum of bare sand (transect 1) at a depth of 8.0 m. Figure 5.18 is a comparison of sand at 8 m (transect 1) and Ecklonia at 1.0 m (transect 8). Both reach about three percent reflectance but the red/brown peak of the Ecklonia at 650 nm with a phaeophytin response at wavelengths beyond indicates that separation of these habitat types should be possible. Figure 5.19 is a comparison of Ecklonia at 1 m (transect 8) and at a greater depth of 3.0 to 4.0 m (transect 10). The position of the red peak and the suggestion of phaeophytin remain evident but the overall reflectance now being of the order of one percent reduce the potential of discrimination of the Ecklonia. This is further emphasised in Figure 5.20 which shows the spectral response of Ecklonia-dominated reef at depths between 3 to 9 m.

At this point it is worth considering the Posidonia in comparison with Ecklonia at the same sort of depths. Comparison of Figure 5.20 and 5.21, ignoring the instrument calibration noise below 500 nm, there is very little potential to reliably separate between Ecklonia and Posidonia, at depths greater than about 3 m, when the sensitivity of most airborne remote sensing platforms is considered.

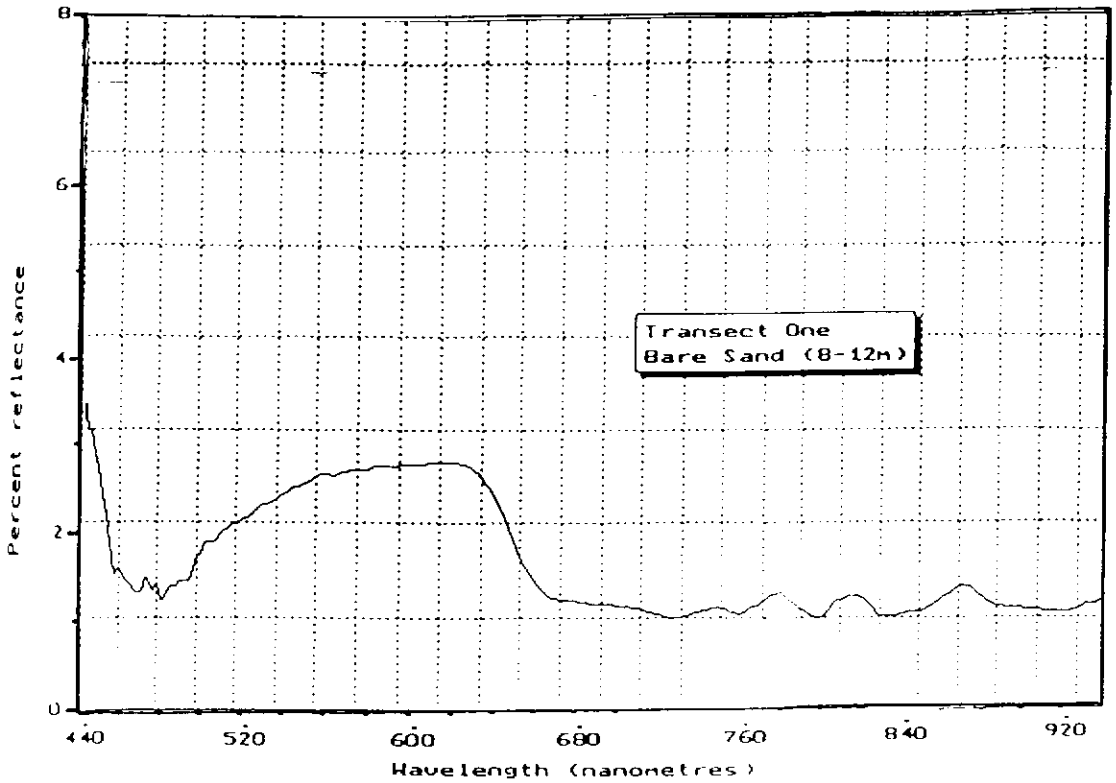

Figure 5.17: Spectrum of bare sand (transect 1) at depth of 8.0 m

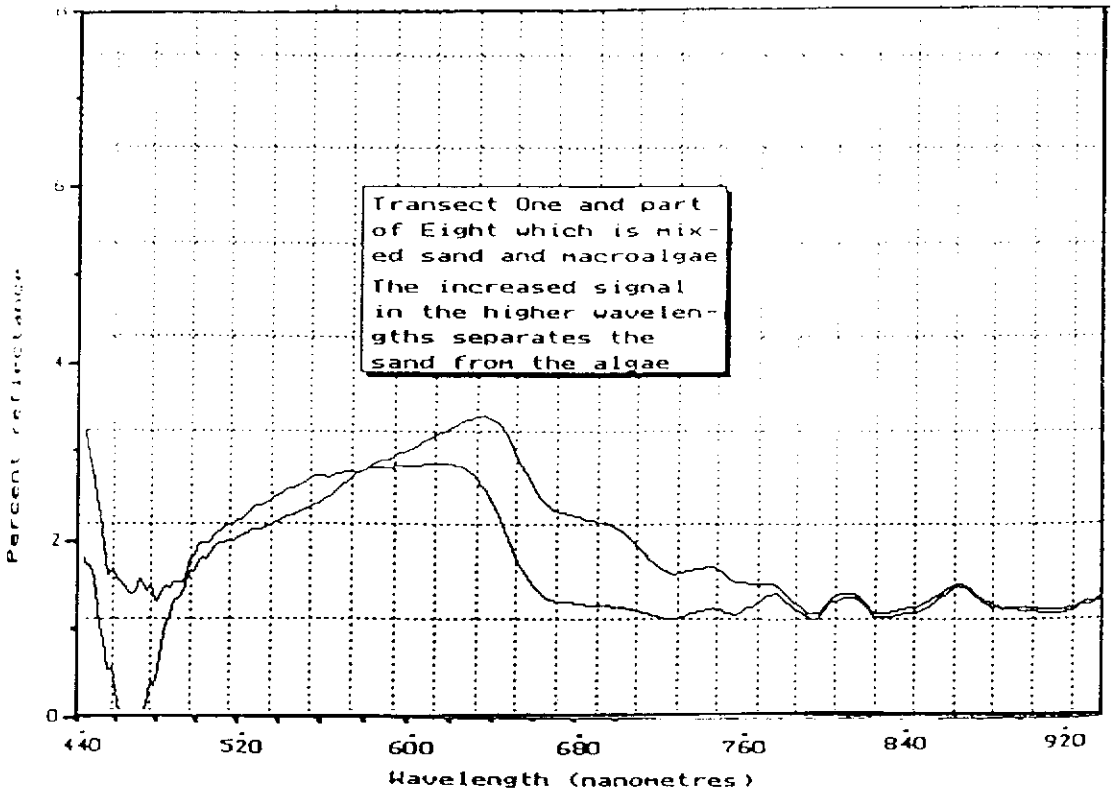

Figure 5.18: Spectra of bare sand at 8.0 m and Ecklonia at 1.0 m

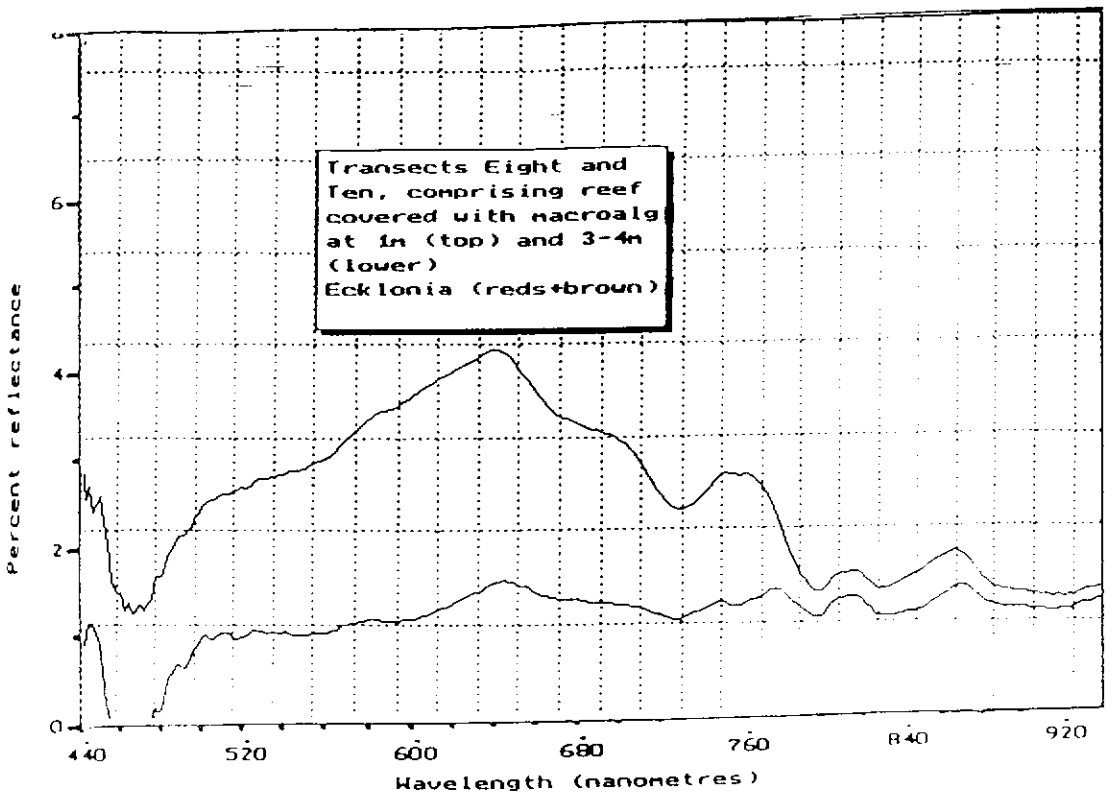

Figure 5.19: Spectra of Ecklonia at 1 m (trans 8) and at 3.0-4.0 m (trans 10)

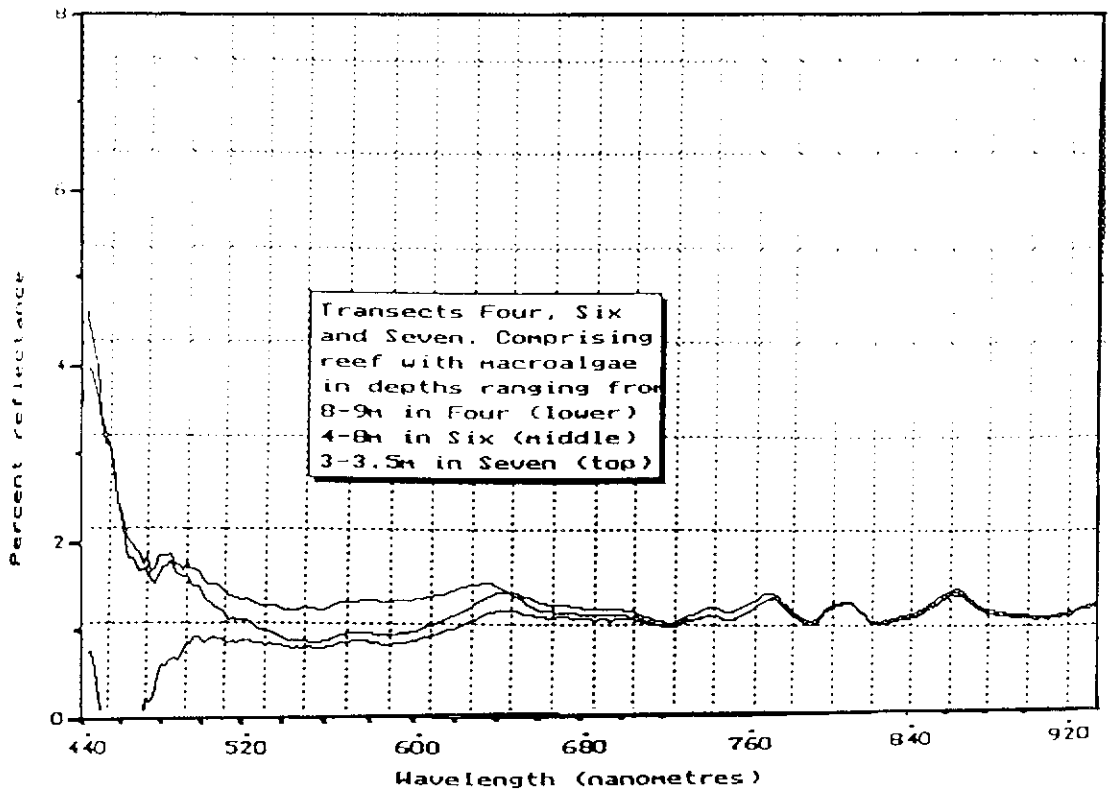

Figure 5.20: Spectra of Ecklonia-dominated reef at depths ranging from 3-9 m

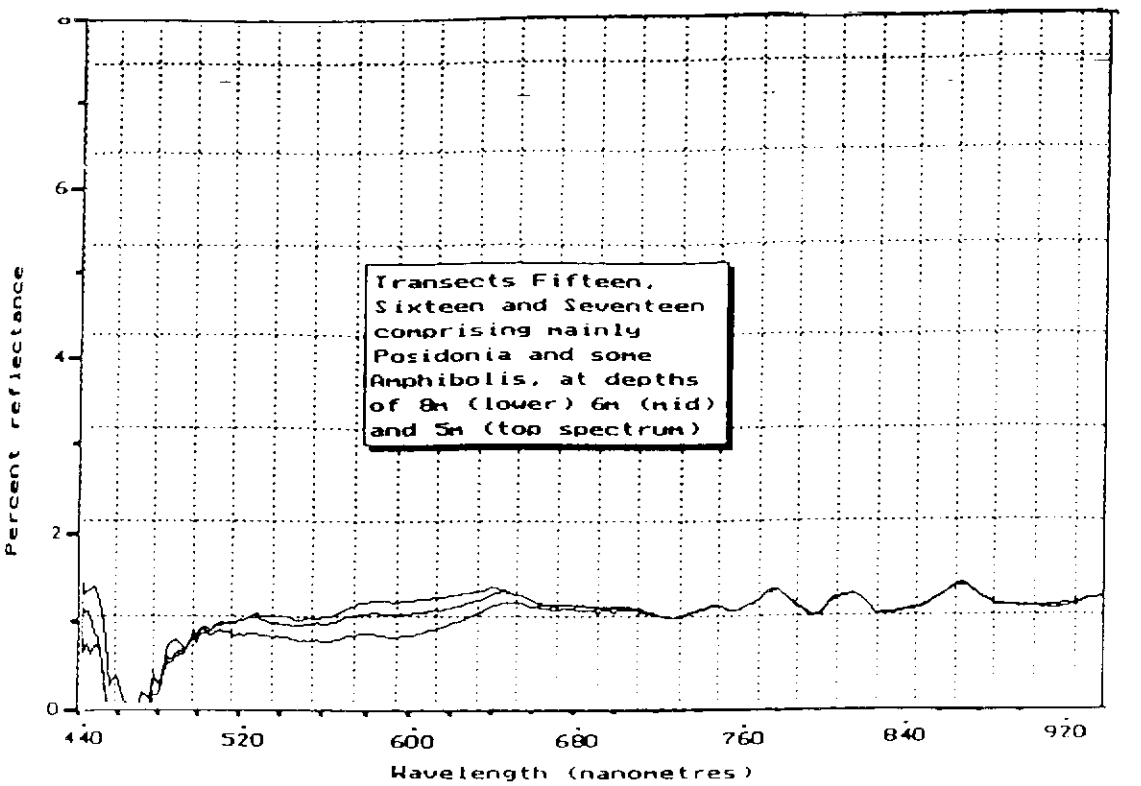

Figure 5.21: Spectra of Posidonia and Amphibolis seagrasses

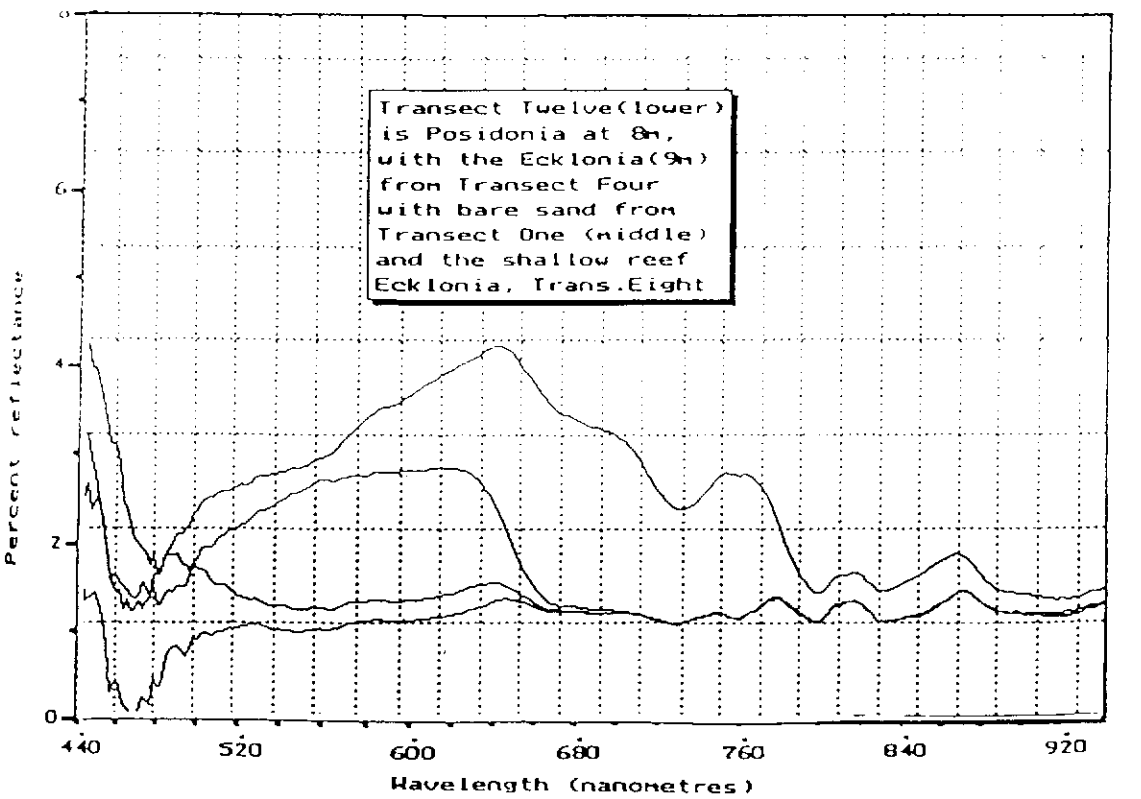

Figure 5.22: Spectra for sand, shallow reef, deeper reef and seagrass

Figure 5.22 combines the spectral response for sand, shallow reef, deeper reef and seagrass. The degree of spectral difference indicates that it should be possible to separate the Ecklonia (with its spectral peak at 650 nm) where it occurs on shallow reefs, from sand areas (with its flatter spectral response between 500-620 nm), and both habitat types are different from the deeper examples of both the algae and seagrasses, which have low and non-diagnostic spectral responses.

5.5.4 Conclusions

The results of this study indicate that for situations such as encountered at the Little Island site, the practical routine use of remotely-sensed data to discriminate major habitat species throughout a depth range is likely to be very difficult. Attenuation of the signal through the water column diminishes the characteristics of the target materials This is clearly evident in both the "at-plant" spectral measurement in the preliminary study and at 3 km above the water using the airborne spectrometer. However, for generic classes, habitat mapping was shown to work reasonably well in the Coastal Waters Study, where depth contours are used as a discriminator in the classification process.

The ability to select specific wavelengths that will provide maximum separation between target materials and or provide the opportunity for algorithms based on positive or negative correlations, such as simple ratio combinations, is the obvious preferred operational outcome. It is realistic to suggest that a combination of spectral bands covering the regions between 450-700 nm could provide the basis for imagery from which reliable habitat maps could be produced, but this could not be achieved

without significant amounts of field spectral analysis of the target materials, field validation of non-training areas and optimum conditions for data acquisition.

5.6 Summary

This chapter has shown that remotely sensed data can provide significant amounts of information about the nature of the near-shore bottom and the characteristics of the benthos it supports. The value of the information is determined by two major influences. These are the conditions at the time of acquisition and the processing steps applied to the data. The benefits of achieving this can mean new information, as was the case in the Broome study which yielded significant production increases. Alternatively, the benefits of this new information in the Geographe Bay study have enabled a conservation strategy to be implemented.

The importance of monitoring change in the coastal environment, especially near populated hinterland, requires the higher spatial resolution offered by airborne multispectral systems, as the rate and extent of critical change indicators is finer that that currently offered by satellite systems. For broad habitat classes such as required in the Perth Coastal Waters Study airborne systems, despite the processing overhead, do have some significant advantages.

The issue of the ability of airborne systems to accurately discriminate between species, or condition of particular species, still appears to be a challenge. However, the amount of interest in the topic currently in the world, and advances in sensor technology, will probably see very significant advances in the near future.

Chapter 6

CONCLUSIONS AND RECOMMENDATIONS

6.1 Conclusions

The aim of this chapter is to summarise some of the already stated conclusions and make recommendations, based on the research in the previous chapters. It is intended to show that the experiments and collaborative case studies, undertaken by the author over the past ten years, provide a coherent assessment the problems that may be expected in applying remote sensing for understanding the surface brightness variation properties, the water column characteristics, and the bottom stratigraphy and benthos in near-shore coastal and riverine environments.

6.1.1 Image Reflectance Characteristics

The problem where imagery of the same area, acquired at different times by an identical sensor, may record very different radiance value is a major limitation to quantitative use of remotely sensed data. These differences can be caused by differences in solar illumination, depending on the time of day or year, differences in the amounts of atmospheric scattering and absorption, or by changes in up-welling radiance at the surface of the area to be studied. The latter is almost always what remote sensing seeks to retrieve from multi-date imagery.

Radiometric correction to compensate for sun elevation differences between image dates and for differences in sensor calibration is an essential precursor to the detection

of change. In some cases it has been shown that a simple correction for solar illumination, based on the cosine of the solar elevation angle, can be used for an arbitrarily fixed solar elevation.

The three experiments in Chapter 3, the Coastal Waters Experiment, the Peel Inlet Experiment and the Swan Estuary Experiment were designed to evaluate the contributions to image brightness of atmosphere, angular variation and hot-spots.

6.1.1.1 Atmospheric and radiometric correction

With some airborne scanners, for example the Geoscan and CASI as used in the Coastal Waters project and in the Swan Estuary experiments, and for imagery from meteorological satellites, radiometric correction is more complicated. The wide scan angle of these systems leads to significant solar elevation differences, or differences in the angles between the sun and sensor across the image, and these may require compensation prior to any quantitative analysis. In its simplest form, the correction is an arithmetic one as was described in the first stage correction for the Coastal Waters Experiment. This was based on a simple model of the scanner angular geometry, although more precise correction may require incorporation of bi-directional reflectance factor or wave facet removal, when determining the characteristics of the water column. These radiometric corrections can remove differences caused by solar elevation or the relative positions of pixels within broad scan swaths.

Atmospheric correction is also a problem and there are a range of techniques of varying complexity to achieve this. It is fortunate that atmospheric effects in

terrestrial applications are usually relatively minor in comparison with solar elevation effects, and some remote sensing can be effective without the need for atmospheric correction. However, the removal of atmospheric effects from visible wavelength data over water is very important, as was shown in the Broome Project.

Over water, where signal is normally relatively low, atmospheric effects can contribute most of the signal reaching a sensor. This is especially true at angular pathlengths and at wavelengths that penetrate water, and is caused by a complex mixture of scattering and absorption by gases, aerosols and solids. Correction models, such as Lowtran, require inputs of sensor and environmental parameters to estimate atmospheric absorption to produce a correction as a function of wavelength.

Ideally, simultaneous spectral measurement of irradiance with the remote acquisition will provide the correction model. This approach was used in the Swan River algal bloom experiments, and the ability to compare imagery between days, and times of day, was possible because of the near-simultaneous reference data.

If neither of these is possible, a common approach for multispectral data is the "darkest pixel" correction method, where the water-leaving radiance in the near infrared is assumed to be zero and the signal received at the sensor is entirely from atmospheric effects. The effects of air molecule scattering can be calculated and removed, leaving the radiance produced from aerosol scattering. Examples show that it is then possible to produce ratios relating the effects of aerosol scattering in the near infrared to the aerosol scattering at other wavelengths, and thus remove atmospheric

effects from visible wavelength data. The corrected radiance values can then be related to physical properties, such as habitat, concentrations of chlorophyll and sediments in the water.

6.1.1.2 Image brightness variation

Imagery obtained over water by a remote sensor contains artefacts of image brightness that relate to the angular effects of the field of view of the instrument. Obvious brightness variation is apparent when the still water surface is acting as a reflector or a mirror and returns an image of the sun to the sensor. The action of wind creates wave facets that increase the reflective region as a function of wave face angle to the sun and the sensor. Increasing wind speed increases the facet angles and, as a consequence, the proportion of an imaged area affected by "sunglint" also increases.

At wind velocities above about 25 km/hr surface waves begin to break causing two major effects. The first is up to a ten-fold increase in the albedo of the breaking wave and the subsequent foam and bubble-stream and, second, in shallow near-shore situations, sediments and biological material may be mixed throughout the water column or resuspended, causing not only increased upwelling radiance from the column, but also a shift toward the red end of the spectral maximum. The spectral study in the Swan Estuary, and the correction technique developed for the Peel Inlet Experiment, were designed to address these issues.

All remotely-sensed data, but especially aerial photographs and "frame-grabbed" airborne video images acquired over land, have brightness variations that must be

considered. They are caused mainly by three things on terrestrial imagery:

(i) Scattering by particles and aerosols in the atmosphere,

(ii) Bi-directional Reflectance Distribution Function (BRDF), and

(iii) Sensor optical geometry.

The same effects are theoretically affecting imagery over water. But over water is the added contribution of the specular reflection of facet scattering. Steps can be taken to inimise these effects at the mission planning stage and by post-processing of the data.

When imaging water, the effect of sunglint, or solar flaring, is the reflection of the sun into the field of view of the sensor. In the case of a "flat" water body, ie. without any surface waves or ripples, the effect on the image, as mentioned earlier, would theoretically be confined to a single spot, which must be avoided by selective acquisition at times when solar elevations are less than the field of view of the sensor. Because the sun is the source of energy for illumination of the target it stands to reason that the best signal to noise ratio, obtained by the sensor, will be at the highest possible solar elevations. The effects of surface roughness or wave facets increases the region around the solar reflection spot and the extent of intrusion into the field of view is a function of windspeed. The experiment in the Swan Estuary, using a particular configuration of spectral radiometer optics, showed the relative trade-offs expected with selection of acquisition planning windows.

6.1.1.3 Hot-spots

The brightness variation (BRDF), sometimes called the "hot-spot", presents problems

that must be addressed on imagery that includes land and water targets. In cases such as river monitoring, where runs of calibrated images are to be produced on a regular time-frame for temporal comparisons, this effect must be removed. It is located on an image at the point on the ground that is in a line with the aircraft and the sun. Theoretically, at the hot-spot centre, the shadow of the aircraft will be located. This point of the image has the potential to provide maximum information from the water column and bottom, but causes processing problems for terrestrial targets. This is because the maximum image brightness appears concentrically around that point.

In typical terrestrial applications, there is no visible shadow from vegetation, or in water applications, from particulate structure and phytoplankton (backscatter only) at the hotspot. As the distance away from that point increases, so does the amount of visible shadow in the image (forward and multiple scattering) causing reduced total reflectance. Again, the spectral experiment in the Swan Estuary indicated that more attention should be given to the issue of hot-spots in studies that can be expected to have high probability of organic or inorganic particulates in the column.

6.1.2 Water Column Characteristics

The need for cost-effective techniques to detect and quantify phytoplankton in the widely-distributed waterbodies throughout Western Australia is an urgent priority for environmental managers. The main problem relates to threats to human and animal health from the toxic effects of blooms of algae in our rivers and coastal waterways. Extensive studies of blue-green algal blooms concluded that the main limitations to using remotely sensed data is a lack of simultaneous in-water and atmospheric

measurements and the importance of using a calibrated data set. The relationship of remotely-sensed data, in the visible-wavelength regions, to chlorophyll-related pigments in water, has been well-established.

The work reported in this thesis occurred in three distinct sequential phases between 1990 and 1995 that represent the evolving availability of airborne instruments to enable the transfer of the technology from the research arena to the practical application of routine monitoring strategies.

The use of remote sensing to detect and quantify algal blooms requires that a relationship exists between in-water data and the remotely-sensed image. Although the detection of, for example, cyanobacterial algal blooms has been highly successful because of the algae's distinctive spectral pigments, detection of the brown-pigmented dinoflagellates was shown in these experiments to be more difficult, especially in humic dominated water such as in the Swan River.

6.1.2.1 Swan-Coastal OCS-Geoscan Comparison

The first study compared the CSIRO Ocean Colour Scanner and the Geoscan Mk2 Airborne Multispectral Scanner to detect and quantify algae-related pigments in coastal waters. Both instruments included wavelengths that are capable of determining the distribution of chlorophyll pigments, and the most useful spectral bands are in overlapping wavebands of the two instruments.

In the analysis the sites were grouped into high- and low-chlorophyll case waters and

the results indicated that band selection is dependant on the expected concentrations. The study showed that a simple universal model could not accurately determine chlorophyll over a wide range of concentrations. Variation in predicting chlorophyll levels came from the physical and chemical nature of the waterbodies. The reflectance from those water bodies was a composite of surface, column and bottom materials. However, the composition could be resolved in some cases as a function of wavelength.

Both instruments performed well when concentrations were grouped at levels that would occur in the independent biophysical systems. The relationship of the chlorophyll to reflectance for high chlorophyll systems, such as the coastal wetlands with values about 50-800 µg/l, is different to the low level systems such as the ocean which recorded levels from 0-50 µg/l. The OCS, as its name implies, performed well in the oceanic levels of pigment concentrations. However, its ability to predict concentrations at higher levels could not be sustained. The Geoscan instrument, with its broader bands, performed reasonably consistently in both case waters.

Determination of speciation of chlorophyll pigments is unlikely with the Geoscan scanner. However, the OCS with its narrow bands in the 400-600 nm regions showed that it may be possible to quantitatively determine pigments. Signal to noise characteristics of the OCS were better than the Geoscan scanner and both instruments appeared to have a higher noise level than specified. Despite this, the image quality was entirely acceptable considering the maximum gain settings that were selected to maximise the low radiances from water bodies.

6.1.2.2 Swan River Study: CASI experiment

This next experiment used data from the CASI instrument to demonstrate:

(i) Characterisation of the spatial and temporal variation of the spectral properties of the water column and the major algal bloom species in the Swan River; and

(ii) Development of spatial and temporal acquisition parameters and image analysis techniques for improved discrimination and early warning of algal blooms.

The majority of algal problems in the eastern states of Australia are caused by cyanobacteria (blue-green algae). However, the Swan River in Western Australia experiences phytoplankton blooms of green algae, diatom and dinoflagellates. The ability to spectrally discriminate between types of blooms was a major objective of the study. The use of airborne instruments was also evaluated as a low cost, operational supplement to traditional boat-based sampling for assessing the spatial and temporal extent of algal blooms. Field studies of in-water reflectance, using multi-band radiometers, supported by laboratory studies indicated that significant spectral differences between cyanobacterial and green algae and diatom/dinoflagellates were measurable.

Two different types of airborne multispectral instruments were evaluated to demonstrate the practical field application of the laboratory results. These were:

(i) CASI which has 288 bands in imaging-spectrometer mode and 14 bands in spatial-imaging mode. It therefore has high spectral resolution but the disadvantage of producing very large data sets that require significant time to

process and analyse. The system is also not available at short notice ; and

(ii) DMSV which provided less spectral resolution although the four bands could theoretically be selected to provide maximum discrimination of algal blooms. The DMSV is less expensive to operate and is locally based, thus normally available at short notice.

The examples used in this study clearly show what the CASI instrument does well. It is sensitive to spectral features of low to moderate concentrations of algal bloom types and other co-varying parameters. The very high spectral resolution gave confidence to the selection of diagnostic wavelengths for the remote sensing of water quality parameters. This study also emphasised the difficulty of obtaining spectral measurements of the water column using conventional field methods. However, the real issue was how few bands, and how broad these bands can be, to still retain reliable diagnostic information.

This phase of the study showed that the classification of water bodies, having low to moderate concentrations of phytoplankton covering six river monitoring sites, is possible. However, it was probably influenced by co-varying parameters such as salinity and turbidity. Strong correlations of image data to total cell counts, and to some of the chlorophyll-dominated phytoplankton, were presented.

The domination of the spectral response by the humic component in the Swan River system needs to be considered if low concentrations of bloom types are to be sensed. In circumstances where major blooms are likely this analysis demonstrates that

spectral separation is possible. To discriminate between bloom types in the major groups of chlorophytes, cryptophytes and diatoms may also be possible with a limited number of bands.

When the comparison of the separation of the best-subset of all CASI bands and the DMSV-like bands was tested with cyanobacteria in the wetland sites there was concurrence in better than 99 percent of cases. The cross-aggregation showed that three DMSV-like bands would be able to separate the algae in the wetlands from the river sites with very high reliability. This finding prompted the next phase of the study into the algal blooms in the Swan River.

6.1.2.3 Swan River Study: DMSV experiment

For monitoring the widely-scattered water bodies in Western Australia, this study showed using the DMSV, that it was likely a simple low-cost airborne system with as few as three or four well-chosen bands could provide the spectral requirements for detection of blooms if supported with some in-water calibration or reference data. It then becomes an economic question as to the temporal frequency that is preferred for monitoring those bloom occurrences.

It was to assess the value of instruments, such as the DMSV, that this evaluation of remotely-sensed data for algal bloom monitoring was initiated. Algal blooms that occur in the Swan River system, such as *Gymnodinium,* are very dynamic in space and time. Although this phase of the study was unable to determine whether the bloom's temporal and spatial patchiness was caused by horizontal advection or vertical

migration of the phytoplankton cells (or a combination of both), it highlighted the need to take account of this variability during in-water sampling for calibration and validation of remote sensing data.

Regardless of the reason for the bloom patchiness, the DMSV study indicated the need to ensure in-water reference sampling is carried out within a short time of the overflight. It also highlighted the problems of collecting enough in-water samples within that restricted time period. The small number of samples at some sites and times within the overflight period may be the reason why several expected trends in the data were poor. A better approach would be to use several fluorometers simultaneously and therefore obtain more samples within a short time period.

The issue of practical spatial resolution is a trade-off between data acquisition and processing volumes against useful information, and the 1.5 m x 1.5 m pixel size of the DMSV provided good discrimination of bloom distribution within the Swan River. It also allowed several replicate pixels within the images to be measured for analyses and interpretation, and it was possible to sample at a similar spatial scale during in-water sampling. However, in an operational context the decision on appropriate spatial resolution would need to be addressed on a site-specific basis, but a larger "foot-print", perhaps as much as 5 m, could be acceptable in rivers such as the Swan.

Earlier work in the previous study, which compared the relationship of different algal blooms with CASI, indicated a variable relationship between spectral bands and the type of phytoplankton. While there was a strong relationship between spectral bands

and cell count for the dominant cryptophyte, *Cryptomonas sp.*, that was occurring in the river at that time of the CASI flight, the relationship for dinoflagellates with the main species *Gymnodinium* was low. A synthesis of the DMSV using the CASI data indicated that even the existing DMSV bands would provide a diagnostic capability for most bloom types in the river system. However, for blooms with spectral characteristics such as *Gymnodinium* that occurred during the DMSV study, this relationship could not be expected to be strong.

The DMSV did not, with its existing band combinations, show any satisfactory relationship with in-situ measurements. This suggests that, for blooms like *Gymnodinium*, the system, as currently configured, could not reliably be used to quantify the bloom concentrations. The lack of characteristic diagnostic features and the dynamic movement of the bloom over time suggests that, even if clear diagnostic bands were available, it may not be possible to estimate *Gymnodinium* concentrations in the river from the air. However, this does not preclude the great potential of the DMSV to reliably detect and perhaps quantify algal blooms that are dominated by chlorophyllous pigments.

Issues of water-clarity and the biology of the particular phytoplankton species may also affect the ability of remote sensing platforms such as DMSV to describe accurately a bloom's distribution and abundance within the water column. This may not be a problem for surface forming blooms that are easily detectable remotely. However, for those blooms, such as *Gymnodinium*, which can alter their distribution within the water column, it is essential that the timing of remote sensing flights be

arranged to coincide with maximum daily abundance at the water surface if the bloom's magnitude and extent is to be determined.

6.1.3 Bottom Characteristics

Landsat TM data have been used to great advantage in the delineation and mapping of substrate features in shallow coastal waters. However, the uncertainty of purchase of what appears on a microfiche quick-look image catalogue to be a clear, cloud-free day, has left many potential users disappointed. Not to mention the realisation that some mathematically-elegant algorithm, that was supposed to deliver contoured bathymetry, is ineffective.

These outcomes led the direction of the research to investigate the practical applied advantages, in terms of the flexibility of timing and spectral selection, of airborne-based digital scanning systems. Research that addressed the shortfalls experienced with satellite-based acquisition included studies designed to produce useful information on benthic habitat using data from the Geoscan scanner, CASI and DMSV. These examples serve to enforce the determination and industry requirement for specific and spatially-coherent information about the near-shore bottom habitats, and the need to monitor change to these environments over time.

The single most important issue in determination of information from beneath a water body is the signal-to-noise ratio. The signal strength is not generally a problem with conventional applications of satellite data. However, for in-water related image processing, the response values between target materials are usually small and

processing is aimed at the maximum information retrieval. Discrimination is limited by the radiometric resolution of the sensors, and the SNR can introduce image degradation which would be unacceptable for most terrestrial applications. However, for qualitative interpretation of linear or reasonably homogeneous patterns, a lower than normal SNR is often acceptable.

6.1.3.1 Broome Project

The earliest recorded use of TM data for commercial fishing purposes was done for the pearling industry in Broome. The aims of that work were to:

(i) Determine quantitative techniques for bathymetric mapping,

(ii) Map the benthic habitats of pearl oyster *(Pinctada maxima)* and Western King Prawn (*Penaeus latisulcatus*),

(iii) Map sub-sea stratigraphy, and

(iv) Evaluate existing remote sensing systems and image enhancement techniques for water penetration.

The relationship between radiance and depth could only be validated in this study when the ocean bottom was uniform and principally sandy. Useful relationships were evident on the image when the bathymetric vector data from the latest hydrographic charts were embedded into the image. Radiometric measurement over different bottom types did support a linear absorption with depth, especially when radiance was converted to reflectance. Ship-borne reflectance measurements were also of the same dynamic range as the radiance measured by the satellite.

Significant relationships were established between the diver assessment of bottom type from the Flinders data for pearl oyster habitat and the information contained in the image. Similarly "rough" and "smooth" trawling ground could reliably be identified on the imagery. The results for trawling indicated a 79 percent success rate in identifying trawlable and non-trawlable bottom. The results for pearl oyster bottom-type indicated 80 percent success.

Inherent positional inaccuracies (from 300 m for SATNAV) may have caused errors in the predictions of bottom-type, and underline the benefits of incorporating the latest GPS technology into the results. The benefits of identifying and accurately locating a set of characteristics which are significantly correlated with the presence or absence of a target species is a saving of unproductive vessel time, with a commensurate increase in the efficiency of a fishing operation.

Evidence of drowned shoreline features as remnants of stillstands during Eocene transgression can be extended from the La Grange image data, used in an earlier study, northward to the Lacipede Islands. Propositions of some explorers as to the likely exit point of an older course of the Fitzroy River through the Roebuck Deep south of Broome may account for the broad sedimentary nature of the areas west of Broome. Exploration trawling for sedimentary diamonds has commenced. This work has contributed significantly to submarine geomorphic and sedimentological studies

.

The study also indicated the importance of careful data selection and processing. High sun angle imagery is of critical importance, but to obtain maximum benefit it

must be coupled with an incoming neap tide (to provide minimum velocity clear oceanic water) and low wind conditions (to reduce wave-induced sediment re-suspension and surface scatter). For tropical environments, where phyto- and zoo-plankton blooms are common during some seasons, local information is also required

The waveband characteristics of Landsat TM band 1 appear to be ideal. However, the usefulness of the SPOT data should not be discounted, despite the longer wavelength, as the higher sun angles, at the later acquisition time (approximately 1 hour), should still retain good water penetrating characteristics. Consideration of SPOT multispectral (20 m) data provides a wider range of potential acquisition dates from which area-specific selection criteria can more closely be followed.

6.1.3.2 Geographe Bay Project

In the light of the above conclusions, and the need to obtain a better understanding of the distribution of high-conservation value seagrass habitat along the entire coast of Western Australia, a small research project was initiated in the Geographe Bay area. Conflicts had arisen between the competing interests of the fishing (trawling) and mining (mineral sand dredging). Anecdotal evidence of great water clarity and extensive seagrass meadows at depths of more than 40 m indicated that Geographe Bay could provide conditions that might support the detection of bottom features at depths approaching 50 m.

The successful use of Landsat TM occurred for several reasons. The weather conditions at the time of acquisition were clear sky, with light normally dry offshore

SE winds. Solar elevation at acquisition was near annual maximum, and the verified depths of penetration were greater than 45 m below mean low sea level.

The research showed the decline in biomass of the meadows with increasing depth. Multiple scattering, caused by the leaf structure of the canopy of the meadow, absorbs light at the wavelength of TM band 1. Crescent-shaped scours observed on the imagery are characteristic of rare storm events on seagrass meadows. These have a scarp edge about 70 cm deep and a lee edge that slopes into the seagrass meadow. They are often colonised by smaller species of seagrass which are more easily scoured out by storms than the surrounding meadow.

6.1.3.3 Perth Coastal Waters Project

Geoscan Airborne Multi-Spectral Scanner imagery was shown, when used in conjunction with other data sets, to be useful for classifying marine benthic habitats. This imagery also provided several significant advantages over other forms of remotely sensed data, such as from satellite and aerial photographs. These include adequate spatial resolution, relatively high water penetration capability and greater logistical discretion to acquire data under optimal environmental conditions. However, satellite data, typically at 20 to 30 m resolution, would not have presented the scattering problems. Aerial photography, which could have provided higher spatial resolution, has limited spectral quantisation, which reduces the potential for multi-band image processing to remove solar flaring effects, and geometric rectification is far more complex.

Water penetration, spatial rectification and the capacity to remove depth effects from confounding the classification of benthic habitats have been the major obstacles to the broad-scale application of remote sensing technology for mapping the marine environment. The approach adopted in this study suggests that airborne scanners, such as Geoscan, can provide marine managers with a technique that produces an accurate, spatially rectified digital habitat map over large areas of the coastal environment, and it was that conclusion that led to further study at Little Island in the Marmion Lagoon.

6.1.3.4 Marmion Lagoon Project

The results of this study indicated that, for situations such as encountered at the Little Island site, the practical routine use of remotely-sensed data to discriminate major habitat species throughout a depth range is likely to be very difficult. Attenuation of the signal through the water column tends to diminish the characteristics of the target materials.

CASI data were used to select specific wavelengths that provide maximum separation between habitat types, and to provide the data for algorithm development, based on positive or negative correlations, such as simple ratio combinations, to separate those types. It is realistic to suggest that a combination of spectral bands covering the regions between 450-700 nm could provide the basis for multi-spectral image acquisition in order to produce reliable habitat maps. However, this cannot be achieved without significant amounts of field spectral analysis of the target materials, field validation of non-training areas and optimum conditions for data acquisition.

The issue of the ability of airborne systems to accurately discriminate between species, or condition of particular species, still appears to be a challenge. However, the amount of interest in the topic currently in the world, and advances in sensor technology, will probably see very significant advances in the near future.

6.2 Recommendations

The following recommendations are given with some explanation to keep them in context with the experiments and conclusions.

6.2.1 Surface Reflectance Effects

Correction procedures need to be undertaken to solve changes in atmospheric conditions and scene brightness variation problems of remotely sensed imagery used in projects involving coastal waters. Atmospheric modelling is a complex and scene specific correction that is well covered in such models as Lowtran, if the ideal and recommended solution of simultaneous spectral calibration is not possible.

Scene brightness correction is also complex but has not received the attention given to atmospheric correction. This research showed that the most common method to remove the BRDF effect relies on calculating an average brightness surface from a sequence of frames in the flight line and subtracting that mean (usually smoothed) surface from the image. Other methods need to be used if multiple uniform frames are not available. These may be based on band-ratios (Hick *et al.*, 1994), or on empirical correction models that account for solar elevation and azimuth and for flight direction (Pickup *et al.*, 1993), or on correlative techniques developed by Hick and Ong (1995) and Ong *et al.* (1995).

(a) Across-track brightness

Rayleigh scattering causes brightness variation in images and varies with particles in the atmosphere and as a function of angular pathlength. The problem increases dramatically with wide FOV instruments and wavelength, especially at the visible wavelengths that provide maximum information both from substrate and water column signal. These effects are most serious in airborne scanners, although correction procedures for wide field of view satellite systems such as the NOAA-AVHRR have similar characteristics, which are further complicated by earth-rotation and curvature effects.

As a result of this research, it is recommended to use column-averaging models to remove across-track brightness effects from Geoscan-type data as long as flight direction and platform stability remains constant. A two-stage correction procedure can be applied to remove across-track illumination and wave facet effects. The first stage involves subtracting smooth column means for deep ocean which contains no detectable bottom features. The product of this subtraction is an image, free of across-track illumination effects, but still containing wave facet effects. A second stage correction, based on band correlations, can remove wave facet effects by regressing the visible and infrared bands. The residual image, with all visibly detectable across-track and wave facet effects removed to within the level of instrument noise, should be acceptable for use in training for classifications and image interpretation.

(b) Solar angle modelling

Conjecture is very evident in the literature on the most useful technique for correction of BRDF. Pickup *et al.* (1993) indicate that a single equation, based on view angle, can be used for brightness normalisation as a function of wavelength for each image. Their findings show that this produces better results than the commonly-used band ratio techniques. However, their work seems to be at variance with King (1991) who, in his analysis of video data, showed that where the linear trends were consistent in all bands, simple band ratios are a very effective means of reducing brightness variations caused by view angle. Pickup *et al.* (1993) produced contingency coefficients for an overlap area on two adjacent images which had different brightness values caused by different view angle. Pickup also suggests the use of multiple flying heights, i.e. correction of very low-altitude acquisitions by comparing derived curves from high-altitude data acquired in the same mission.

The most significant conclusion that can be drawn from this conjecture is based on a simple premise. After correction it is reasonable to expect that the digital values in two adjoining images, in the area of image overlap, should be the same. Most empirical models have been derived for uniform surfaces where they may work reasonably well, but there are two significant points that are sometimes overlooked. These are that the brightness curve on an image is (i) material-dependent, and is also (ii) wavelength-dependent. The correlative correction work of Hick and Ong (1995) produced outcomes and a technique that considers these factors, and seems to be able to produce consistent results for highly-variable target surfaces. Therefore this technique is recommended for terrestrial applications.

(c) Correlative corrections over water

Similar approaches to correlative correction have been developed for the same purposes, but over water bodies, for aquatic and marine applications (Hick and Ong, 1995; Ong *et al.*, 1995). These techniques use simultaneously-acquired satellite data with corresponding wavebands to determine BRDF effects and hence create a correction surface. This technique has been used extensively, and successfully by the author, to remove scene-brightness effects in airborne video data acquired for monitoring condition of salt concentrator ponds in the north-west of Western Australia where significant bottom reflectance contributes to the signal. The technique is therefore also recommended for correction of high resolution imagery that is required to be mosaicked for spatial interpretation or that is to be used in any form of multi-temporal monitoring using automatic supervised or unsupervised classifiers.

(d) Wave-facet scattering and removal techniques

The example using DMSV data in Peel Inlet showed that, with the knowledge of the expected variability between pixels caused by wave facet reflectance, a kernel and a brightness differential could be chosen to select and remove (or enhance) the bright pixels caused by the wave facets or targets. This form of data filtering should be used to provide user control that may not be possible in Fourier Transformation or other image processing techniques. In this case a trade off between image clarity and the need to locate control points (fixed position boats and markers) is important. In high spatial resolution imagery the S/N ratio will change between different datasets and this depends to a large extent on the conditions of the day and the spatial configuration of

the instrument to optimise signal. This technique is recommended for site-specific correction where interactive control over the level of facet smoothing may vary between frames, or the user has specific targets to extract from the data.

6.2.2 Water Column Characteristics

The findings of the research into the operational use of high-resolution remote sensing of the Swan River and surrounding waterways, using airborne systems such as the DMSV, identified some important advantages and limitations to the generic use of this technology. The following points illustrate some of the important considerations.

(a) Effectiveness

Remote sensing is recommended as an effective means to rapidly map the extent of the highly dynamic, widely-spread algal blooms. Airborne sensors have advantages over traditional sampling methods such as the ability to sample large expanses, in an inexpensive manner, over very short periods of time. They can be used to provide a "birds-eye view" of blooms and a unique means to identify specific sites of interest, such as in-flowing drains and point-source sites, which may be difficult to identify or locate from the ground. A good relationship between the ground data and the images is obviously necessary for detection and quantification of bloom concentrations. However, in situations where blooms are rapidly changing, remote sensing provides an effective tool for describing in a qualitative sense, the dynamic nature of the bloom at a particular moment over large spatial scales.

(b) Discrimination

Most discrimination of algal bloom types can be made with few spectral bands in the

visible spectrum that cover the major combination of pigments. For routine monitoring, simple instruments such as the DMSV, should be sufficient provided that bandpass filters are selected that provide maximum discrimination of the bloom of interest in the water column. Generic or filter combinations that are optimised for terrestrial applications will not have sufficient discriminant functions in most cases.

(c) Water column components

More research on the spectral contribution of water column components, eg. humics, suspended solids and the atmospheric scattering contribution, will provide a more quantitative description of bloom type and severity through the development of specific algorithms for image analysis.

(d) Flight times

Flight times are very site- and mission-specific, and over water should be limited as a general rule to sun angles of no more than 45 degrees (i.e. in summer, flights should be between 8 am and 10 am and from 3 pm to 5 pm for latitudes and time zones like Perth). Some algal blooms, eg. *Gymnodinium*, alter their position within the water column so that their maximum abundance in the surface layers occurs in the latter part of the day. Thus flights need to be planned to coincide with both physical and biological factors for maximum accuracy.

(e) Sunglint

Increased overlap of the image frames will also minimise the effects of sunglint but increase the data handling burden. Optimum data quality is obtained when calm wind conditions prevail. This will reduce wave ripples to minimise the facet sunglint area

and also reduce mixing of the upper water column. The central flight-line for the aircraft can be set to favour the same side of the river as the sun to minimise sunglint effects.

(f) Flight altitudes

Flight altitudes of 3,500 m, the practical maximum altitude for low-cost, un-pressurised aircraft, provide DMSV images with a nominal ground resolution of 2 m pixels. That resolution provides spatial discrimination that is considered ideal for research purposes. However, a larger spatial resolution for operational purposes in rivers as wide as the Swan, would also be satisfactory. DMSV data, when de-convolved to as much as 10 m, still provides adequate description of bloom variability.

(g) Calibration

Calibration targets should be included in every mission, and gains and offsets of cameras should not be altered without reflight over those targets. This aspect is often ignored and is essential for quantitative monitoring.

(h) Band registration

Camera alignment, or band registration, on video-based systems should be precise to ensure a minimum post processing registration of 1.5 m to 2 m pixels. Algorithms based on multi-band spectral response demand good pixel registration. However, this becomes less critical if individual frames are to be mosaicked as an overlay on 10 m pixel satellite data such as panchromatic SPOT.

(i) Auto-correlation

Further development of automatic correlation-based software procedures, for both band and image registration, for near-real time information products is essential. Using procedures developed for this study the delivery time for image products is of the order of two to three days. This could be reduced to less than 24 hrs which is becoming the normal requirement for environmental managers.

(j) Reference data

Remote sensing requires reference sampling to be done simultaneously or within a very short period of the remote sensing flight. For accurate assessment of bloom distribution, flights must coincide with the biological activity of the phytoplankton, and at times of the day that will minimise sunglint. If flights are not carefully planned, the relationships between bloom distribution and abundance, and remotely sensed images will be poor. Ground truthing must be done within $\pm$ 30 min of flight times or bloom distribution and abundance may have significantly changed and have little resemblance to the precise patterns captured in the image. A way to ensure better ground truthing at the time of the overflight is to deploy multiple fluorometers from stations or boats equipped with differential GPS.

(k) Field spectrometry and fluorometry

The advancing technology of solid-state miniature field spectrometers is an area of research and development that should be pursued. These low-cost instruments have the potential to supplement the use of multiple fluorometers, and also be useful installations for remote location monitoring and identification of algal types based on

characteristic spectra, as well as for validating airborne multi-spectral imagery.

6.2.3 Bottom Characteristics

Two main conclusions can be drawn from the experimental use, in this thesis, of remotely sensed data for the characterisation of the sea-floor. Firstly, if the acquisition conditions are optimum, significant upwelling radiance can be attributed to materials on the bottom. Secondly, the potential to divide that upwelling radiance into meaningful spectral diagnostic functions is very limited and rapidly diminished by the attenuation of the water column.

(a) Radiance and depth

The earliest study using Landsat TM data to determine the relationship between radiance and depth could only be sustained when the ocean bottom is uniform and principally sandy. Radiometric measurement over different bottom types did support a linear absorption with depth, although this aspect of the research has been explored by other authors and therefore was not given as high priority in this work as the detection and characterisation of bottom materials. The major recommendation on the use of remotely sensed visible data for quantitative bathymetric determinations is that the outcome will be site-specific without significant reference data for atmosphere, attenuation coefficients for the column, and uniform or known bottom characteristics.

(b) Assessment of bottom type

Significant relationships were established between the diver assessment of bottom type for pearl oyster and prawn trawl habitat. Also, rough and smooth trawling ground could reliably be identified on the early applications of this type of imagery.

This opportunity-cost can be justified in a fishery where the identified productive grounds support economic catches. This method is recommended as having the greatest potential benefit in the exploration and development of any new benthic-related fishery, where the distribution of target species and habitat is unknown, and in many instances where the bathymetry is uncharted.

(c) Data selection

Both the Broome and Geographe Bay studies indicated the importance of careful data selection and processing. High sun angle imagery is of critical importance, but to obtain maximum benefit it must be coupled with low wind and swell conditions. For tropical environments, where phytoplankton blooms, coral spawning and spat release are evident at certain times of the year, tide and local information is also required.

The waveband characteristics of Landsat TM band 1 appear to be ideal. The usefulness of the SPOT data should not be discounted despite the longer wavelength band, as the higher sun angles, due to the later acquisition time, can still retain good water penetrating characteristics.

(d) Processing airborne scanner data

The desire to improve spatial and spectral characteristics, seen as a limitation to Landsat data, introduce additional disadvantages. Raw Geoscan imagery, chosen for the Coastal Water study, was affected by several artefacts, especially sun-glint and specular reflection long-period swell waves. The heuristic approach used to remove these effects from the image relied on the inclusion of a uniform area across the image

(eg. deep ocean) in order to separate sun-glint from real features.

Water penetration, spatial rectification and the capacity to remove depth effects from confounding the classification of benthic habitats have been the major obstacles to the broad-scale application of remote sensing technology for mapping the marine habitats. This study suggests that airborne scanners, such as Geoscan and subsequent multi-band systems, can provide marine managers with a technique that produces an accurate, spatially rectified digital habitat maps over large areas of the coastal environment. However, it is recommended that the attenuation of signal as a function of depth be considered and incorporation of bathymetry as a discriminant function be implemented before subdivision of habitat types is made.

(e) Water column properties

Although, as concluded above, the results of both the in-situ spectral measurements and the CASI spectral-mode data indicated a relatively low and uniform reflectance at each depth, the pattern changed with depth. While it is possible to obtain a relatively diagnostic response in one location and depth, unique characteristics of the water column properties, can mask the effect. This interpretation is supported by the differing response of the radiance immediately above species, without the contribution of the water column on the upwelling radiance. It is therefore recommended that studies that assume uniform water column characteristics, without calculation of attenuation coefficients, require careful interpretation.

The results for situations, such as encountered at the Little Island site, show the practical routine use of remotely-sensed data to discriminate major habitat species throughout a depth range is likely to be very difficult. However, it should be possible, and was shown to work reasonably well in the Coastal Waters Study, where depth contours are used as a discriminator in the classification process, and where the opportunity exists to select wavelengths that will provide maximum separation. It is realistic to suggest that a combination of spectral bands covering the regions between 450-700 nm could produce the basis for imagery from which reliable habitat maps could be produced, but this could not be achieved without significant amounts of field validation and optimum conditions. These considerations must be factored in to any program that seeks quantitative data.

In summary, upwelling reflectance is affected by the light attenuated by the water column and the underlying substrate. It may therefore be possible to distinguish not only among species but also their density of cover. This ability will be influenced by other masking features such as the water column. The ability to distinguish between factors, such as species and density, relies on the ability to unambiguously separate the characteristic reflectance components.

REFERENCES

Ackleson, S.G. and Klemas, V. (1987) Remote sensing of submerged aquatic vegetation in Lower Chesapeake Bay: A comparison of Landsat MSS to TM imagery, *Remote Sensing of Environment*, Vol. 22, pp. 235-248.

Anthony, C., Hick, P.T. and Wallace J.F. (1991) Spectral relationships of water chemistry for the wetlands of Rottnest Island, *CSIRO/SCITECH Report*, Scitech Discovery Centre, Perth, WA, pp.1-12.

Babey, S.K. and Anger, C.D. (1989) A Compact Airborne Spectrographic Imager (CASI), *Proceedings of 12th IGARSS Canadian Symposium on Remote Sensing*, Vancouver, BC, Canada, pp.10-14.

Bierwirth, P.N., Lee, T.J. and Burne, R.V. (1993) Shallow sea floor reflectance and water depth derived by unmixing multispectral imagery, *Photogrammetric Engineering and Remote Sensing*, Vol. 59, No. 3, pp. 331-338.

Bell, J.D. and Pollard, D.A. (1989) Ecology of fish assemblages and fisheries associated with seagrass, in *Seagrasses: A Treatise in Seagrasses with Special Reference to the Australian Region*, Larkum, McCombe and Shepherd (eds), Elsevier, Amsterdam, pp. 565-609.

Benjamin, K.J. (1985) Studies of the intertidal flora of the Point Peron region, Western Australia, *Honours Thesis*, School of Biological and Environmental Sciences, Murdoch University, WA (unpublished).

Bird, E.C.F. (1976) *Coasts*, 2nd Ed., Vol. 4 Australian National University Press, Canberra, ACT, 52pp.

Burt, J.S., Kendrick, G.A., Masini, R.J. and Simpson, C.J. (1995) Light and *Posidonia* seagrass meadows in the temperate coastal waters of Western Australia: The effect of epiphyte biomass and species assemblage on attenuating light to the leaf surface, *Technical Series Report Number 62*, Department of Environmental Protection, Perth, WA.

Cambridge, M.L. (1975) Seagrasses of south-western Australia with special references to the ecology of *Posidonia australis* Hook. F. in a polluted environment, *Aquatic Botany*, Vol. 1, pp. 149-161.

Cambridge, M.L. and McComb, A.J. (1984) The loss of seagrass in Cockburn Sound, Western Australia: The time course and magnitude of seagrass decline in relation to industrial development, *Aquatic Botany*, Vol. 21, pp. 229-243.

Campbell, N.A. (1984) Canonical variate analysis - A general model formulation, *Australian Journal of Statistics*, Vol. 26, No. 1, pp. 86-96.

Campbell, N.A. and Atchely, W.R. (1981) The geometry of canonical variate analysis, *Systematic Zoology*, Vol. 30, No. 3, pp. 268-280.

Carpenter, D.J. and Carpenter, S.M (1983) Modelling inland water quality using Landsat data, *Remote Sensing of Environment*, Vol. 13, p. 345.

Clark, D.K. (1981) Phytoplankton algorithms for the Nimbus-7 CZCS, in *Oceanography from Space*, Gower, J.R.F. (ed), Plenum, New York, pp. 227-238.

Collins, L.B. (1988) Sediments and history of the Rottnest Shelf. southwest Australia: a swell dominated, non-tropical carbonate margin, in *Sedimentary Geology*, No. 60, pp.15-49.

Cox, C. and Munk, W. (1954) Measurement of the roughness of the sea surface from photographs of sun glitter, *Journal of Optical Society of America*, Vol. 44, pp. 838-850.

Cox, C. and Munk, W. (1956) Slopes of the sea surface deduced from photographs of sun glitter, *Bulletin of Scripps Institute of Oceanography*, Vol. 6, pp. 401-488.

Craig, M.D. and Green, A.A. (1987) Registration of distorted images from airborne scanners, *Australian Computer Journal*, Vol. 19, No. 3, pp. 148-153.

Dekker, A.G., Malthus, T.J. and Seyhan, E. (1991) Quantitative modelling of inland water quality for high-resolution MSS systems, *IEEE Transactions on Geoscience and Remote Sensing*, Vol. 29, pp. 89-95.

Dervieux, A. and Tamisier, A. (1987) Submerged macrophyte beds of Camargue wetlands: Estimation of their distribution and size by the interpretation of air photos, *Oceanocologica Acta*, Vol. 8, pp. 371-385.

Doak, E., Livisay, J., Lyzenga, D., Ott, J. and Polcyn, F. (1980) Evaluation of water depth extraction techniques using Landsat and aircraft data, *Final Report, 1359000-2-F 1980*, Defence Mapping Agency, Washington DC, Hyd/Topo Centre, 208 pp.

Dwivedi, R.M. and Narain, A. (1987) Remote sensing of phytoplankton: an attempt from the Landsat Thematic Mapper, *International Journal of Remote Sensing*, Vol. 8, p. 1563.

Fairbridge, R.W. (1961) Eustatic changes in sea level, *Physics and Chemistry of the Earth*, Vol. 14, pp. 99-185.

Gordon, H.R., Clark, K., Brown, W., Brown, B., Evans, H. and Broenkow, W. (1983) Phytoplankton pigment concentration in the Middle Atlantic Bight: comparison of ship determination and CZCS estimates, *Applied Optics*, Vol. 22, p. 20.

Gordon, H.R. and Jacobs, M.M. (1977) Albedo of the ocean-atmosphere system: influence of sea foam, *Applied Optics*, Vol. 16, p. 2257.

Gordon, H.R. and McCluney, W.R. (1975) Estimation of sunlight penetration in the sea for remote sensing, *Applied Optics*, Vol. 14, No. 2, pp. 413-416.

Gordon, H.R. and Morel, AY. (1983) Remote assessment of ocean color for interpretation of satellite visible imagery, a review, in *Lecture Notes on Coastal and Estuarine Studies*, Springer-Verlag, New York, pp. 113.

Guzzi, R., Rizzi, R. and Zibordi, G. (1987) Atmospheric correction of data measured by a flying platform over the sea: elements of a model and its experimental validation, *Applied Optics*, Vol. 26, pp. 3043-3051.

Harding, L.W. Jr., Itsweire, E.C. and Esias, W.E. (1992) Determination of phytoplankton chlorophyll concentrations in the Chesapeake Bay with aircraft remote sensing, *Remote Sensing of Environment*, Vol. 40, pp. 79-100.

Hick, P.T. (1978) A descriptive classification and its use in the genetic interpretation of the coast of the south-west of Western Australia, *Report to Western Australian Institute of Technology*, CSIRO, Perth, WA, 42 pp.

Hick, P.T. (1979) Remote sensing techniques applied to an estuarine environment problem in Western Australia, *Australian Journal of Instrumentation and Control*, Vol. 60, No. 1, pp. 4-6.

Hick, P.T. and Jernakoff, P. (1994) Algal bloom research using CASI data in Western Australia, *Proceedings of 7th Australasian Conference on Remote Sensing*, Melbourne, March, Vol. 2, pp. 736-744.

Hick, P.T. and Ong, C. (1995) Evaluation of part of the 1995 DMSV dataset of the Andoom Minesite, *Report from CSIRO Minesite Rehabilitation Program for Comalco Minerals and Alumina*, CSIRO, Perth, WA.

Hick, P.T., Pattiaratchi, C. and Wyllie, A. (1992) A comparison of two Airborne Multispectral Scanners for determination of chlorophyll pigments in riverine, lacustrine and oceanic environments, *Proceedings of 6th Australian Remote Sensing Conference*, Wellington, NZ, November, Vol. 1, pp. 215-225.

Hick, P.T. and Scoones, R.J.S. (1988) Satellite data use for studies of benthic and bathymetric characteristics of sub-sea stratigraphy in the Eighty-Mile Beach region of Western Australia, *Exploration Geoscience Restricted Report EG5R*, 14 pp.

Hick, P.T. and Scoones, R.J.S. (1990) Satellite derived imagery for water penetration and its relevance to fisheries in the Kimberley region of Western Australia, *CSIRO DEG Restricted Report 122R*, CSIRO, Perth, WA, pp.1-28.

Hick, P., Wyllie, A. and Kirkman, H. (1994) Marine substrate feature delineation from Thematic Mapper data: the Geographe Bay example, *Proceedings of 7th Australasian Conference on Remote Sensing*, Melbourne, Vic, March, Vol. 2, pp.706-713.

Hodgkin, E.P. (1959) The salt lakes of Rottnest Island. *Journal of Royal Society of WA*, Vol. 42, pp. 84-85.

Hodgkin, E.P. and Birch, P.B. (1984) Algal problems in the Estuary *Western Australian Journal of Agriculture*, Vol. 25, No. 3, pp. 80-81.

Honey, F.R. and Byrne, P. (1978) Air survey and satellite imagery: tools for shallow water bathymetry, *Proceedings of 20th Australian Survey Congress*, Darwin, NT, 17 pp.

Honey, F.R. and Hick, P.T. (1976a) Classification of the wetlands of the south-east corridor, *Report to Wetlands Advisory Committee for the Environmental Protection Authority of WA*, March, CSIRO, Perth, WA, 20 pp.

Honey, F.R. and Hick, P.T. (1976b) Aerial photographic specifications for land resource management, *CSIRO Land Resource Management Report*, CSIRO, Perth, WA.

Honey, F.R., Hick, P.T. and Brown, J.M. (1980) Multilevel inventory and monitoring of wetlands, *Report to the Department of Conservation and Environment, WA*, CSIRO, Perth, WA, 20 pp.

Jensen, J.R., Estes, J.E. and Tinney, L. (1980) Remote sensing techniques for kelp surveys, *Photogrammetric Engineering and Remote Sensing*, Vol. 46, pp. 743-755.

Jerlov, N.G. (1976) *Marine Optics*, Elsevier Oceanography Series, No. 14, Elsevier, Amsterdam, 231 pp.

Jernakoff, P. and Hick, P.T. (1994) Spectral measurement of marine habitat: simultaneous measurements and CASI data, *Proceedings of 7th Australasian Conference on Remote Sensing*, Melbourne, Vic, Vol. 2, pp. 706-713.

John, J. (ed) (1987) Swan River estuary, ecology and management, *Curtin University Environmental Studies Group Report No 1*, Curtin University of Technology, Perth, WA.

Johnsen, G., Oddgeir, S., Lois, G. and Egil, S. (1994) *In vivo* absorption characteristics in 10 classes of bloom-forming phytoplankton: taxonomic characteristics and responses to photo-adaptation by means of discriminant and HPLC analysis, *Marine Ecology Progress Series*, Vol. 105, pp. 149-157.

Jupp, D.L.B. (1988) Background and extensions to depth of penetration (DOP) mapping in shallow coastal waters, *Proceedings of International Symposia on Remote Sensing of the Coastal Zone*, Gold Coast, Qld, September, pp. IV.2.1-IV.2.19.

Jupp, D.L.B., Held, A., Byrne, G., Hutton, P. and McDonald, E. (1992a) The potential use of airborne scanning for monitoring algal dynamics in Australian inland waters, *COSSA Report No. 03*, Canberra, ACT, pp. 1-124.

Jupp, D.L.B., Kirk, J.T.O. and Harris, G.P. (1994) Detection, identification and mapping of cyanobacteria - using remote sensing to measure the optical quality of turbid inland waters, *Australian Journal of Marine and Freshwater Research*, Vol. 45, pp. 801-828

Jupp, D.L.B., McVicar, T.R., Walker, J., Held, A., Kalma, J.D. and McDonald, E. (1992b) Remote sensing of change in components of the regional water balance of the Murray Darling Basin using satellite imaged and spatially registered environmental data, *Final Report on LWRRDC Project CWA6: CSIRO Division of Water Resources Consultancy Report No. 92/31*, CSIRO, Perth, WA.

King, D. (1991) Determination and reduction of cover type brightness variations with view angle in airborne multispectral video imagery, *Photogrammetric Engineering and Remote Sensing*, Vol. 57, pp. 1571-1577.

Kirk, J.T.O. (1981a) Monte Carlo study of the nature of the underwater light field in, and the relationships between optical properties of, turbid yellow waters, *Australian Journal of Marine and Freshwater Research*, Vol. 32, pp. 517-532.

Kirk, J.T.O. (1981b) Estimation of the scattering coefficient of natural waters using underwater irradiance measurements, *Australian Journal of Marine and Freshwater Research*, Vol. 32, pp. 533-539.

Kirk, J.T.O. (1983) *Light and Photosynthesis in Aquatic Ecosystems*, Cambridge University Press, Cambridge, UK, 401 pp.

Kirkman, H. (1990) Seagrass distribution and mapping, in: *Seagrass Research Methods*, UNESCO Monographs in Oceanographic Methodology, pp. 19-25.

Kirkman, H. and Kuo, J. (1990) Pattern and process in southern Western Australian seagrasses, *Aquatic Botany*, Vol. 37, pp. 367-382.

Kneizys, F.X., Shettle, E.P., Gallery, W.O., Chetwynd, J.H. Jr, Abreu, L.W., Selby, J.E.A., Clough, S.A. and Fenn, R.W. (1983) *Atmospheric Transmittance/Radiance: Computer Code LOWTRAN 6*, AFGL-TR-83-0187, Airforce Geophysics Laboratory, Massachusetts, 200 pp.

Koepke, P. (1985) The reflectance factors of a rough ocean with foam. Comment on remote sensing of seastate using the 0.8-1.1 by Wald and Monget, *International Journal of Remote Sensing*, Vol. 6, pp. 787-799.

Lavery, P., Pattiaratchi, C., Wyllie, A. and Hick, P. (1993) Water quality monitoring in estuarine waters using the Landsat Thematic Mapper, *Remote Sensing of Environment*, Vol. 46, pp. 268-280.

Lillesand, T.M., Johnson, W.L, Deuell, R.L., Lindstrom, O.M. and Miesner, D.E. (1983) Use of Landsat data to predict the trophic status of Minnesota lakes, *Photogrammetric Engineering and Remote Sensing*, Vol. 49, p. 219.

Lyons, K.G. (1976) *Evaluation of an experimental bathymetric map produced from LANDSAT data*, Department of Surveying, Western Australian Institute of Technology, Perth, WA.

Lyzenga, D.R. (1978) Passive remote sensing techniques for mapping water depth and bottom features, *Applied Optics*, Vol. 17, No. 3, pp. 379-383.

Lyzenga, D.R. (1981) Remote sensing of bottom reflectance and water attenuation parameters in shallow water using aircraft and Landsat data, *International Journal of Remote Sensing*, Vol. 2, No. 1, pp. 71-82.

MacArthur, W.M. and Bettenay, E. (1960) The development of the soils of the Swan Coastal Plain, Western Australia, *Soil Publication Series*, No. 16, 55 pp. CSIRO, Perth WA.

McRoy, C.P. and Helfferich, C. (1977) in: *Seagrass ecosystems: a scientific perspective*. Marcel Dekker Inc., New York, pp. 1-5.

Milton, E.J. (1987) Principles of field spectroscopy, *International Journal of Remote Sensing*, Vol. 8, No. 12, pp. 1807-1827.

Monahan, E.C. and O'Muircheartaigh, I.G. (1986) Whitecaps and the passive remote sensing of the ocean surface, *International Journal of Remote Sensing*, Vol. 7, No. 5, pp. 627-642.

O'Neill, N.T., Kalinauskas, A.R., Borstad, G.A., Edal, H., Gower, J.F. and Van der Piepen, H. (1987) Imaging spectrometry for water applications, *SPIE Imaging Spectroscopy II*, Vol. 834, pp. 129-134.

Ong, C., Hick, P.T., Craig, M., Warren, P. and Newman, C. (1995) A correlative technique for correction of shading effects in digital multispectral video imagery, *Proceedings of International Symposium on Spectral Sensing Research*, Melbourne, Vic, November, CD-ROM.

Ong, C., Wyllie, A. and Hick, P.T. (1994) Mapping marine habitats using Geoscan Mk2 Airborne Multispectral Scanner Data, *Proceedings of 7th Australasian Conference on Remote Sensing*, Melbourne, Vic, March, Vol. 2, pp. 698-705.

Patriquin, D.G. (1975) Migration of blowouts in seagrass beds at Barbados and Carriacou, West Indies, and its ecological and geological implications, *Aquatic Botany*, Vol. 1, pp. 163-189.

Pattiaratchi, C., Lavery, P., Wyllie, A. and Hick, P. (1992) Multi-date algorithms for predicting surface water quality parameters in estuarine and coastal waters using Landsat TM data, *Proceedings of Central Symposium on International Space Year*, Munich, Germany, April, pp. 709-714.

Pattiaratchi, C., Pearce, A.J. and Hick, P.T. (1990) Application of Coastal Zone Colour Scanner (CZCS) imagery for productivity and circulation studies of the Leeuwin Current, Western Australia, *Proceedings of 5th Australian Remote Sensing Conference*, Perth, WA, October, pp. 252-256.

Pearce, A.F. and Griffiths, R.W. (1991) The mesoscale structure of the Leeuwin Current: a comparison of laboratory model and satellite images, *Journal of Geophysical Research*, Vol. 96, No. 9, pp. 16739-16757.

Penn, J.W. and Dybdahl, R. (1988) A survey of pearl oyster and prawn resources in waters off Broome, *West Australian Fisheries Report No. 81*, Western Australian Fisheries Department, Perth, WA, 20 pp.

Pickup, G., Chewings, V.H. and Pearce, G. (1995) Procedures for correcting high resolution airborne video imagery, *International Journal of Remote Sensing*, Vol. 16, No.9, pp. 1647-1662

Savastano, K.J., Faller, K.H., McFadin, L.W., and Holley, H. (1981) Mapping of submerged vegetation using remote sensing technology, *NOAA Technical Memorandum*, NOAA/ NMFS; NSTL Station, MS (USA), No. 73, 101 pp.

Scoones, R. and Hick, P.T. (1990) Bathymetric imagery and its relevance to fisheries in the tropical regions of Western Australia, *Proceedings of 5th Australian Remote Sensing Conference*, Perth, WA, October, Vol. 1, pp. 811-814.

Simpson, C.J., Burt, J.S., Cary, J.L., D'Admano, N., Masini, R.J. and Mills, D.A. (1993) Southern metropolitan coastal waters study (1991-1994): progress report, Environmental Protection Authority, Perth, WA, *Technical Series 53*, 65 pp.

Smith, R.C. and Baker, K.S. (1981) Optical properties of the clearest natural waters (200-800 nm), *Applied Optics*, Vol. 20, pp. 177-184.

Smith, R.C. and Wilson, W.H. (1981) Ship and satellite bio-optical research in the California Bight, in *Oceanography from Space*, Gower, J.F. (ed), Plenum Press, New York, p. 281.

Sorokin, A.L., Kil'dyushevskij, E.I., Gurevich, D.S. and Vanyukhin, B.I. (1988) Aerial photography in marine ecological and landscape studies of the White Sea, *Izvestia Vgo*, Vol. 120, pp. 314-321.

Stumpf, R.P. and Tyler, M.A. (1988) Satellite detection of bloom and pigment distributions in estuaries, *Remote Sensing of Environment*, Vol. 24, pp. 395-404.

Sturm, B. (1981) Ocean colour remote sensing and quantitative retrieval of surface chlorophyll in coastal water using NIMBUS CZCS data, in *Oceanography from Space*. Gower, J.F. (ed) Plenum Press, New York, p. 267.

Tapley, I.J. (1990) The perception of submerged strandlines on night thermal NOAA-AVHRR satellite imagery, *Proceedings of 5th Australian Conference on Remote Sensing*, Perth, WA, October, Vol. 2, pp. 928-942.

Tassan, S. (1987) Evaluation of the potential of the Thematic Mapper for marine applications, *International Journal of Remote Sensing*, Vol. 8, pp. 1455-1478.

Tassan, S. and Sturm, B. (1986) An algorithm for the retrieval of sediment content in turbid coastal waters from CZCS data, *International Journal of Remote Sensing*, Vol. 7, pp. 643-655.

Van Stokkom, H.T.C., Stokman, G.N.M. and Hovenier, J.W. (1993) Quantitative use of passive optical remote sensing over coastal and inland water bodies, *International Journal of Remote Sensing*, Vol. 14, No. 3, pp. 541-563.

Verdin, J.P. (1985) Monitoring water quality conditions in a large western reservoir with Landsat imagery, *Photogrammetric Engineering and Remote Sensing*, Vol. 51, p. 343.

Wald, L. and Monget, J.M. (1983) Remote sensing of the sea-state using the 0.8-1.1 micron spectral band, *International Journal of Remote Sensing*, Vol. 4, No. 2, pp. 433-446.

Wallace, J.F., Palmer, M.J. and Furby, S. (1991) Vegetation mapping and dieback hazard assessment in the Northern Jarrah Forest using remotely sensed data, *CSIRO WA Remote Sensing Group, Division of Mathematics and Statistics report to ALCOA Australia*, CSIRO, Perth, WA.

Yamaguchi, Y. and Lyon, R.J.P. (1985) A comparative field study of spectroradiometers and radiometers as used in geologic mapping of a porphyry copper at Yerrington, Nevada, Proceedings of *19th International Symposium on Remote Sensing of Environment*, Ann Arbor, Michigan, July, pp. 523-532.

Young, F.R. (1984) Remote sensing for bathymetric mapping of the shallow water areas of Papua New Guinea, *MSc Thesis*, Papua New Guinea University of Technology, 156 pp.

Zibordi, G., Parmiggiani, F. and Alberotanza, L. (1990) Application of aircraft multispectral scanner data to algae mapping over the Venice Lagoon, *Remote Sensing of Environment*, Vol. 34, pp. 49-54.